DIAGENESIS IN THE CREEDE FORMATION,

SAN JUAN MOUNTAINS, CREEDE, COLORADO

by

Marie Taaffe McCrink

Submitted in partial fulfillment
of the Requirements for the Degree of
Master of Science in Geochemistry

New Mexico Institute of Mining and Technology

Socorro, New Mexico

January 22, 1982

CONTENTS

Figures

ABSTRACT

The Creede Formation located in the San Juan Mountains of southcentral Colorado, is a volcaniclastic unit derived from the erosion of numerous surrounding ash-flow tuffs. Sediments, ash-falls, ash-flows, a few thin lava flows, and numerous travertine bodies have been deposited in a structural moat which formed in response to resurgent doming of the Creede caldera. Sediments and some ash-fall material fill in the moat on the western, northern, and eastern sides of Snowshoe Mountain, the resurgent dome. On the south side, Creede Formation sediments are interbedded with Fisher Quartz Latite lava flows and breccias. The Fisher Quartz Latite has been dated at 26.4 m.y., a date which also fixes the age of the Creede Formation.

Sediments in the Creede Formation have undergone varying degrees of diagenetic alteration. Diagenesis has produced a large variety of authigenic silicate minerals. The most important diagenetic reaction to occur is the hydration and solution of unstable pyroclastic material. From this solution montmorillonite, celadonite, clinoptilolite, mordenite, and silica minerals precipitate. It is believed that analcime, illite, and potassium feldspar then form by replacement of zeolite precursors. Heulandite is also present in samples which were collected for the detailed analysis of this project. However, it is uncertain

whether heulandite formed by precipitation from the glassy solution, or by replacement of zeolite precursors.

Lacustrine siltstones and sandstones were deposited in small playa lakes which formed in the central and deepest portions of the moat. Fluvial sandstones, conglomerates, and breccias were deposited near the caldera rim and along the caldera sides. It is suggested that diagenesis of the lacustrine facies occurred in a saline alkaline lake environment. Pore fluids in the lacustrine sediments were moderately alkaline and saline. Diagenesis of the fluvial and breccia facies occurred by ground waters percolating down towards the playa lakes. Pore fluids in these sediments were mildly saline and moderately alkaline.

ACKNOWLEDGEMENTS

Completion of this thesis was the result of many peoples' efforts, and I would like to sincerely thank the following people. My advisors, M. W. Bodine, David I. Norman, Phillip M. Bethke, and George S. Austin, each spent a great deal of time carefully reading, and making constructive criticisms on the text. In particular, George S. Austin, deputy director of the New Mexico Bureau of Mines, joined the thesis committee at the last minute in order to fill in for P. M. Bethke who was unable to attend the thesis defense. Managers of the Wason and Phipps Ranches willingly allowed access to their lands, and gave permission to collect as many samples as necessary for the use of acedemic persuits. R. A. Sheppard with the U. S. Geologic Survey in Denver, Colorado, donated 8 zeolite samples of known composition from which standards were prepared for X-ray fluorescence analysis. Babette Faris, XRF laboratory manager, New Mexico Bureau of Mines, Socorro, New Mexico, set up calibration curves for the zeolite standards. Charles E. Chapin, New Mexico Bureau of Mines volcanologist, was instrumental in helping with the petrography. Karen Couch, scanning electron microscope technician, New Mexico Institute of Mining and Technology, Socorro, New Mexico, helped to scan chips from every sample collected and analyzed for this thesis. Mark Leo, geologist

and computer scientist, patiently provided detailed instructions on how to use the New Mexico Tech computer system for typing, editing, and producing the final copy of this thesis. Finally, encouragement from my husband, Tim McCrink, always made it easier to keep working.

INTRODUCTION

The Creede Formation is a volcaniclastic unit derived from the erosion of numerous surrounding ash-flow sheets. It is situated in and around the town of Creede, and is located in the San Juan Mountains of southcentral to southwestern Colorado (Fig. 1). The San Juan Mountains represent the largest erosional remnant of a major composite volcanic pile that once extended over most of the southern Rocky Mountains in middle Tertiary time (Steven and Epis, 1968; Steven, 1975). The San Juan Mountains presently cover approximately 25,000 square kilometers (Lipman and others, 1970).

The Creede Formation is exposed along the western, northern, and eastern margins of the Creede caldera (Fig. 2). The sediments were deposited in a structural trough which formed in response to resurgent doming of the Creede caldera. The Creede Formation forms an irregular arc spanning nearly 270°C degrees from Lime Creek, 3.0 km northwest of Spar City, along the Rio Grande River to Wagon Wheel Gap, and south up Goose Creek for nearly 9.4 km (Steven and Ratte, 1964). This arc covers a distance of approximately 35 km.

Sediments in the Creede Formation have undergone varying degrees of alteration. The effects of diagenesis, and possibly hydrothermal alteration, appear to be

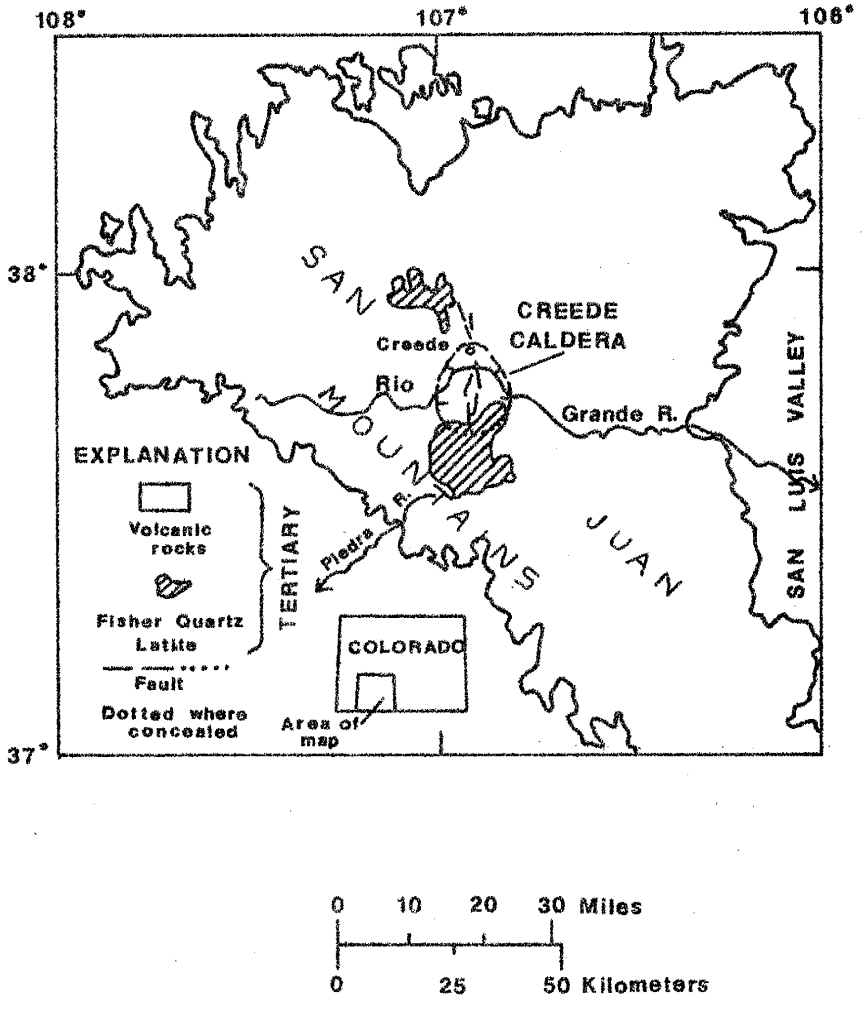

Figure 1. Location map of southwestern Colorado showing outline of the San Juan volcanic field. Modified from two sources, Steven and Ratte (1965), and Steven and Friedman (1968).

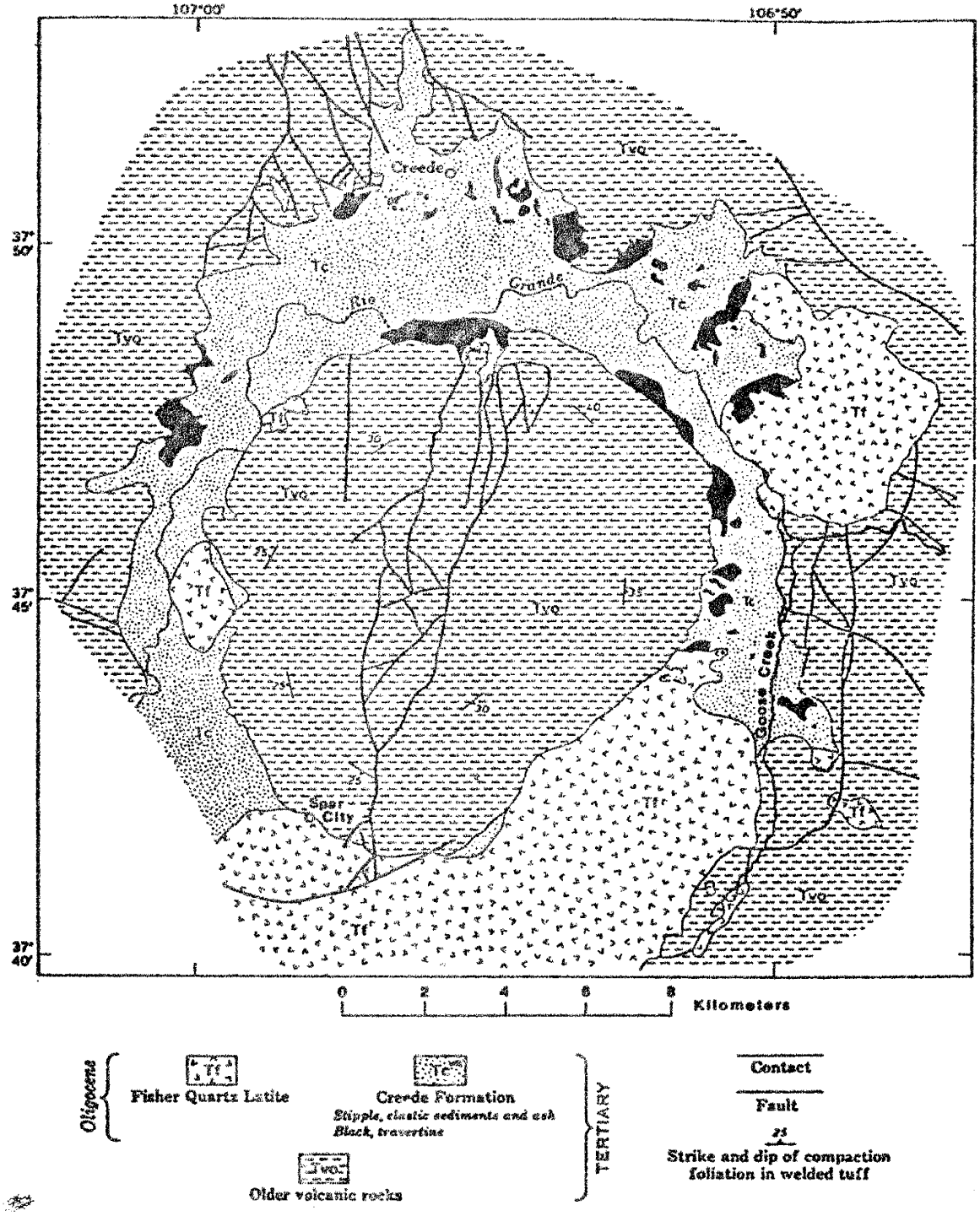

Figure 2. Geologic map of the Creede caldera. Modified from Steven and Friedman (1968).

widespread throughout the unit. Several types of authigenic minerals have formed: the zeolites heulandite, clinoptilolite, analcime, and mordenite; montmorillonite clays, kaolinite, and traces of chlorite; chalcedony, opal, and quartz; and potassium feldspar. Diagenetic alteration involves hydration and solution of volcanic glass. From this solution clay minerals, alkalic zeolites, and silica minerals precipitate. A sodium-rich zeolite (analcime), illite, and potassium feldspar then form by replacement of zeolite precursors. Few of the primary crystalline minerals are replaced and only in a small number of localities has the mesoscopic textural character of the rocks changed due to alteration.

A few brief descriptions of the Creede Formation currently exist in the literature. The two earliest references reported the Creede Formation as a series of sedimentary beds and lava flows. These flows accumulated in a deep valley that had much the same character and position as the present Rio Grande River between Wagon Wheel Gap and Trout Creek (Emmons and Larsen, 1923; Larsen and Cross, 1956). However, since the late nineteen fifties the Creede area has been recognized as a resurgent caldera complex (Smith and Bailey, 1968).

The early investigators attempted to divide the Creede Formation into two members. They reported a considerable thickness of fine grained tuffs, a few breccias, and

abundant travertine bodies in the lower part; and coarser grained tuffs with some intercalated lava flows in the upper part. Today it is recognized that the earlier subdivisions are laterally equivalent facies which cannot be separated stratigraphically (Steven and Ratte, 1964).

Mapping of the Creede Formation was completed in 1973 by T.A. Steven and J.C. Ratte. The only subdivision they have indicated is the numerous travertine bodies occurring throughout the formation.

The primary objective of this thesis is to begin a comprehensive description of the Creede Formation. The project involves stratigraphy, petrography, mineralogy, and major element geochemistry. Particular emphasis has been placed on investigating the origin of authigenic minerals which form through diagenetic alteration of pyroclastic material.

Field work for this project involved the measurement and preparation of two detailed stratigraphic columns. The columns represent a thorough description of Creede Formation geology with specific references to exposures found in sections 3, 4, 9, and 10 on the Creede quadrangle, Mineral County, Colorado (Fig. 3). The measured sections cover a vertical thickness of approximately 180 meters and include detailed rock descriptions of the immediate surrounding 10.24 square kilometers. While the exact thickness of the Creede Formation is not known, it probably averages between

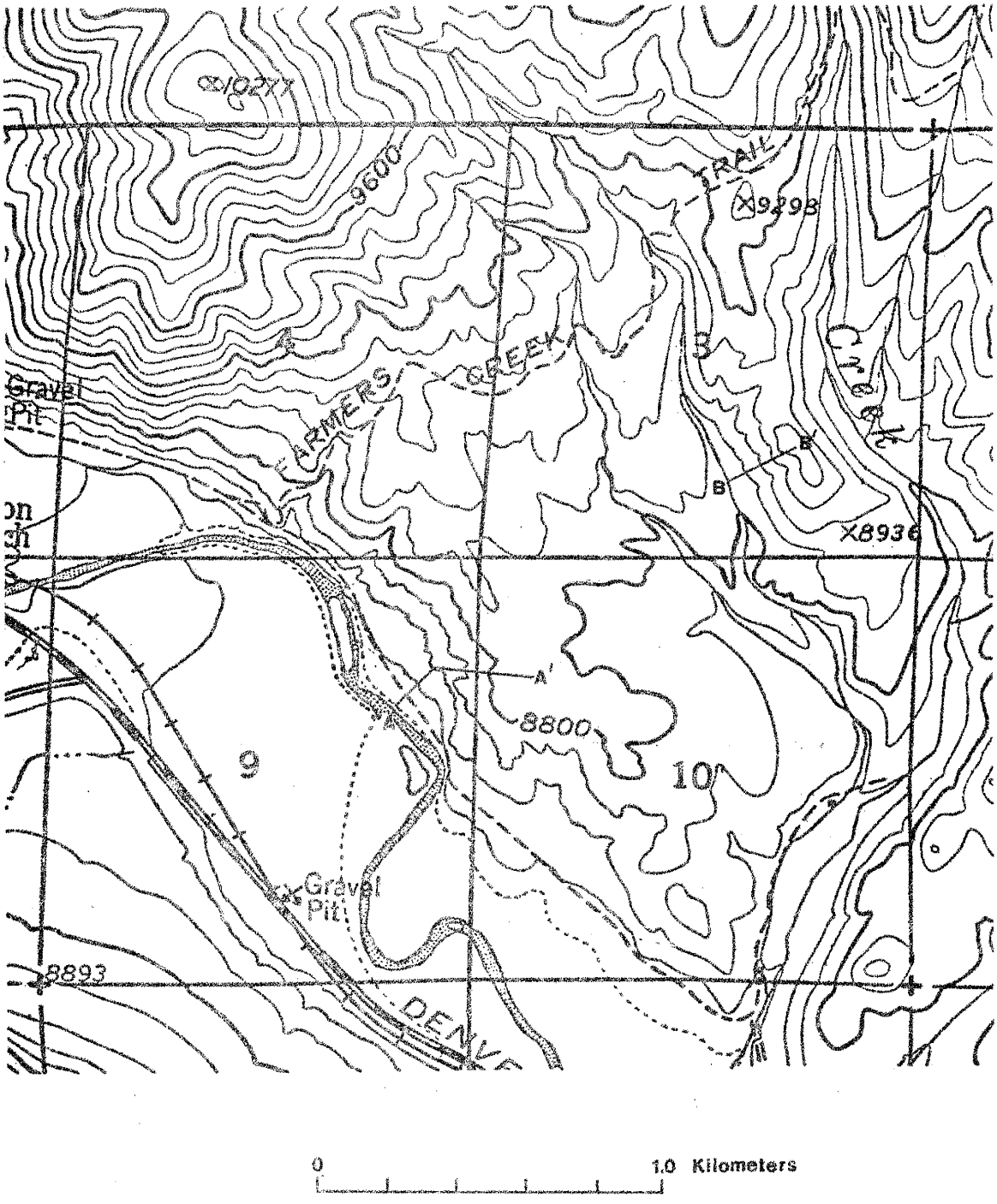

Figure 3. Enlarged map of the Creede quadrangle showing sections 3, 4, 9, and 10. Lines A-A' and B-B' indicate where measured sections under investigation are located.

700 and 750 meters. Furthermore, the sediment filled moat spans a 35 km arc. Thus, this study focuses on only a small portion of the Creede Formation in comparison to the total volume of sediments which fill the Creede caldera moat.

Analytical work for this thesis relied foremost on x-ray diffraction analysis. Scanning electron microscopy, petrographic microscopy, and x-ray fluorescence analysis were also extensively employed.

SAMPLE PREPARATION AND ANALYTICAL PROCEDURES

Whole rock samples were prepared for all rock types collected from two measured sections. Approximately 50 g. of all samples were dry ground on a Microjet 5 high speed rotary grinder to less than 200 mesh in an agate mortar and pestle. Pressed powder pellets containing approximaely 3.0 g of sample material were prepared in duplicate by pressing under 20 tons of pressure into briquettes using boric acid or bakelite backing.

1. X-ray Diffraction Analysis: A conventional Norelco X-ray generator and diffractometer was used to obtain all whole rock diffraction patterns and initially identify most minerals present. A Rigaku generator and diffractometer was used for clay analyses and size fractionation studies. All X-ray patterns were obtained using nickle-filtered copper radiation, a curved crystal monochrometer, a scanning speed of two degrees 2θ per minute, a chart speed of one inch per minute, and slit sizes of 1-4-1 and 1-3-1 for the Norelco and Rigaku respectively.

2. Size Fractionation Study: From the minus 200 mesh powder 20 samples were chosen for preparation of the less than 13, 9, 5, 3, 2, and 1 micron fractions. Each fraction was removed by gravity settling and X-rayed for relative amounts of minerals present in the different size ranges.

3. Clay Analysis: Ten samples were chosen for analysis

of clay content. The less than two micron fraction was removed by gravity settling and three slides were prepared for each of the clay samples. These slides were X-rayed after air-drying, solvation with ethylene glycol, heating for one hour at 350°C, and one hour at 550°C.

4. X-ray Fluorescence Analysis: Pressed powder whole rock pellets were analysed for SiO_2, Al_2O_3, total Fe as Fe_2O_3, MgO, CaO, Na_2O, K_2O, and TiO_2. A wavelength dispersive Rigaku 3064 vacuum spectrometer and electronic accessories were used for the analyses. For each element counts were collected in excess of 10,000 thereby insuring a standard deviation of 1% or less in counting statistics. Oxide concentrations were obtained by correlating net counts of sample with net counts of the drift pellet. The calibration curves for each element except Na, were derived from linear and multiple regression calculations using U.S.G.S. zeolite standards. Na required the addition of some U.S.G.S. igneous standards. The fit of the standard data to the curve was acceptable for corrrelation coefficients better than 0.99. Regression coefficients obtained from the least squares fit were then used to determine the unknown concentrations in the samples collected. Matrix effects were corrected using multiple linear regression of influencing elements where necessary (Si, Al, Mg, and Ca).

For all samples the following instrumental conditions

remained constant throughout the analyses: use of first order K alpha peaks only; KV/MA settings of 50/50; and use of a rhodium target. Tables of calibration curve statistics and of those instrumental conditions that varied are located in Appendix I.

5. Scanning Electron Microscope Study: One cm square chips of all samples were mounted on Al stubs and coated with a mixture of 40% Au and 60% Pd using a C.S.C. mini sputter coater. All samples were examined using an Hitachi HHS-2R scanning electron microscope. An Ortec energy dispersive X-ray analyser, Model 260, was used to obtain relative abundances of cations present on selected surfaces and crystals.

6. Authigenic Mineral Identification: Initial identification of authigenic silicates was made on the Norelco diffractometer; size fractionation studies indicated which minerals were present in the authigenic size range; and scanning electron microscope studies confirmed their presence by allowing identification based on crystal morphology and grain relationships.

GEOLOGIC SETTING

THE SAN JUAN MOUNTAINS

The general geology and petrologic evolution of the San Juan Mountains is described in detail in Steven and Lipman (1976), and Lipman and others (1978). Therefore, only the fundamental sequence of volcanic events will be summarized based on facts obtained in those papers. Most specific age designations mentioned below are also from those papers.

EARLY INTERMEDIATE LAVAS AND BRECCIAS

Volcanism probably began between 40 and 30 m.y. ago in the latest Eocene or earliest Oligocene time, and was most intense from 34.7 to 31.1 m.y. ago. The early phase of volcanism was characterized by complex local sequences of intermediate composition lavas and breccias. Rocks were principally alkali andesites, rhyodacites, and mafic quartz latites erupted from numerous widely spread stratovolcanos. This early suite of volcanics is estimated to have once covered more than 40,000 square kilometers and averaged approximately 1 km in thickness (Lipman and others, 1978).

ASH-FLOW TUFFS

Approximately 30 m.y. ago voluminous pyroclastic eruptions of quartz latitic and rhyolitic ash-flow tuffs began. These volcanics were derived primarily from calderas in the western and central portions of the San Juan volcanic field. Ash-flow sheets were generally emplaced directly on top of the early lava flows and breccias, however they were only about half as voluminous (Lipman and others, 1978). K-Ar data indicate the time span of major ash-flow eruption was slightly less than or equal to 4 m.y. During this time at least 18 major ash-flow sheets were erupted from 15 known and three postulated calderas (Steven and Lipman, 1976).

Caldera collapse also began during this period and was followed by some later ash-flow eruptions which were largely ponded within their associated subsiding caldera (Steven and Lipman, 1976). After caldera collapse, the cores of many were resurgently domed following the typical caldera sequence outlined by Smith and Bailey (1968).

LAVAS AND ROCKS RELATED TO ASH-FLOW TUFFS

In most places caldera collapse was also closely followed by eruption of post subsidence lavas and breccias. In the western part of the San Juan mountains eruptions were mainly of intermediate composition and often barely

ASH-FLOW TUFFS

Approximately 30 m.y. ago voluminous pyroclastic eruptions of quartz latitic and rhyolitic ash-flow tuffs began. These volcanics were derived primarily from calderas in the western and central portions of the San Juan volcanic field. Ash-flow sheets were generally emplaced directly on top of the early lava flows and breccias, however they were only about half as voluminous (Lipman and others, 1978). K-Ar data indicate the time span of major ash-flow eruption was slightly less than or equal to 4 m.y. During this time at least 18 major ash-flow sheets were erupted from 15 known and three postulated calderas (Steven and Lipman, 1976).

Caldera collapse also began during this period and was followed by some later ash-flow eruptions which were largely ponded within their associated subsiding caldera (Steven and Lipman, 1976). After caldera collapse, the cores of many were resurgently domed following the typical caldera sequence outlined by Smith and Bailey (1968).

LAVAS AND ROCKS RELATED TO ASH-FLOW TUFFS

In most places caldera collapse was also closely followed by eruption of post subsidence lavas and breccias. In the western part of the San Juan mountains eruptions were mainly of intermediate composition and often barely

distinguishable from those rocks of the early stratovolcanos. In the central San Juan calderas post subsidence eruptions were of viscous quartz-latitic and rhyolitic lavas closely related in composition to the ash-flow tuffs (Steven and Lipman, 1976). During this time, moats, which formed in response to resurgent doming of the calderas, were filled with volcaniclastic rocks derived principally from surrounding ash-flow sheets.

Ash-flow eruption began to decline in the western calderas about 28 m.y. ago. In the central calderas highly explosive activity continued until approximately 26.6 m.y. ago. In the Creede area the final phase of late Oligocene volcanism was marked by eruption of the Fisher Quartz Latite; K-Ar data has yeilded a mean age of 26.4 m.y. for this event (Steven and others, 1967).

LATE BASALTS AND RHYOLITES

In the early Miocene, approximately 25 m.y. ago, the character of volcanism changed markedly once again. The change was to a bimodal suite of basaltic lavas and high-silica, alkali-rich rhyolite lavas and tuffs. This phase produced a widespread but very thin veneer of volcanic material compared to thick accumulations of ash flows which were produced by the late Oligocene phase of volcanism. Early Miocene volcanic history in this area was also

characterized by the onset of basin and range faulting immediately to the east of the San Juan Mountains in the San Luis Valley segment of the Rio Grande trough. Thus, it appears that the change to bimodal volcanism approximately coincided with this major tectonic event (Lipman and Mehnert, 1975).

Eruption of basalts and rhyolites associated with rifting continued intermittantly from early Miocene into Pliocene time until about 5.0 m.y. ago. Only one large volume ash-flow tuff, the Sunshine Peak Tuff, was deposited during this time. It was erupted very early in this phase of volcanism, approximately 22.5 m.y. ago (Mehnert and others, 1973). A concise summary of the volcanic stratigraphy reviewed here is found in Table 1.

THE CREEDE CALDERA

The Creede caldera is part of the central San Juan caldera complex and lies at the southern end of four nested calderas (Fig. 4). The oldest of these calderas is the La Garita caldera where subsidence took place 27.8 m.y. ago in response to eruption of the Fish Canyon Tuff (Lipman and others, 1970). Along the western margin of the La Garita caldera, the Bachelor caldera formed next in response to eruption of the Carpenter Ridge Tuff. This event occurred sometime between 27.8 and 26.7 m.y. ago, which are the ages

Table 1. Generalized Tertiaty volcanic stratigraphy of the San Juan Mountains, Colorado

VOLCANIC UNIT	K-AR AGE (MILLION YEARS)
Late Basalts and Rhyolites	
Basalts of Servilleta Fm	3.6 to 4.5
Hinsdale Formation	
Basalt	4.7 to 26.4
Rhyolite	4.8 to 22.4
Sunshine Peak Tuff (ash-flow sheets of Lake City caldera)	22.5
Lavas and Rocks Erupted Concurrent With Ash-flow Tuffs	
Fisher Quartz Latite	26.4
Local andesitic-quartz latitic flows and breccias.	>26.4
Main Ash-Flow Tuffs	
Snowshoe Mountain Tuff	>26.4
Nelson Mountain Tuff	
Rat Creek Tuff	
Wason Park Tuff	
Mammoth Mountain Tuff	26.7
Carpenter Ridge Tuff	
Fish Canyon Tuff	27.8
Masonic Park Tuff	28.2
Sapinero Mesa Tuff	
Dillon Mesa Tuff	
Blue Mesa Tuff	
Tuff of Ute Ridge	28.4
Treasure Mountain Tuff	
Ra Jadero Member	
Ojito Creek Member	
La Jara Canyon Member	
Tuff of Rock Creek	
Early Intermediate-Composition Lavas and Breccias	
Local andesitic-quartz latitic rocks of the Conejes Fm and related units	31.1 to 34.7

Modified from Lipman and others (1978)

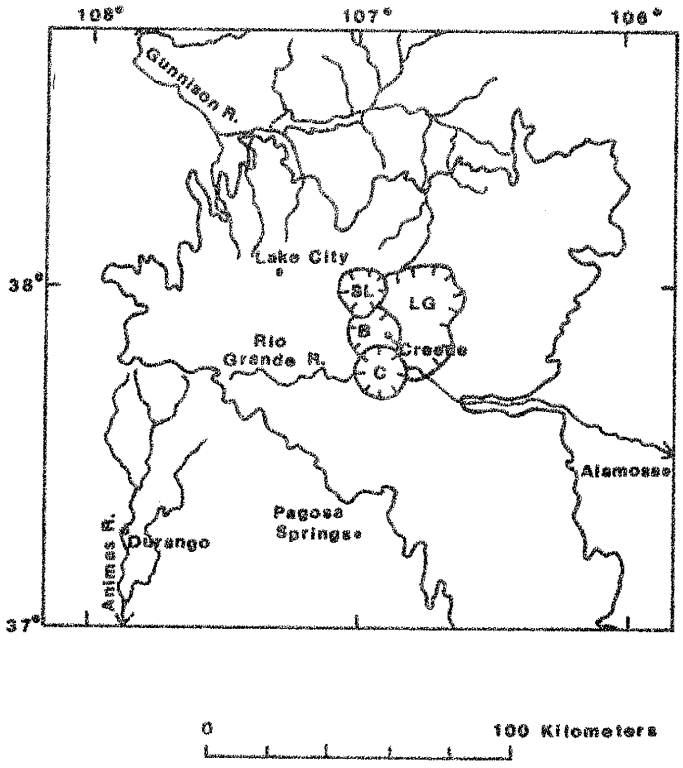

Figure 4. Location of central San Juan calderas showing position of the Creede caldera on the southern end of four nested calderas. Modified from Steven and Lipman (1976).

Calderas (in order of increasing age)

C Creede caldera
SL San Luis caldera
B Bachelor caldera
LG La Garita caldera

of the older Fish Canyon Tuff and younger Mammoth Mountain Tuff, respectively (Steven and Lipman, 1976). Based on textural evidence in the Mammoth Mountain Tuff, the formation of another caldera after the Bachelor Mountain caldera, has been postulated. However, most of this caldera was destroyed by the younger Creede caldera or covered by younger rocks.

Another problematic issue is the source of the Wason Park Tuff which, like the Mammoth Mountain Tuff, may be related to a buried or destroyed caldera. This unit also seems centered on the younger Creede caldera, and is exposed in the upper parts of the same topographic areas as the Mammoth Mountain Tuff. Yet, no caldera structure nor even indirect evidence linking this unit to caldera formation can be found (Ratte and Steven, 1967).

After formation of the Bachelor Mountain caldera, the next caldera to form in the cluster was the San Luis caldera. This caldera destroyed the northwest rim of the La Garita and the north rim of Bachelor calderas. It appears the San Luis caldera is a compound structure of two overlapping subsided blocks, an earlier and a later, which formed during eruption of the Rat Creek and Nelson Mountain Tuffs respectively (Steven and Lipman, 1976).

The youngest subsidence structure in the cluster (and in the central caldera complex) is the Creede caldera which formed in response to eruption of the Snowshoe Mountain Tuff

about 26.5 m.y. ago (Steven and Lipman, 1976). Subsidence produced a caldera 12 to 15 km wide with unstable walls 1 to 1.4 km high. These walls soon collapsed depositing talus and rockfall breccia across the caldera floor (Steven and Lipman, 1976). After collaspe, resurgent doming occurred, followed by eruption of Fisher Quartz Latite flows around the perifery of the caldera (Steven and Lipman, 1976). Resurgence of the Creede caldera caused the formation of an arcuate structural moat between the dome and caldera rim. Stream and lake sediments of the Creede Formation were deposited in the moat concurrently with eruption of the Fisher Quartz Latite (Steven and others, 1967) about 26.4 m.y. ago. A summary of age relationships and volcanic stratigraphy of the central San Juan calderas is found in Table 2.

About 2 m.y. after the Creede caldera subsided, strong local faulting occurred, probably due to the intrusion of a local stock into broken zones at the buried base of the caldera (Steven, 1972; Steven and Eaton, 1975). In north trending faults along the northern rim of the caldera, a complex fracture zone developed. The southern end of this zone cut into the Creede Formation just north and west of the present location of the town of Creede. The fracture zone was subsequently mineralized by fluids of hydrothermal-meteoric origin, an event which occurred approximately 24.6 m.y. ago (Bethke and others, 1976).

Table 2. Volcanic stratigraphy of the central San Juan Mountains

LAVAS AND SEDIMENTARY ROCKS	ASH-FLOW TUFFS (CALDERA SOURCES)	COMPOSITION	K-Ar AGE (M.Y.)
Fisher Quartz Latite and Creede Fm.		Fisher: quartz latite lavas and breccias Creede: stream, lake, tuff, travertine deposits	26.4
	Snowshoe Mtn Tuff (Creede)	Phenocryst-rich quartz latite	>26.4 <26.7
	Nelson Mtn Tuff (San Luis)	"	"
	Rat Creek Tuff	"	"
Local rhyolite, quartz latite, and andesite flows and breccias between ash-flows	Wason Park Tuff	Phenocryst-rich rhyolite	>26.4 <26.7
	Mammoth Mtn Tuff (Mammoth Mtn?)	Phenocryst-poor rhyolite to phenocryst-rich quartz latite	26.7
	Carpenter Ridge Tuff (Bachelor)	Phenocryst-poor rhyolite	>26.7 <27.8
	Fish Canyon Tuff (La Garita)	Phenocryst-rich quartz latite	27.8
Conejos Fm.		Andesite flows and breccias	>30.0 <35.0

Modified from Steven and Eaton (1975)

GEOLOGY OF THE CREEDE FORMATION

From 1977 to 1981 the International Union of Geological Sciences (IUGS) Subcommission on the Systematics of Igneous Rocks questioned geologists around the world on descriptive nomenclature of pyroclastic deposits and fragments. A classification scheme and set of recommended definitions were compiled from their results in an attempt to standardize a very confusing segment of geologic nomenclature. All lithologies mentioned in this thesis will be classified and defined according to the recommendations of this subcommittee (Appendix II).

Tuffaceous sandstones are the dominant rock type encountered throughout the Creede Formation. Numerous travertine deposits plus a few locally interbedded lentils and tongues of igneous material are also present. Both sediments and volcanics fill in the structural moat that surrounds Snowshoe Mountain on three sides (Fig. 2). Deposition of the Creede Formation is responsible for preserving the excellent topographic form of the Creede caldera. Due to burial of all but the higher parts of the dome, the moat structure remained protected from erosion and was not exposed until some of the Creede deposits were removed during Quaternary time (Steven, 1968).

AGE OF DEPOSITION

The age of the Creede Formation is now known with certainty. Along the eastern margin of the caldera, Creede Formation deposits intertongue laterally with lava flows of Fisher Quartz Latite. According to Steven and Ratte (1960; 1965), the source of the flows was from vents located in the Fisher Mountain area due south of the Creede caldera. Plagioclase, sanidine, biotite, hornblende, and glass concentrates were collected from type Fisher lavas and yeilded a mean age of 26.4 m.y. (Steven and others, 1967). Thus, this date fixes the age of the Creede Formation and the age of abundant fossil plant material found within it. The Fisher lavas were also the last flows to be erupted during the intensive period of Oligocene volcanism which formed the San Juan mountains.

STRUCTURE AND THICKNESS

Location of Creede Formation deposits is controlled by the arcuate moatlike valley representing the Creede caldera. This structure has been well preserved along the western caldera margin from just northwest of Spar City, and clockwise around the caldera to Goose Creek on the eastern caldera margin (Fig. 2). The southern part of the caldera has been entirely covered up by Fisher lava flows, and

Quaternary landslide debris or glacial drift.

Dip measurements of Creede Formation beds yeild angles ranging from five to 30 degrees. Near the center of the moat lower angle dips prevail and in most places beds are nearly horizontal. Along the caldera rim higher angle dips prevail but horizontal beds are not uncommon. Strike measurements do not all run tangential to the caldera margin, as one might expect. They reflect the paths which old stream valleys cut down the caldera wall into the moat fill.

The original thickness of the Creede Formation is not known but has been estimated by Steven and Ratte (1965) to extend over a vertical range of at least 1000 meters. The lowest exposure of Creede Formation occurs along the Rio Grande River near the mouth of Farmers Creek at an altitude of 2630 meters. Water wells drilled at ranches on the river have not yet found the bottom of the Creede Formation. It may extend from one hundred to several hundred meters below this level (Steven and Ratte, 1965). The highest exposures are found on Bachelor Mountain and on the south-facing slopes of Mammoth Mountain east of Creede. Both of these occur at 3350 meters. In all places an unknown amount of material has been eroded away.

GENERAL DESCRIPTION

The Creede Formation is composed of a variety of facies which locally are extremely diversified. Distribution of the various facies depends on local conditions of deposition and on proximity to sources of different constituent materials (Steven and Friedman, 1968). All facies present are complexly interbedded and it is impossible to separate them on a geologic map. However, for descriptive purposes the facies present can be broken into five groups: lacustrine; fluvial; breccia; and travertine and bedded carbonate rocks (Table 3).

A1. Lacustrine facies: Thin-bedded lacustrine deposits are the most common type of facies encountered in the lower lying, more centrally located portions of the Creede Formation. The lake deposits are composed of tuffaceous siltstones, tuffaceous sandstones, and air-fall tuffs. Tuffaceous siltstones and sandstones complexly interbed throughout the lacustrine facies , and all gradations between them exist. Tuffs however, have a much more restricted distribution. According to Steven and Friedman (1968) tuffs are confined to the southern parts of the caldera, while reworked tuffaceous sediments prevail in the western, northern, and eastern parts. Thus, tuffs comprise a very small portion of the lascustrine facies and of the entire Creede Formation.

Table 3. Sedimentary rocks present in the Creede Formation

A. Siltstones, sandstones, conglomerates, breccias
   1. Lacustrine facies
      a. tuffaceous siltstones
      b. tuffaceous sandstones
      c. tuffs
   2. Fluvial facies
      a. tuffaceous sandstones
      b. tuffaceous conglomerates
   3. Breccia facies (epiclastic)
      a. volcanic talus breccia
      b. water-laid breccia
      c. mudflows

B. Travertines

C. Bedded carbonates

Lacustrine tuffaceous siltstones are typically buff yellow or pale gray to white in color. They occur mostly in beds of paper thin layers with some beds up to five cm in thickness. Reworked fine grained tuffaceous material is the major constituent. In most places siltstones are extremely fissile and friable. Numerous carbonized plant remains occur along shaley partings of the paper thin variety.

Lacustrine tuffaceous sandstones are relatively fine-grained, uniform in texture, and occur in beds from approximately 1 to 30 cm in thickness. In color and composition, they are very similar to the siltstones. Yet, they differ by being thicker bedded, slightly better consolidated, and by containing less carbonized plant remains.

Pale gray to white lacustrine tuffs occur in centimeter thin layers and in beds up to five meters thick. Although overall they are not abundant, several different types of tuffs are present: air-fall tuffs; non to poorly welded ash-flow tuffs; and densely welded ash-flow tuffs. Air-fall and non to poorly welded varieties are moderately abundant, compared to welded ash-flows. Air-fall bodies occur in massive, well sorted deposits. Internally they contain many feldspar phenocrysts that are remarkably unbroken. Air-fall bodies are usually very well bedded. However, at the bentonite mine southwest of Creede and the zeolite adit southeast of Creede, alteration of pyroclastic material is

pervasive and has destroyed most bedding features.

A few thin layers of densely welded ash-flow tuffs have been noted by Steven and Ratte (1965). Ash-flow material can be distinguished from air-fall deposits in several ways: by the presence of a eutaxitic texture resulting from compaction of pumice and other vitroclasts during a welding process; by a total lack of sorting; and internally by the presence of distinctly broken up feldspar phenocrysts.

Many features exhibited by the lacustrine facies indicate shallow water deposition. Syndepositional features include abundant ripple marks, laminations, horizontal bedding, and local cut-and-fill structures. Post-depositional features include small scale slump structures and associated convoluted bedding (Plate A). Mudcracks, the best indicator of shallow water, are widespread throughout the lacustrine facies. These observations suggest the presence of many small isolated shallow ponds, instead of one large ancient lake which filled the entire moat.

A2. Fluvial Facies: Fluvial deposits of tuffaceous sandstones and tuffaceous conglomerates are the next most common facies observed in the Creede Formation. They occur in and around buried stream valleys, and are often interbedded with the sandstones and siltstones of the lacustrine facies. Both fluvial and lacustrine sandstones also complexly intergrade at most localities where they

Plate A. Small scale slump structures and associated convolute bedding. Outcrop located 2.4 km southwest of Creede on Hwy. 149.

interbed. However, the fluvial sandstones are generally coarser grained, more poorly sorted, and form relatively thicker exposures ranging from one to five meters. Fluvial conglomerates are poorly sorted, exhibit a very crude stratification, graded bedding, or a somewhat oriented fabric indicated by clasts which are joined in an imbricate fashion.

Of particular interest are the fluvial deposits found in the old stream valley extending across Bachelor Mountain to the Amythyst fault (Steven and Ratte, 1965). These are extremely poorly sorted conglomerates, breccias, or possibly mudflows containing angular to subangular clasts of pale pink rhyolite in a densely silicified fine-grained matrix. According to Steven and Ratte (1965) these rocks have been impregnated with barite and black manganese oxides, and a few beds contain valuable quantities of silver.

A3. Breccia facies: Along the caldera rim tuffaceous epiclastic volcanic breccias of several types occur: volcanic talus breccia; water-laid breccia; and mudflows. The following descriptions of these rocks are based on definitions taken from R.V. Fisher (1961).

Talus breccia are probably the most common type that were deposited into the Creede moat. A volcanic talus breccia is composed of angular volcanic fragments, with or without a matrix, formed by mass transfer in volcanic regions. In this case over-steepening of the caldera walls

caused landslides and rock avalanches to form the breccias.

Water-laid volcanic breccias are the next most common type. These contain angular to subangular volcanic rock fragments and occur in regions undergoing relatively rapid erosion by stream action. They are deposited in streams and lakes, and in this area are extremely hard to distinguish from fluvial conglomerates with which they complexly interfinger.

Mudflows have also been noted in the moat fill. These deposits contain angular to subrounded clasts of volcanic origin which were transported in a viscous slurry of volcanic ash and debris. Mudflows are more easily distinguished from the other breccias and conglomerates by several features. They form massive deposits exhibiting totally random fabrics. Yet the key distinction is that the clasts never touch and always appear to be floating in the matrix. Heavy rains and rapidly melting snow or ice, falling on, or flowing over unconsolidated ejecta is the most likely mechanism of mudflow formation in the Creede area.

Fluvial and breccia facies represent deposition under a wide variety of conditions. Completely unsorted beds containing clasts which float in a muddy matrix, represent deposition by mudflow. Poorly sorted gravels probably represent deposition by swiftly flowing water. Gravels which contain boulders up to 50 cm in diameter are probably

indicative of deposition by torrential streams (Steven and Friedman, 1968). However, mudflows are also known to carry boulders of this size. Finally, moderately sorted fluvial sandstones indicate deposition by more slowly flowing streams.

B. Travertines: Concurrent with deposition of the Creede Formation, numerous mineral springs produced and deposited large quantities of travertine. Many bodies, ranging from one meter to 300 meters in length and of unknown thickness, are somewhat randomly distributed throughout the moat. The travertine bodies tend to occur along the interior and exterior sides of the moat (Fig. 2).

According to Steven and Friedman (1968), travertine occurs in several kinds of deposits: as inclined sheetlike masses deposited along steep outer caldera walls which cement talus accumulations; as intertongued wedges, emanating from a central travertine mass which grade laterally into normal stream or lake deposits with little or no carbonate; as plug-like openings representing original spring orifices (Plate B); and as hard sedimentary strata from deposition in shallow ponds fed by mineral springs (Plate C).

Steven and Friedman (1968) have discussed in detail the possible source of the carbonate. Geologic and isotopic evidence support a model which calls upon an upwelling resurgent magma intruding a sedimentary carbonate unit below

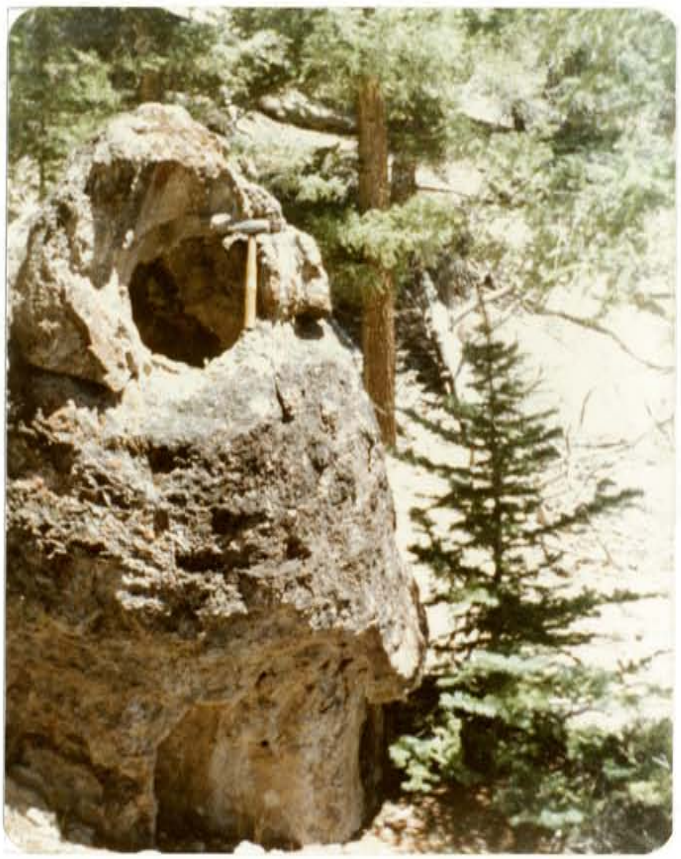

Plate B. Plug-like opening representing an original travertine spring orifice. Outcrop located at base of North Phipps stratigraphic section.

Plate C. Travertine beds occurring as hard sedimentary strata from deposition in shallow ponds fed by mineral springs. Outcrop located 10.5 meters above base of North Phipps stratigraphic section.

the San Juan volcanic field. This event remobilized the calcium carbonate by a process related to contact metamorphism or solution and replacement.

C. Bedded carbonates: Beds of limestone and limey siltstone or sandstone apparently not directly related to a travertine source occur in many places in the Creede Formation (Steven and Ratte, 1965). These beds have probably formed by evaporation in shallow ponds that contained carbonate rich waters derived from mineral springs located elsewhere. Another possible origin is that chemical changes occurring during alteration of volcanic parent rock may have also provided sufficient carbon dioxide to form carbonate minerals (Garrels and MacKenzie, 1971, p. 244).

STRATIGRAPHY AND PETROGRAPHY

LOCATION OF THE SAMPLING SITES

Two stratigraphic sections were measured in as much detail as exposure permitted (Figs. 5 and 6). One section is located on the Wason Ranch about 4.0 km southeast of Creede, Colorado on Highway # 149. From the main buildings on the ranch, the section is situated approximately 2.0 km to the southeast along the northeast bank of the Rio Grande where the river has cut through Creede Formation and left well exposed cliffs. The bottom of the section lies in the base of the NE 1/4 of the NE 1/4 of Section 9 and extends up into the NW 1/4 of the NW 1/4 of Section 10, T41N, R1E on the Creede, Colorado quadrangle (Fig. 3). Thirty-five samples were collected at this locality. The section begins at 2654 meters (12 meters above the river), and extends to an elevation of 2738 meters covering a vertical distance of approximately 84 meters.

The Wason section was chosen for its moderately good exposure along cliffs cut by the river. It represents an area from the lower lying, more centrally located portions of the moat. It was hoped that this section would represent the lacustrine facies. However, analysis of these sediments has shown the section may be approximatelty 1/3 lacustrine facies and 2/3 fluvial facies.

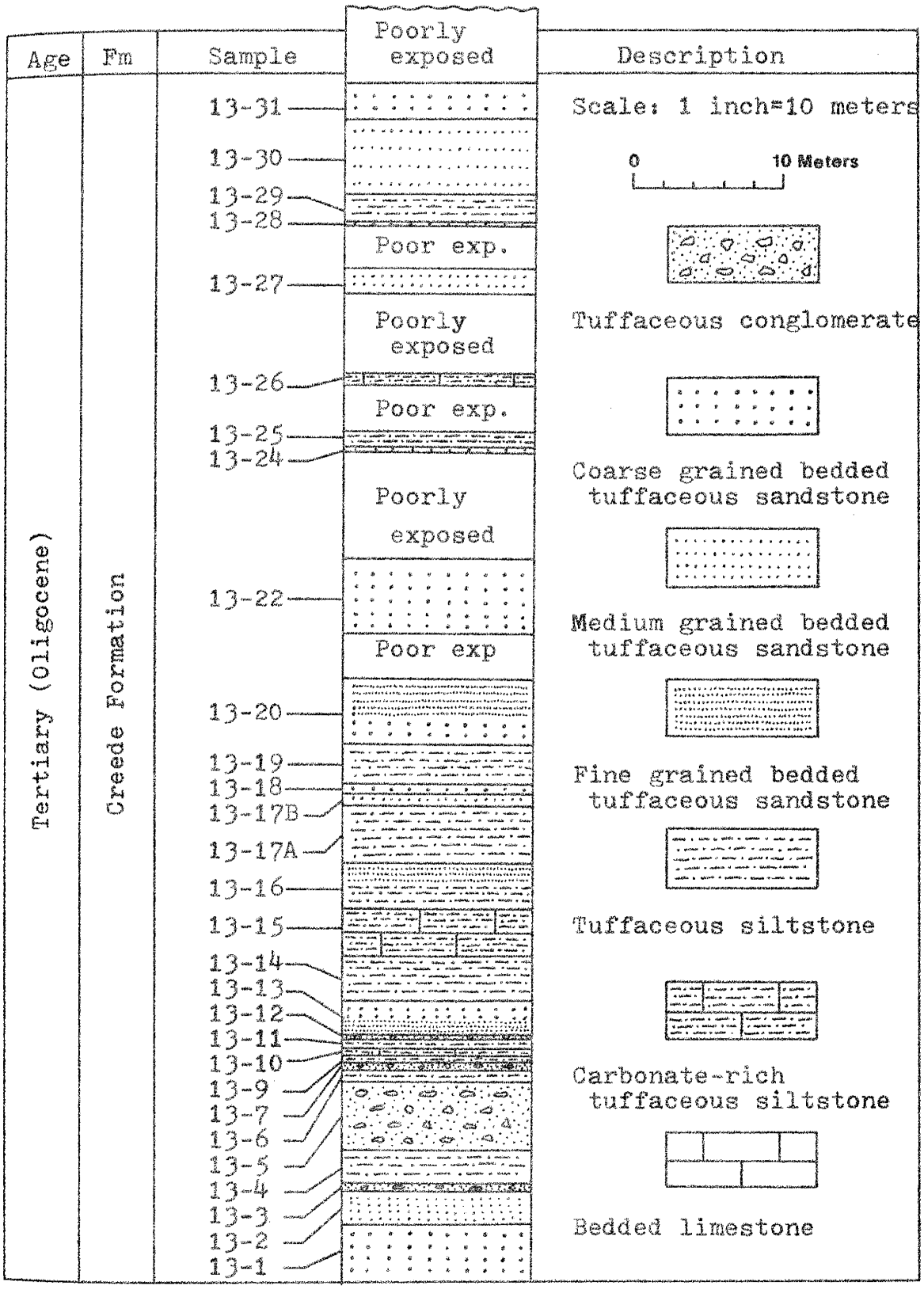

Figure 5. Wason stratigraphic section.
Total vertical thickness: 83.71 meters

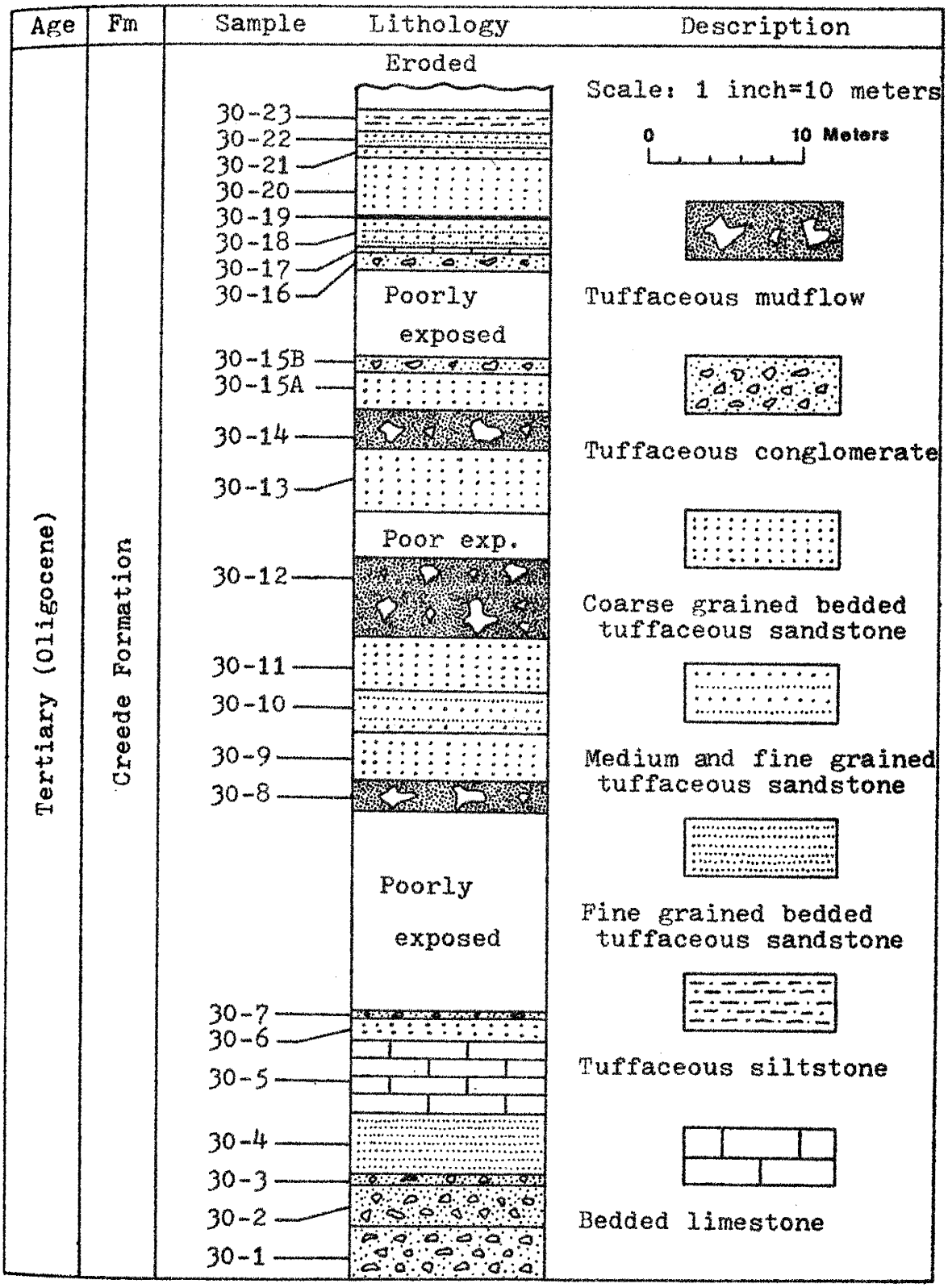

Figure 6. North Phipps stratigraphic section.
Total vertical thickness: 76.34 meters.

The other section is located 3.2 km due northwest of the main buildings on the Phipps Ranch, and is here designated the North Phipps section. It is reached by traveling along Highway # 149 to the Farmers Creek trailhead 4.4 km southeast of Creede, hiking 2.4 km east along the trail, turning south at the second major ravine encountered in Section 3 on the Creede quadrangle, and hiking 1.2 more km south along the ravine. This section lies in the W 1/2 of the SE 1/4 Section 3, T41N, R1E on the Creede, Colorado quadrangle (Fig. 3). Thirty samples were collected at this location. This section begins at 2755 meters and extends to an elevation of 2831 meters covering a vertical distance of approximately 76 meters.

The North Phipps section was chosen because it lies very near the contact between the Creede Formation and the surrounding volcanics. This section lies over what may be the approximate caldera margin at depth. Analysis of these sediments has shown the section to represent the fluvial and breccia facies deposited near the caldera rim and along the caldera sides.

PETROGRAPHIC DESCRIPTIONS

The following descriptions pertain specifically to samples collected in the Wason and North Phipps sections. All tuffaceous rocks present in these sections are reworked

pyroclastic material. They are classified according to terms defined in Appendix II for tuffites, and contain greater than 25% epiclasts and less than 75% pyroclasts. Even though these rocks are sedimentary, they have textures strongly resembling those found in extrusive igneous rocks. Many beds have well preserved vitroclastic texture and often appear porphyritic, particularly the tuffaceous siltstones. If they are classified according to a sedimentalogical classification scheme such as Folk (1957), there is no indication of the important volcanic association. For that reason the IUGS scheme is being used to ensure a given rock name is as descriptive as possible. Mineral percentages given in the text are visual estimates of thin section constituents. Thin section plate number's 1 through 20 to which the reader is referred in this section are located in Appendix III.

1. Tuffaceous Siltstones: The tuffaceous siltstones comprise 1/4 of the lithologies found in this area of the Creede Formation. Of these, more than 90% are located in the more centrally located portions of the moat and are best represented by samples from the Wason section.

Matrix material in the tuffaceous siltstones comprises 40-60% of the rock. The matrix is a mixture of unaltered glass, altered glass, devitrified glass, and optically indistinguishable siliceous material. From X-ray diffraction data, siliceous material in the matrix contains

abundant chalcedony; moderate amounts of feldspar, heulandite group zeolites, Na-montmorillonite, and illite; sometimes a small amount of gypsum; occasional traces of kaolinite; and highly varying amounts of carbonate (Fig. 7). The zeolitic material present is heulandite, clinoptilolite, and mordenite, in approximate order of abundance.

All the tuffaceous siltstones contain two distinct detrital grain sizes, the siltsize matrix, and medium sand size grains. Euhedral, unbroken feldspar laths are the most abundant type of sand size grains and comprise 20-35% of the rock. They range in size from 0.1 to 0.5 mm. Biotite flakes make up 5-15% of the rock and are about the same size as the feldspars. Quartz comprises 5-10% of the rock. Sand size grains, along with thin stringers of organic laminae and siliceous material, tend to align and produce a very finely bedded rock (Plate 1). Pumice fragments are often present (Plate 2), and are replaced by carbonate (Plate 3), or siliceous intergrowths of chalcedony, zeolites, opaline silica, tridymite, or feldspar.

Matrices are too fine grained to show any specific textures except for overall alteration and devitrification to the various siliceous materials discussed above. Optical measurements are also impossible to obtain on matrix materials due to the fine grained nature of the minerals present.

In hand specimen very thin laminations of carbonaceous

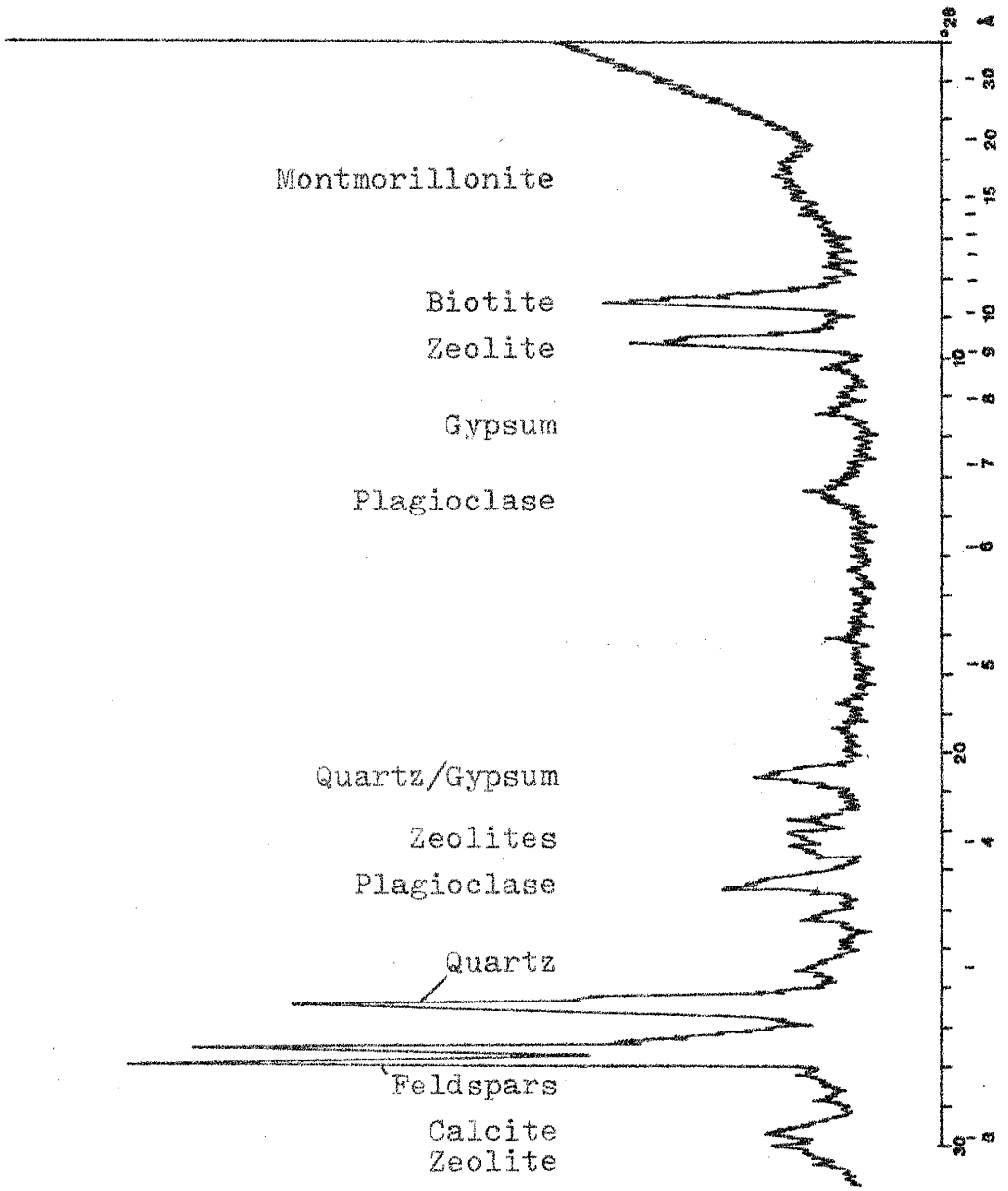

Figure 7. Whole rock X-ray diffraction pattern of a typical tuffaceous siltstone and sandstone.

material less than a millimeter thick occur in nearly all the tuffaceous siltstones. Carbonized leaf and wood imprints are found in 25% of the siltstones and are exposed along shaley partings. Without the sedimentary laminations and fossil material, these siltstones could easily be mistaken for fine ash deposits containing abundant feldspar phenocrysts, which resulted directly from volcanic activity. However, the presence of sedimentary structures confirms their reworked nature, and forces them to be classified as rocks of mixed pyroclastic-epiclastic origin.

2. Tuffaceous sandstones: The tuffaceous sandstones are by far the most abundant rock type found in the Wason and North Phipps sections. They comprise 1/2 the lithologies found in the area and are equally distributed between interior and exterior portions of the moat.

Sixty-five percent of the sandstone samples fall in the course grained size range (Plate 4). Visual estimates of mineral percentages found in thin section yeild results very similar to the tuffaceous siltstones. The sandstone matrix, however, is coarser grained and contains 35-50% fresh, altered, or devitrified glass, and optically indistinguishable siliceous material. This reduction in matrix material is accompanied by the introduction of 10-20% lithic fragments. Feldspar laths comprise approximately the same percentages as those in the siltstones, but are sometimes more broken up. Accessory minerals include

hornblende, clinopyroxene, orthopyroxene, and occasionally tiny bits of opaque iron oxide material.

In the ground mass X-ray diffration data indicates the presence of abundant silica minerals; moderate amounts of feldspar, heulandite, Na-montmorillonite, and illite; small amounts of clinoptilolite, mordenite, and celadonite; sometimes moderate to small amounts of gypsum; occasional traces of kaolinite; and highly varying quantities of carbonate (Fig. 7).

Chalcedony is the dominant variety of silica minerals present. This mineral's X-ray pattern matches that of quartz. However, quartz fragments are not abundant in thin section, and the characteristic radial structure and mossaic texture of chalcedony is frequently observed (Plate 5). Furthermore, chalcedony is commonly associated with zeolites and calcite, both of which occur in more than 85% of the samples collected. Tridymite is also present and appears in 45% of the samples in moderate or trace amounts. It is easily identified by its occurrence in pumice fragments and by its wedged shaped twins (Plate 6). Opal is found as coliform crusts (Plate 7), in veinlets, and lining cavities. Minor amounts of volcanic detrital quartz which are present can be identified by perfect dipyramidal crystal terminations indicative of their volcanic source (Plate 8).

Feldspar grains range in size from 0.5 to 2.0 mm. Plagioclase and orthoclase are the major varieties present

and occur in a 2:1 ratio respectively. A few sanidine crystals have been noted in nearly every thin section (Plate 9). Plagioclase content was determined by the Michael-Levy method and values range from An 24 to An 35. Thus, oligoclase and andesine are the dominant types of plagioclase present. Overall, plagioclase, orthoclase, and sanidine, all appear remarkably unaltered, frequently show near perfect crystal terminations, but are sometimes more broken up than feldspar laths found in the tuffaceous siltstones (Plates 9 and 10).

A wide variety of lithic fragments is present and most are chips from surrounding ash-flow sheets. This is readily evident from the distinctive eutaxitic flow and compaction textures contained in the lithic fragments (Plate 11).

The zeolites heulandite, clinoptilolite and mordenite occur in 85% of the samples collected. However, zeolitic material is only half as abundant as feldspar and silica minerals. Individual zeolite crystals are rarely seen with certainty in thin section due to their minute sizes which range from five to 30 microns. As single crystals they characteristically grow into cavities (Plate 12). As massive varieties they are present in the altered glass matrix, replacing glass shards, or filling in cavities (Plate 13 and 14) (Hay, 1966; Mariner and Surdam, 1970; Steven and Van Loenen, 1971).

Biotite grains are ubiquitous. In many samples they

are bent (Plate 15), a feature resulting from their pyrogenic origin. Calcite is present as crystal fragments, replacement material, or cement. Gypsum is found coating many joint surfaces and also occurs as cement. Hydromica was observed in sample 30-2 (Plate 16). According to Kerr (1977, p. 461) hydromica is a variety of illite which grows in irregular matted flakes that my be intercalated with flakes of montmorillonite or kaolinite.

Montmorillonite is present in at least 60% of the samples collected, illite is also found in at least 60%, and traces of kaolinite are present in at least nine samples. The usual occurrence of the clay minerals is as dark reaction rims around other grains (Plate 17), filling in fractures within grains (Plate 18), and as alteration coronas around glass shards (Plate 19).

A vitroclastic texture is well preserved in many of the sandstones. Relict glass shards are found in more than 75% of the samples (Plates 16 and 19), and vessicles are equally abundant (Plate 17).

3. Tuffaceous Conglomerates and Mudflows: Like the tuffaceous siltstones, the tuffaceous conglomerates and mudflows comprise 1/4 of the lithologies present in this area. However, in this case more than 70% of the samples are located near the caldera rim and are best represented by specimens from the North Phipps section.

Matrix comprises 25-40% of this rock type. The most

obvious change in composition between the sandstones and the conglomerates is a significant increase in lithic fragments. Tuffaceous conglomerates contain between 20 and 40% lithic fragments. Fragments range in diameter from 2.0 to 10 mm and have been seen as large as 50 cm across at one mudflow outcrop in the North Phipps section (Plate D). The fragments are angular to subrounded and elongate to subequant (Plate E). They come from the surrounding volcanics as well as from earlier segments of the Creede Formation.

As stated in an earlier section, the key distinctions between the conglomerates and the mudflows are in the nature of the clast-matrix relationships. In mudflows the clasts do not touch. They appear to float in the matrix due to deposition in a viscous slurry of volcanic ash and mud.

4. Carbonates: Calcite and variety travertine are the only carbonates found in these rocks. Some amount of carbonate is present in greater than 85% of the rocks in this area, yet the amount in each specimen is highly variable. Of that 85% carbonate, 10% occurs as individual beds of pure limestone. The rest occurs as non-descript patchy replacement material, replacing siliceous material in pumice fragments, occasionally as individual crystal fragments in matrix materials, and rarely carbonate was observed replacing a plagioclase grain (Plate 20).

Relative abundances of all lithologies and a comparison

Plate D. Mudflow outcrop located 40.2 meters above base of North Phipps stratigraphic section. Boulder at far right side of photograph is 50 cm in diameter.

Plate E. Detail of photographic Plate D.

of sandstone grain sizes discussed above are found in Tables 4 and 5 respectively. Comparative mineralogies of major minerals present in the Wason and North Phipps sections are summarized in Tables 6 and 7 respectively.

Table 4. Comparative lithologies from the Wason and North Phipps Sections

ROCK TYPE	WASON SECTION	N. PHIPPS SECTION
Siltstones	12	1
Sandstones	15	12
Conglomerates	4	5
Mudflows	0	4
Carbonates	1	2

Table 5. Comparison of tuffaceous sandstone types in the Wason and North Phipps sections

SIZE GRADE	WASON SECTION	N. PHIPPS SECTION
Fine	2	1
Fine to Medium	0	3
Medium	5	0
Medium to Coarse	0	0
Coarse	8	6
Very Coarse	0	2

Table 6. WASON SECTION: comparative mineralogy of major minerals present

SAMPLE	QTZ	TRD	PLG	KSP	HEU GRP	ILL	CAL
13-1	xx	t	xx	xx	s	s	s
13-2	xx	-	xx	xx	s	s	s
13-3	xx	t	xx	xx	s	s	s
13-4	xx	-	s	s	s	s	s
13-5	xx	-	xx	xx	s	s	s
13-6A	xx	-	s	s	s	t	s
13-6B	xx	-	s	s	s	t	s
13-7	s	-	s	s	s	-	xx
13-9	xx	-	s	s	s	t	s
13-10A	s	-	xx	xx	s	-	s
13-10B	s	-	t	t	s	-	xx
13-11	xx	-	s	s	s	t	s
13-12	s	-	xx	xx	s	s	xx
13-13A	s	s	xx	xx	s	s	s
13-13B	xx	s	s	s	s	s	s
13-14	xx	-	s	s	s	s	s
13-15	xx	-	s	s	s	s	s
13-16A	xx	-	t	t	s	s	xx
13-16B	s	s	s	s	s	s	xx
13-17A	s	s	s	s	s	s	xx
13-17B	xx	s	xx	xx	s	s	s
13-18	s	s	xx	xx	s	s	s
13-19	xx	s	s	s	s	s	s
13-20A	s	t	xx	xx	s	s	s
13-20B	s	s	xx	xx	s	s	s
13-22	s	s	xx	xx	s	s	s
13-24	s	t	xx	xx	s	s	t
13-25	s	-	t	t	t	t	xx
13-26A	s	-	t	t	t	t	xx
13-26B	s	-	t	t	-	t	xx
13-27	s	s	xx	xx	s	s	s
13-28	s	-	s	s	t	s	xx
13-29	xx	s	s	s	s	s	s
13-30	s	t	xx	xx	s	s	-
13-31	s	t	xx	xx	s	s	-

xx: dominant phase
s: significant phase
t: trace amount
-: not detectable

QTZ-quartz; TRD-tridymite;
PLG-plagioclase; KSP-K-feldspar;
HEU GRP-heulandite group zeolite;
ILL-illite; CAL-calcite.

Table 7. NORTH PHIPPS SECTION: Comparative mineralogy of major minerals present

SAMPLE	QTZ	TRD	PLG	KSP	HEU GRP	ILL	CAL
30-1	xx	s	s	s	s	s	t
30-2	xx	s	xx	xx	s	s	t
30-3	xx	t	xx	xx	s	s	s
30-4	xx	-	xx	xx	s	s	s
30-5	s	-	-	s	-	-	xx
30-6	s	-	s	s	s	t	xx
30-7	xx	t	xx	xx	s	t	t
30-8	s	t	xx	xx	-	s	-
30-9	xx	-	s	s	s	s	-
30-10A	s	xx	xx	s	s	s	-
30-10B	xx	-	s	s	s	s	t
30-10C	xx	-	xx	xx	s	s	s
30-10D	xx	t	xx	xx	s	s	-
30-10E	s	s	xx	xx	s	s	-
30-10F	xx	-	s	s	s	s	-
30-10G	xx	t	xx	xx	s	s	s
30-11	xx	t	xx	xx	s	s	xx
30-12	s	s	xx	xx	-	t	-
30-13	xx	s	xx	xx	s	s	s
30-14	s	t	xx	xx	-	t	-
30-15A	s	-	xx	xx	s	t	t
30-15B	xx	-	s	s	s	s	s
30-16	s	-	xx	xx	s	t	-
30-17	s	-	-	s	s	-	xx
30-18	s	-	xx	xx	s	s	s
30-19	s	t	xx	xx	-	t	-
30-20	s	-	xx	xx	s	s	s
30-21	xx	-	xx	xx	s	s	s
30-22	s	-	s	s	s	t	xx
30-23	s	s	s	s	s	-	xx

xx: dominant phase
s: significant phase
t: trace
-: not detectable

QTZ-quartz; TRD-tridymite;
PLG-plagioclase; KSP-K feldspar;
HEU GRP-heulandite group zeolite;
ILL-illite; CAL-calcite.

AUTHIGENIC MINERALOGY

Most parts of the Creede Formation have undergone varying degrees of diagenetic alteration to form a variety of authigenic minerals. In particular, alteration resulting in zeolitization has been widespread. Zeolitic alteration can vary considerably over short distances both laterally and vertically. Some beds show only minor amounts of zeolitization, while other beds can form extensively zeolitized, massive deposits. However, no pattern of cyclic repetition from minor to extensively zeolitized strata can be detected in the Wason and North Phipps sections.

Poorly welded to nonwelded ash-flows, ash-falls, and poorly consolidated tuffaceous sediments provide an excellent environment for alteration reactions to occur. Freely circulating meteoric waters cause unstable glassy sediments to respond very quickly to processes of diagenesis and/or low temperature hydrothermal alteration.

In the Wason and North Phipps sections tuffaceous sediments share three basic features which allow these rocks to be hosts for several types of alteration reactions. First, most beds have formed from silicic volcanic material which once contained a large amount of glass. Second, all beds, except those composed mostly of carbonate, are poorly indurated. A rare few could be considered moderately indurated. Finally, high porosity and permeability are

characteristic of sediments in this area of the Creede Formation. A necessary concequence of these features is that nearly all silicate-rich beds in the study area have undergone some amount of diagenetic alteration.

Authigenic minerals are identified by a combination of X-ray diffraction analysis and scanning electron microscopy, and by the scanning electron microscope alone. From a combination of the two methods montmorillonite, kaolinite, clinoptilolite, heulandite, mordenite, chalcedony, opal, quartz, potassium feldspar, and gypsum have been identified. With only the use of the scanning electron microscope one other authigenic mineral has been identified. Chlorite is present in very minute quantities which do not show up on X-ray diffraction patterns but can be observed with the scanning electron microscope. All scanning electron microscope plates to which the reader is referred in this section are located in Appendix IV.

1. Clay Minerals: Montmorillonite, illite, celadonite, kaolinite, and chlorite are the clay minerals which occur in this area. In thin section clay minerals form reaction rims around primary minerals or coat glass fragments and cannot be precisely identified. Under the scanning electron microscope clays can be identified quite accurately by their morphology.

Illite is present in a minimum of 60% of the samples collected. It commonly forms as an alteration product of

feldspar and biotite, both of which are abundant in these samples. On whole rock X-ray diffraction patterns it is not possible to distinguish illite from biotite. However, on X-ray patterns from the less than 13 micron size fraction, detrital biotite is not present. Illite is distinguished from montmorillonite by the presence of a strong sharp 10-A spacing and by its lack of expansion with water or other solavating agents.

Under the scanning electron microscope illite forms irregular haphazzardly oriented sheet-like flakes with very distinctive wispy fibrous terminations that often bridge large pore spaces in sediments (Scholle, 1979). Although authigenic illite morphology as described above has not been observed in these samples under the scanning electron microscope, it does not mean that the majority of illite present is detrital. Many non-descript, unidentifiable surfaces which often show strong potassium peaks with energy dispersive analysis, are commonly seen. Perhaps much of the authigenic illite is present on these unidentifiable surfaces. In addition, many small grains which form characteristic stacks of thin micaceous plates have been observed (Plate 21). Based on close proximity of volcanic source rocks for all Creede sediments, and the common occurrence of authigenic illite in volcaniclastic sediments, these grains are much too small for a detrital origin to be their most likely mechanism of formation. Authigenic illite

has also been observed forming on the edges of corroded feldspar grains (Plate 22).

Montmorillonite is present in at least 60% of the samples collected, and is represented by the Na variety. Identification of montmorillonite is based on the fact that glycolation swells the basal spacing from approximately 12-A to 17 or 18-A . Heating to 350^{o}C causes collapse back to a mica structure at slightly less than 10-A (Fig. 8). Ten samples were analysed for clay material present in the less than 2 micron fraction. All samples were found to contain only the Na variety of montmorillonite.

Under the scanning electron microscope montmorillonite occurs in highly crenulated, honeycombed, interlocking crystals which pervasively cover surfaces (Plates 23, 24, and 25) (Scholle, 1979). Montmorillonite is less frequently reported forming irregular wavy plates or sheets with a highly swirled texture. These structures would represent relict eutaxitic structure composed of fused glass shards from ash-flow tuffs (Scholle, 1979).

Very small amounts of kaolinite are detectable in four diffraction patterns on samples from the North Phipps section and in five specimens from the Wason section studied with the scanning electron microscope. With X-ray diffraction, kaolinite is identified by a 7-A reflection which is destroyed after heating to 550^{o}C. Under the

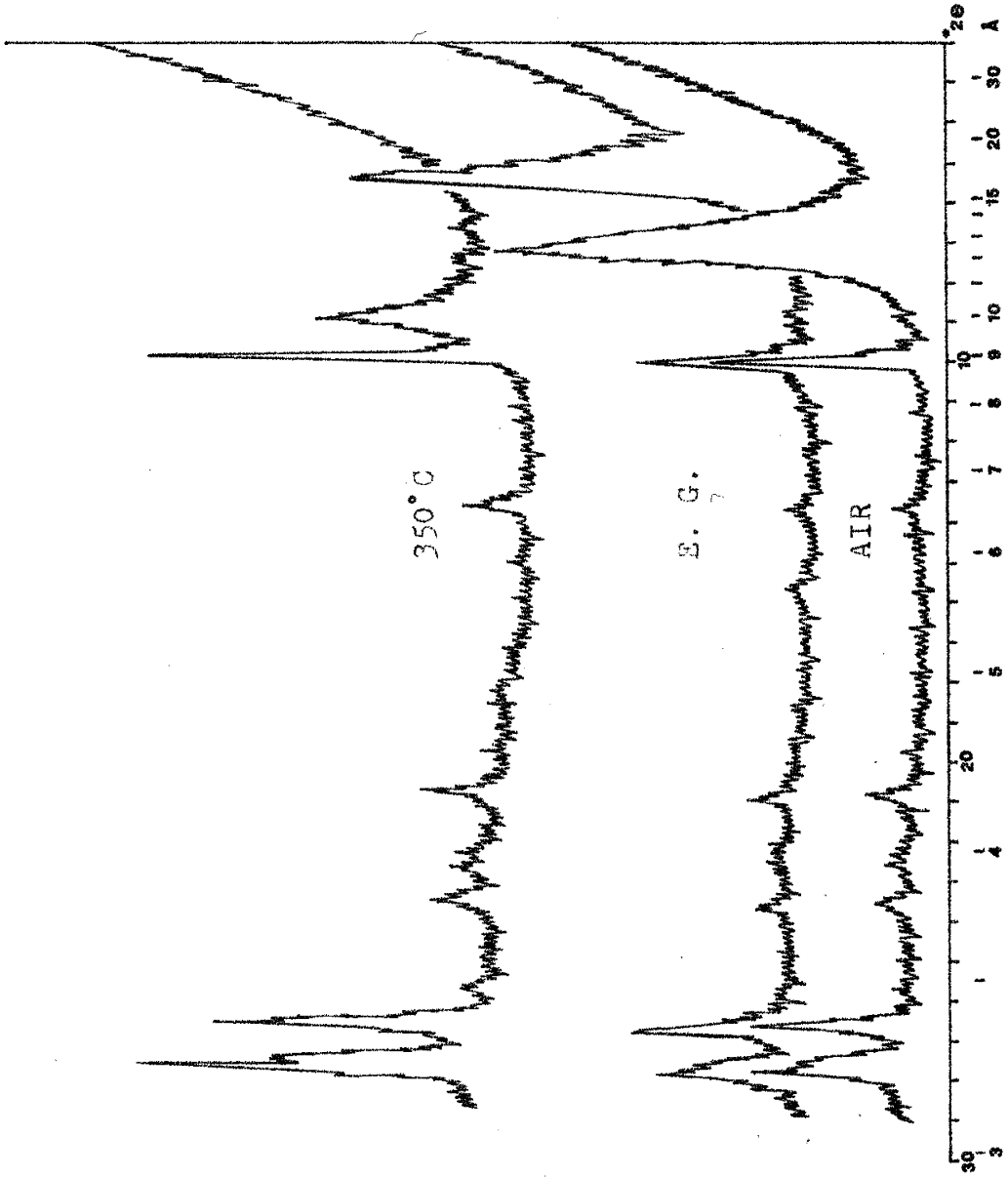

Figure 8. Na-montmorillonite clay patterns.

scanning electron microscope kaolinite forms distinctly well developed pseudohexagonal basal scales, between five and ten microns in diameter (Plates 26 and 27) (Keller,1976; Scholle, 1979).

Celadonite, a dioctahedral mica group clay mineral, is present in small quantities in 30% of the samples and in trace amounts in 20%. According to Barrows (1980), tuffs of more silicic compositions corresponding approximately to rhyolites or quartz latites, produce authigenic clay minerals from both the montmorillonite and celadonite groups. Whole rock chemical analyses indicate the average silica compositions to be 61.76% (mode=63.00%) and 61.18% (mode=65.00%) for the Wason and North Phipps sections respectively. These values suggest the rocks are silicic enough to form celadonite in addition to montmorillonite, and X-ray diffraction analysis confirms this. The most intense celadonite peak at 2.58-A is not masked by any other mineral in these samples, and where present it is a positive identification of celadonite (Fig. 9).

From the scanning electron microscope study it appears that minute amounts of chlorite are present. Under the microscope the most common chlorite habit observed is in clusters, rosettes, or spherules of extremely thin individual clay plates (Plate 28) (Scholle, 1979). The rosettes range in diameter from five to ten microns. These structures were observed in five specimens. However, no

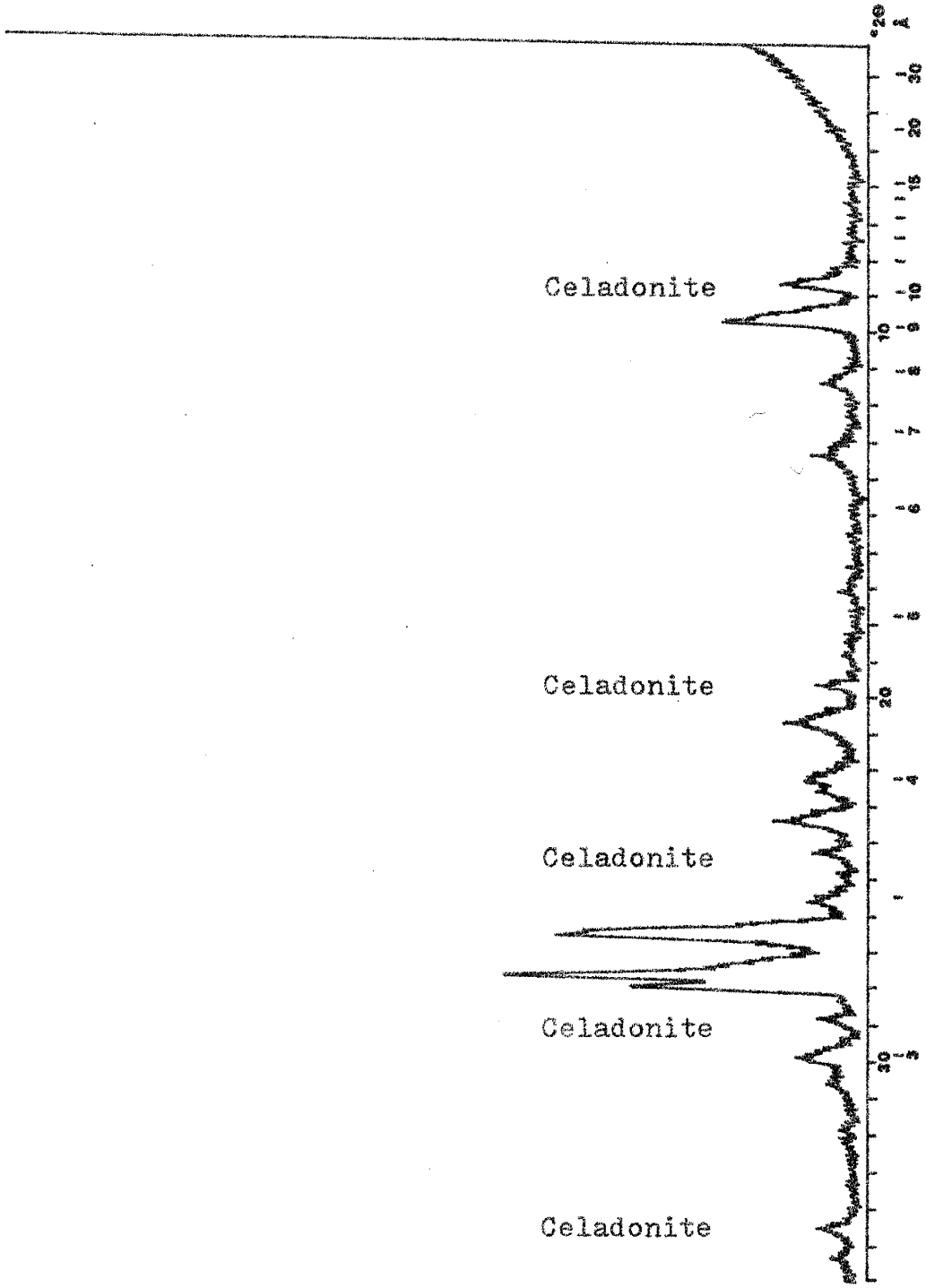

Figure 9. Whole rock X-ray diffraction pattern indicating minor amounts of celadonite present.

evidence for chlorite is present on X-ray patterns. Through X-ray diffraction analysis chlorite is identified by a strong reflection near 14-A which remains unaffected by any solavating process and is not destroyed by heating to either 350°C or to 550°C. Such properties were not observed in any of these samples. The 7-A reflection mentioned above and identified as kaolinite was not mistaken for a 7-A chlorite because the 7-A kaolinite peak was destroyed by heating to 550°C.

2. Zeolites: Clinoptilolite, heulandite, and mordenite are present in the altered tuffs of the Wason and North Phipps sections. All occur as cryptocrystalline aggregates complexly intergrown with other authigenic minerals, replacing glass shards or pumice fragments, as matrix material, or as precipitates lining cavities and growing into voids.

Most of the zeolites identified in these samples belong to the heulandite crystal chemistry group of zeolites. Within this group a heulandite solid-solution series exists between a Ca-rich end member, pure heulandite, and a K-rich end member, pure clinoptilolite (Boles, 1972). Boles (1972) has reported the Si/Al ratio increases from 2.9 to 5.1 between heulandite and clinoptilolite respectively. Boles (1972) has proposed the following classification of zeolites in the heulandite solid-solution series: those minerals with Si/Al ratios less than 3.5 are pure heulandites; those

between 3.5 and 4.0 are Si-rich heulandites; those between 4.0 and 4.5 are Si-poor clinoptilolites; and those greater than 4.5 are pure clinoptilolites.

X-ray diffraction patterns for heulandite and clinoptilolite are virtually identical. Therefore, when a Si/Al ratio cannot be obtained, thermal stability tests must be used to determine which type of heulandite group zeolite is present on a given diffractogram. Thermal stability tests indicate that 85% of the heulandite group zeolites present in these samples are heulandite (Fig. 10).

All samples were heated for 16 hours at 450°C and X-rayed immediately. Heating powdered heulandite at 260°C for 4 hours causes structural contraction of the 020 spacing; heating at 450°C for 16 hours causes this spacing to collapse; the clinoptilolite 020 spacing remains unaffected through these treatments (Munpton, 1960; Merkle and Slaughter, 1968; Alietti, 1972; Boles, 1972). Clinoptilolite 020 peaks remained after heating in only 15% of the samples from this study area (Fig. 11).

The presence of both heulandite and clinoptilolite is further substantiated with evidence from the scanning electron microscope. Plates 29 and 30 show their characteristic monoclinic symmetry and wafer-thin, coffin-like morphology. In most plates it appears that heulandite and clinoptilolite are complexly intergrown with authigenic potassium feldspar.

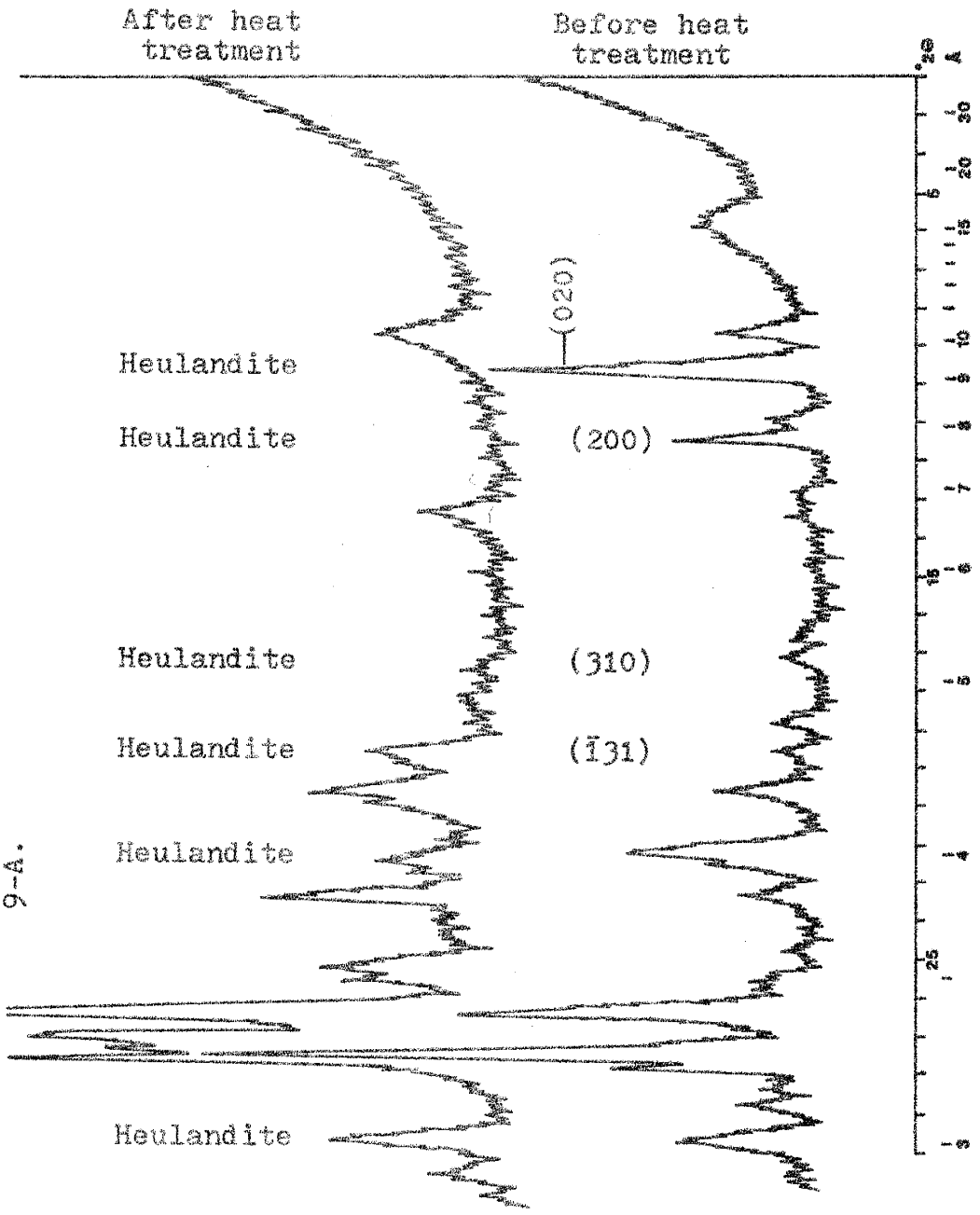

Figure 10. Whole rock X-ray diffraction pattern showing heulandite before and after heat treatment. Note the destruction of the (020) spacing at 9-Å.

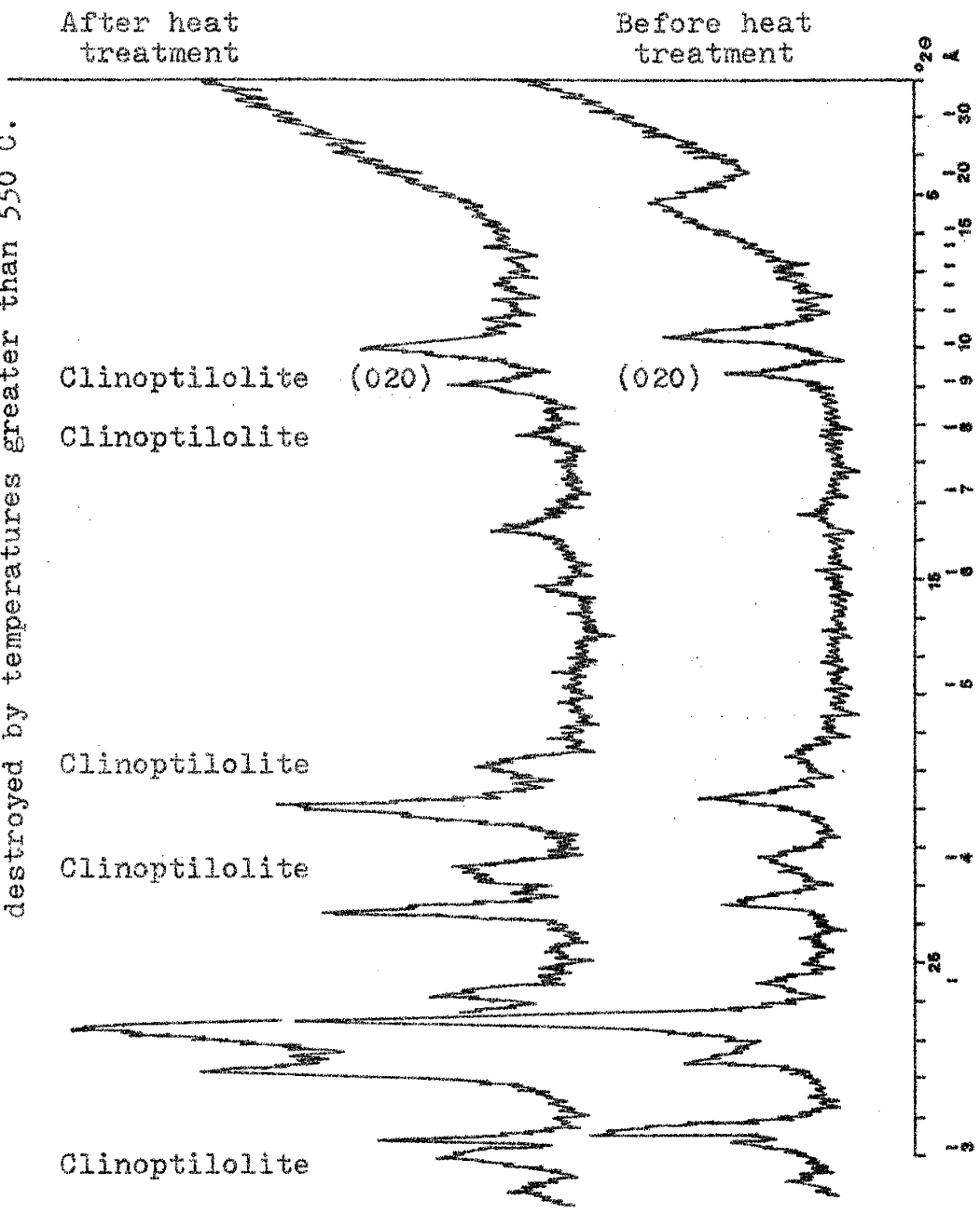

Figure 11. Whole rock X-ray diffraction pattern showing clinoptilolite before and after heat treatment. Note the (020) spacing at 9-A is not destroyed by temperatures greater than 550 C.

The heulandite group zeolites are distinguished from authigenic potassium feldspar by a different shaped lath and by a lack of abundant cleavage traces. Clinoptilolite and heulandite laths are very slender, ranging from 1-5 microns in width and from 10-30 microns in length. The zeolite crystal surfaces are remarkably unmarred. Potassium feldspar crystals occur as stubby prismatic, domed laths which range from 20-30 microns in length and 10-20 microns in width. They often show small, slightly angled, step-like cleavage indentations (Scholle, 1979), and sometimes crystals twinned according to the Carlsbad law can be observed. Extremely perfect crystal morphology occurring in such minute sizes strongly suggests an authigenic origin for both the zeolites and potassium feldspar.

Mordenite may be present in as many as 75% of the rocks but cannot be conclusively identified by X-ray data alone. Where present it occurs in minor quantities and the diffraction pattern is consequently very weak. The four most intense reflections and most of minor ones are all masked by heulandite, clinoptilolite, quartz, and feldspar peaks. However, scanning electron microscope photographs confirm its presence.

Mordenite is a fibrous zeolite very commonly associated with clinoptilolite due to their similar chemical composition and requirements for crystallization. Mordenite occurs as thin, curved, haphazzardly oriented hair-like

masses, highly oriented radiating fibrous clusters, or as single acicular crystals. Plates 31 and 32 very clearly show these habits respectively. Length width ratios of mordenite fibers have been determined by Mumpton and Ormsby (1978) to average 100 or more. Therefore, the diameter of a single mordenite fiber is on the order of a few tenths of a micron.

Mordenite can easily be misidentified for the zeolite erionite which grows in very similar habits. However, two factors establish that in these samples mordenite has been correctly identified. Erionite and mordenite rarely occur together. Erionite is a low silica zeolite and its precipitation is favored only in a low silica environment. Thus, if either erionite or mordenite can be detected in an X-ray pattern, the likelihood that both minerals would be present in the same sample is very slim. Secondly, according to Mumpton and Ormsby (1976) erionite fibers are thin but not as thin as mordenite, and in many cases a hexagonal symmetry can be detected if the crystal is properly oriented. Mordenite is orthorhombic and has rarely been reported thick enough to see the crystal symmetry. All fibrous crystals observed in these samples are much too thin to observe any crystal symmetry.

3. Silica Minerals: Silica minerals are present in greater than 95% of the samples collected, and in half of them a silica mineral is the dominant phase (Table 5).

Based on a common association with zeolites and a characteristic occurrence as a secondary mineral filling voids and forming cementing material, the finely crystalline variety chalcedony is the dominant authigenic silica mineral present. Opal is also frequently observed. It is most commonly reported as the silica mineral which in combination with clinoptilolite replaces glass shards (Hay, 1966; Mariner and Surdam, 1970; Steven and Van Loenen, 1971). Authigenic quartz as individual crystals has not been positively identified in these samples under the scanning electron microscope. If present, they should be easily recognized by smooth, partially interlocking, extremely well formed crystal faces (Scholle, 1979).

In the Wason section altered tuffaceous sediments form resistant cliffs. This may be attributable to the presence of a silica mineral(s) as the dominant phase. In particular, the lower 1/3 of the Wason section forms cliffs. Table 5 correspondingly indicates that in the lower 30 meters of section a silica mineral is the dominant phase in 66% of the rocks. Upper portions of the section form rounded, knobby, gentle slopes and Table 5 indicates that often, much less resistant feldspar minerals are the dominant phase.

4. Potassium Feldspar: Alkali feldspar is present in more than 90% of the samples collected. Although primary crystals of alkali feldspar are seen in most thin sections,

where detectable they are often outnumbered two to one by plagioclase crystals. However, on the X-ray patterns relative abundances of the two feldspars as suggested by peak intensities are approximately equal. Thus, cryptocrystalline, authigenic potassium feldspar must be present in the siliceous groundmass or less likely in the cementing material to explain this phenomena.

Size fractionation studies provide the most concrete evidence that authigenic potassium feldspar is present. In 17 of 20 samples on which size fractionation studies were performed, authigenic potassium feldspar can clearly be identified. X-ray diffraction patterns for authigenic potassium feldspar are only slightly different from those patterns for igneous potassium feldspar (Fig. 12). When used alone to identify authigenic potassium feldspar, whole rock X-ray diffraction patterns are not conclusive. Size fractionation data must be considered for a positive identification. The presence of authigenic potassium feldspar is not evident until the larger detrital feldspar grains are removed.

The pattern used to aid in the identification of authigenic potassium feldspar present in these samples is taken from Sheppard and Gude (1969). Authigenic potassium feldspar appears to be most abundant in the 13 through 9 micron size range. Figure 13 shows a typical diffraction pattern from this size range obtained by gravity settling.

Figure 12. Comparison of primary and authigenic potassium feldspar X-ray diffraction patterns.

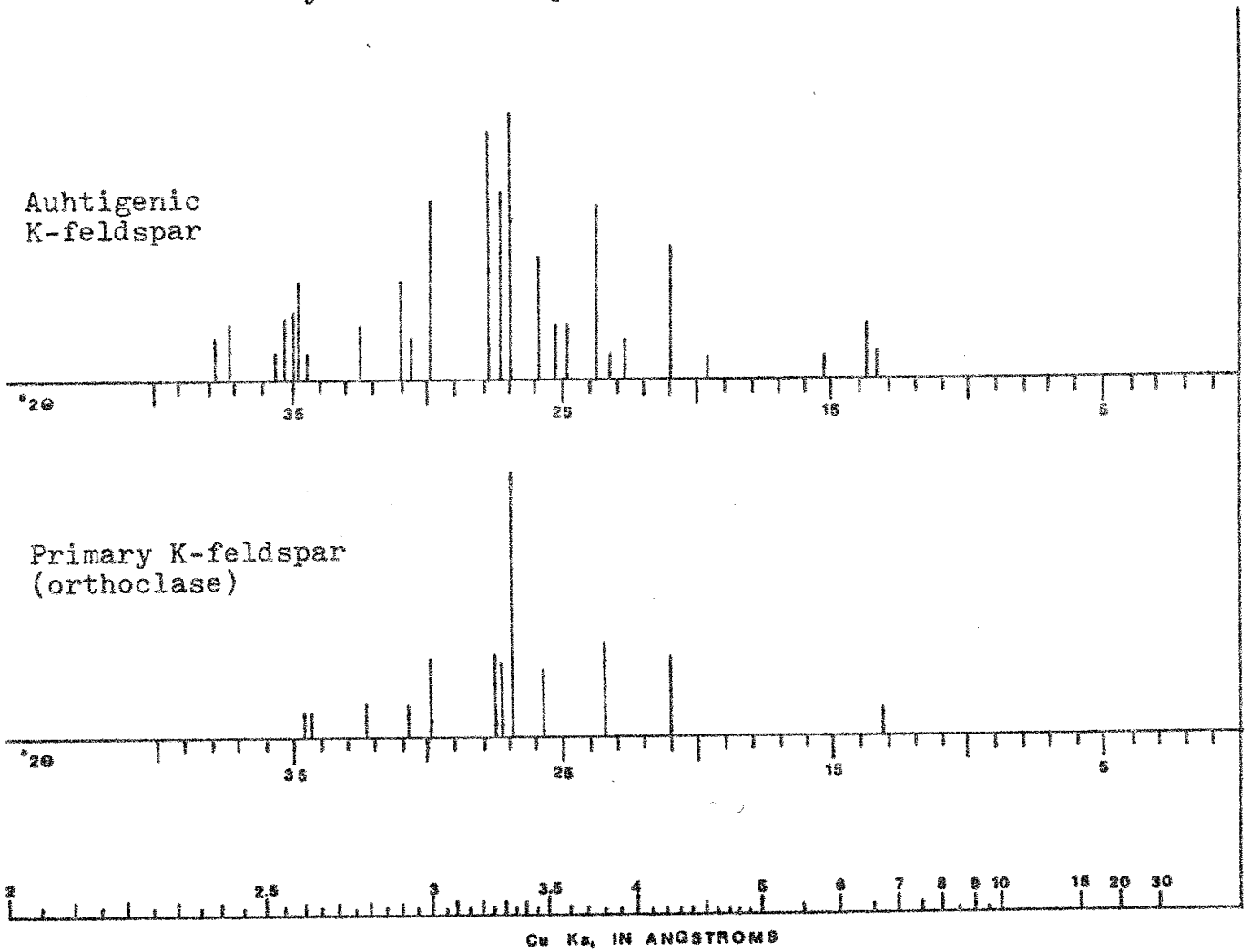

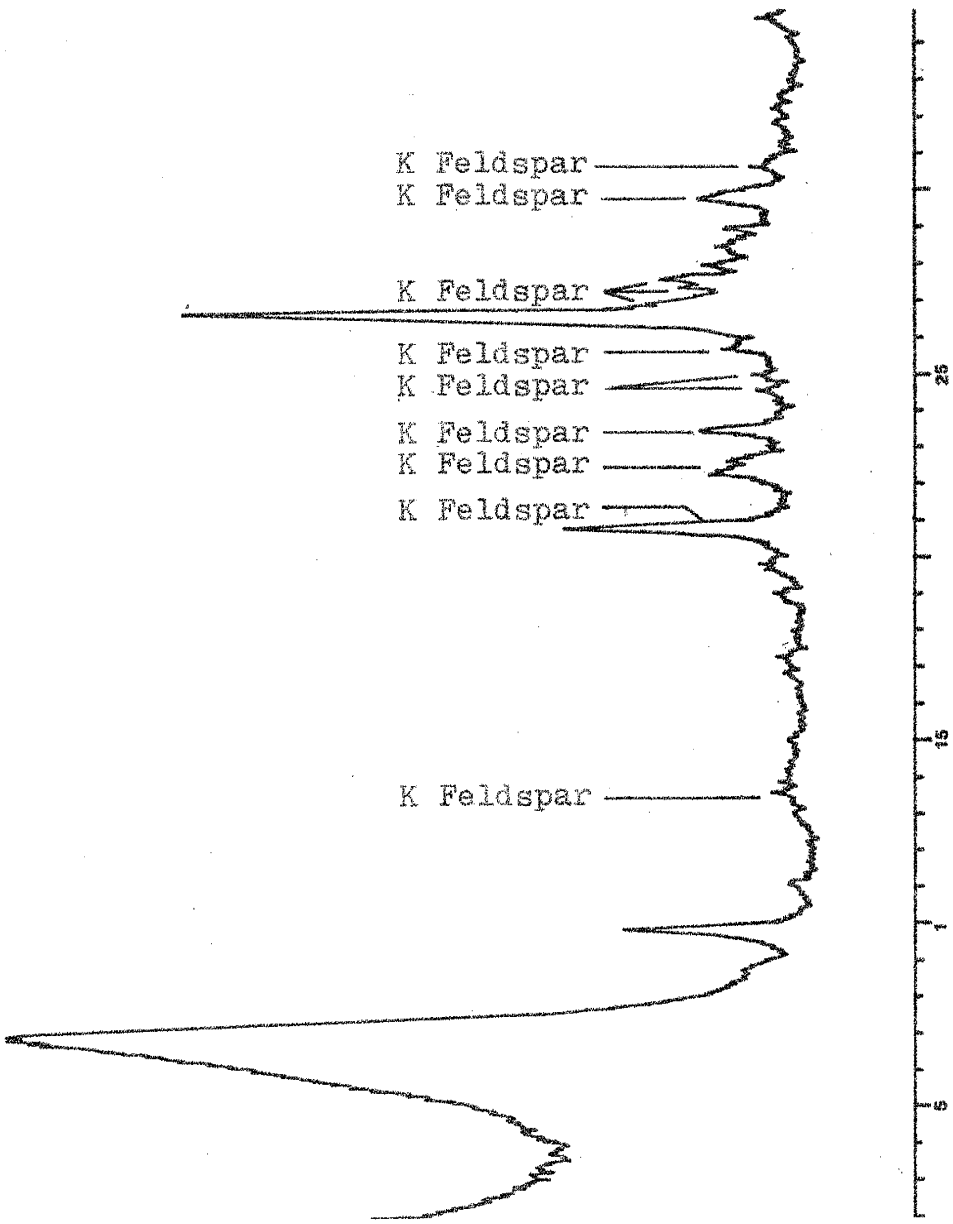

Figure 13. Authigenic potassium feldspar X-ray diffraction pattern of the less than 13 micron fraction.

Authigenic potassium feldspar was observed with the scanning electron microscope in ten other samples not chosen for size fractionation studies. Thus, it is probably present in highly varying quantities in a minimum of 50% of all samples collected in the Wason and North Phipps sections. Plates 33 and 34 show the most common habit of stubby prisms which occur in these samples. Plate 35 shows a well developed crystal with characteristic orthoclase crystal form. Frequently authigenic potassium feldspar is complexly intergrown with clinoptilolite and heulandite laths as discussed above (see photos listed for clinoptilolite and heulandite). Like the zeolites, the euhedral nature and minute size of all crystals in these photographs strongly suggest an authigenic origin for potassium feldspar in this size range also.

The presence of authigenic gypsum has been observed under the scanning electron microscope. Plate 36 shows a monoclinic tabular crystal that strongly resembles the variety selenite. In outcrop secondary gypsum coats joint surfaces where exposures form cliffs and many rocks impart a strong sulfur smell when struck with a hammer. Thus, gypsum is probably present as cementing material also, and its presence is clearly confirmed on numerous X-ray patterns in moderate to minor amounts.

In summary, data from size fractionation studies support the presence of authigenic montmorillonite,

heulandite, clinoptilolite, silica minerals, and potassium feldspar. A mica group clay (illite +/- celadonite) was also present in all size fractions prepared. Montmorillonite reflections are strongest in the less than five micron fraction. Heulandite and clinoptilolite reflections are strongest in the less than 13 through 5 micron size range. Potassium feldspar appears most abundant in the less than 13 through 9 micron size fraction. Opal is present in minor quantities through all the size ranges examined by size fractionation studies.

WHOLE ROCK CHEMISTRY

Eight major element oxide compositions are listed in Tables 8 and 9 for all silicate-rich samples collected in the Wason and North Phipps sections respectively. They are listed by rock types because it is not valid to compare sedimentary rocks of different grain sizes. According to Garrels and Mackenzie (1971), chemical compositions of sandstones and shales are related to grain size and, in general, % SiO_2 tends to decrease with decreasing grain size while, Al_2O_3, K_2O, and Fe oxides tend to increase. Table 10 contains average weight percents of the eight major element oxides for each rock type in the Wason and North Phipps sections. Examination of Table 10 indicates that overall the siltstones, sandstones, and conglomerates follow this compositional behavoir pattern. However, the mudflows do not follow this pattern. Although the mudflows are the coarsest grained rock type represented here, their compositional trend behaves more like a fine grained sediment. This can be explained by the fact that the mudflows are deposited in a viscous slurry of fine grained volcanic ash. Mudflow compositions indicate that the amount of matrix material must significantly outweigh the amount of clast material. The % SiO_2 is substantially lower than all other rock types while % Al_2O_3 and K_2O are higher.

SiO_2 and Al_2O_3 are the most abundant oxides present.

Table 8. WASON RANCH SECTION: Whole rock chemistry of silicate-rich samples (wt. %)

	SiO_2	Al_2O_3	TOTAL FE AS Fe_2O_3	MgO	CaO	Na_2O	K_2O	TiO_2	TOTAL
Tuffaceous Siltstones									
4	60.70	9.99	1.49	1.10	0.90	0.51	4.09	1.5	80.27
6A	60.99	12.24	1.09	0.91	2.38	0.76	4.82	.50	83.69
6B	60.94	12.43	2.81	1.42	4.71	1.10	4.51	.38	88.32
9	58.28	8.91	1.55	1.18	0.55	0.38	2.83	.53	74.20
10A	60.10	13.84	2.41	1.37	2.39	1.05	2.98	2.4	86.56
11	66.48	9.75	1.17	1.22	0.85	0.67	3.08	.40	83.61
13A	59.09	14.22	1.71	1.35	3.09	1.05	3.39	.52	84.41
13B	58.46	13.68	1.58	1.75	2.69	0.71	3.49	.50	82.85
14	59.67	13.40	1.07	1.41	2.06	0.70	4.20	.48	82.99
15	59.34	13.35	1.88	1.59	1.89	0.82	4.61	.48	83.97
17A	65.69	11.20	1.95	1.10	8.29	0.85	3.73	.38	93.20
19	68.78	8.25	2.99	0.96	3.19	0.93	3.10	.42	88.63
29	63.82	11.01	1.64	1.23	1.74	1.01	4.16	.49	85.10
Tuffaceous sandstones									
1	59.60	14.45	3.18	1.24	2.50	2.09	3.10	.65	86.79
2	60.52	13.22	2.32	1.25	2.01	1.44	3.08	.52	84.35
16B	70.63	9.41	1.36	0.94	12.51	0.83	3.35	.30	99.32
17B	60.39	12.34	3.40	1.43	2.45	0.70	3.11	.51	84.34
18	59.05	13.93	2.92	1.50	4.55	1.89	2.64	.59	87.08
20A	59.88	13.39	3.53	1.55	3.10	1.62	2.91	.61	86.60
20B	61.34	13.35	2.08	1.56	3.02	1.57	2.90	.56	86.37
22	62.27	12.92	5.11	0.91	3.15	2.18	2.27	.46	89.26
24	61.66	13.74	2.77	1.23	3.28	2.30	2.44	.53	87.96
27	61.67	12.65	1.30	1.50	2.66	0.98	3.25	.59	84.61
30	60.67	13.46	2.72	1.46	2.84	1.16	3.42	.59	86.34
31	59.92	14.40	4.24	1.57	3.57	1.89	2.69	.71	89.00
Tuffaceous Conglomerates									
3	62.64	11.51	1.77	0.78	1.33	1.67	4.28	.42	84.40
5	62.16	11.80	1.75	0.49	2.68	1.25	4.05	.40	84.58
12	66.45	10.60	1.79	0.48	12.33	1.43	3.51	.26	96.84

Table 9. NORTH PHIPPS SECTION: Whole rock chemistry of silicate-rich samples (wt. %)

	SiO_2	Al_2O_3	TOTAL FE AS Fe_2O_3	MgO	CaO	Na_2O	K_2O	TiO_2	TOTAL
Tuffaceous Sandstones									
4	65.65	12.13	0.74	1.00	3.33	1.24	2.20	.33	86.63
9	59.11	15.09	2.76	0.97	2.32	1.83	3.55	.53	86.15
10A	59.43	14.43	2.54	1.21	2.86	1.83	3.34	.47	86.11
10B	65.00	12.14	2.72	1.10	2.68	1.02	2.10	.42	87.18
10C	64.37	12.45	2.68	0.89	2.46	1.57	2.93	.42	87.77
10D	64.24	12.63	2.41	1.09	2.89	1.24	2.29	.42	87.21
10E	57.40	15.13	3.09	1.39	3.49	1.76	3.34	.61	86.22
10F	64.64	12.00	2.81	1.11	2.83	1.08	2.19	.40	87.06
10G	58.23	16.65	1.97	1.31	3.47	2.19	3.02	.72	87.56
11	64.48	12.44	2 56	0.87	8.66	1.63	2.81	.42	93.86
13	57.39	15.26	4.20	0.91	2.42	2.11	3.83	.78	86.89
15A	59.35	12.34	4.29	1.23	2.98	1.99	2.94	1.0	86.13
18	56.74	16.13	2.49	1.51	2.98	1.96	2.96	.55	85.32
19	58.14	14.72	1.90	0.12	3.14	3.37	6.25	.41	88.06
20	66.34	12.11	1.75	1.01	10.46	1.06	2.06	.34	95.14
21	62.88	14.17	2.23	1.11	8.66	1.44	2.60	.41	93.49
Tuffaceous Conglomerates									
1	64.78	12.16	1.16	0.77	2.24	2.03	3.30	.43	86.88
2	64.24	12.90	1.17	0.42	2.62	2.39	3.71	.35	87.80
3	61.72	13.43	1.98	0.48	2.28	2.35	4.78	.39	87.42
7	64.31	12.62	1.01	0.48	2.27	2.33	3.91	.50	87.43
15B	64.62	11.75	2.00	1.13	2.51	1.01	2.22	.51	85.76
16	58.51	15.08	4.01	0.74	2.17	2.33	3.79	.80	87.43
Tuffaceous Mudflows									
8	55.09	17.14	1.71	0.12	1.00	4.07	6.48	.44	86.04
12	55.90	16.46	1.78	0.22	1.01	3.95	6.21	.46	85.99
14	56.83	15.88	1.97	0.23	1.22	3.75	5.80	.44	86.13

Table 10. Average % SiO_2, Al_2O_3, Fe_2O_3, and K_2O for each rock type represented in the Wason and North Phipps sections (wt. %)

		SILTSTONES	SANDSTONES	CONGLOMERATES	MUDFLOWS
SiO_2	WS	61.72	61.47	63.75	
	NPS		61.27	63.03	57.27
Al_2O_3	WS	11.71	13.11	11.30	
	NPS		13.74	12.99	16.49
Fe_2O_3	WS	1.80	2.91	1.77	
	NPS		2.57	1.89	1.82
K_2O	WS	3.77	2.93	3.95	
	NPS		2.97	3.62	6.16

(Note: WS=Wason Section; NPS=North Phipps Section)

The average % SiO_2 for each section reflectes a dominantly quartz-latitic source. MgO and TiO_2 are the least abundant major oxides and are most likely present in clay minerals along with Fe oxides and Na_2O. Their minor presence reflects the small amount of clay occurring overall in the study area. The average amounts of Na_2O present are low and not enough to suggest the presence of abundant evaporites or Na-rich zeolites. Since all clay analyses indicate that Na-montmorillonite is the dominant variety of smectite clay present, some of the Na_2O is present in this clay. The rest is probably contained in abundant plagioclase grains present which have an average An content of approximately 30.

Weight percents of K_2O and CaO relative to Na_2O are particularly important because they reflect the feldspar and zeolite compositions. Although petrographic studies nindicate that plagioclase grains are more abundant than potassium feldspar grains, petrography cannot be used to determine what minerals are present in the fine grained matrix. In all rocks studied, weight % K_2O and CaO are consistantly greater than weight % Na_2O through approximately 160 vertical meters of measured section. This compositional relationship suggests that authigenic potassium feldspar and a K-Ca-rich zeolite variety occur in the groundmass. The presence of these minerals is well documented with X-ray diffraction analyses and scanning electron microscope studies.

Table 11 contains the average overall composition of each major element oxide in the two measured sections. In this table mean calculations are not divided into rock types. For comparison, means of the major element chemistry for the three youngest tuffs in the Creede area, and of the Fisher Quartz Latite which was erupted concurrently with Creede Formation sedimentation, are also included in Table 11. According to Steven and Eaton (1975), following subsidence, resurgence, and moat filling, Snowshoe Mountain Tuff, Nelson Mountain Tuff, and Rat Creek Tuff were all exposed on the north side of the moat above the topographic wall of the caldera rim. On the south side Fisher Quartz Latite was exposed. Although Creede Formation sediments are derived from numerous surrounding tuffs, the Fisher Quartz Latite and the three youngest tuffs have probably contributed significantly more material to the Creede sediments than the older tuffs of the area due to their paleotopographic position above the caldera rim.

Between the Wason and North Phipps sections, % SiO_2 generally decreases with progressively younger beds. Although this decrease is minute compared to the decreasing trend found among all the ash flows and volcanic rocks associated with the Creede caldera, it still reflects the general trend of the central San Juan calderas. According to Ratte and Steven (1967), the Creede caldera sequence shows a change with time from alkali-rich rhyolites to

Table 11. Means of major element compositions for the Wason section, North Phipps section, Fisher Qtz L., Nelson Mtn. Qtz L., Rat Creek Qtz L., and Snowshoe Mtn. Qtz L.

	SiO_2	Al_2O_3	TOTAL FE AS Fe_2O_3	MgO	CaO	Na_2O	K_2O	TiO_2
Wason Section	62.91	12.27	2.27	1.23	3.45	1.20	3.43	0.60
N. Phipps Section	61.18	13.89	2.32	0.85	3.32	2.06	3.54	0.50
Fisher Qtz L.	62.96	15.93	5.07	1.77	4.33	3.58	3.96	0.78
Nelson Mtn Qtz L.	64.97	15.57	5.06	1.45	4.29	3.53	3.82	0.58
Rat Creek Qtz L.	66.42	14.39	3.78	1.11	2.96	2.99	3.79	0.49
Snowshoe Mtn Qtz L.	63.37	15.65	4.17	1.13	3.21	3.46	4.04	0.56

Note: Averages for the quartz latite tuffs are taken from data in Ratte and Steven (1967). Qtz L.=Quartz Latite

quartz latites and rhyodacites.

In weight % SiO_2 the Wason and North Phipps sections most closely reflect the Fisher Quartz Latite. However, Figure 14B indicates a possible bimodal distribution in % SiO_2 for the North Phipps section. The higher SiO_2 values are generally present in the younger tuffaceous sandstone beds of that section and may reflect a lesser degree of leaching and alteration caused by groundwaters.

If the four volcanic units mentioned above are the dominant sources of the Creede sediments, then some other trends can also be noted: Si, Al, Fe, and Na are all present in lower quantities in the volcaniclastics compared to the source rocks; and Mg, Ca, K, and Ti all remain relatively constant. Al is usually found to behave as an immobile component. However, based on quantitative electron microprobe studies between fresh glass and its surrounding alteration products, Al has been reported as a mobile component in this type of environment by several investigators (Robinson, 1966; Barrows, 1980).

Of particular interest are the chemical compositions of heulandite, clinoptilolite, and mordenite, all of which occur complexly intergrown with other authigenic silicates. No zeolite crystals large enough to be studied individually have been found, and attempts to separate zeolites from other minerals were unsuccessful. Therefore, no chemical analyses of only the zeolite minerals have yet been

A. Wason section

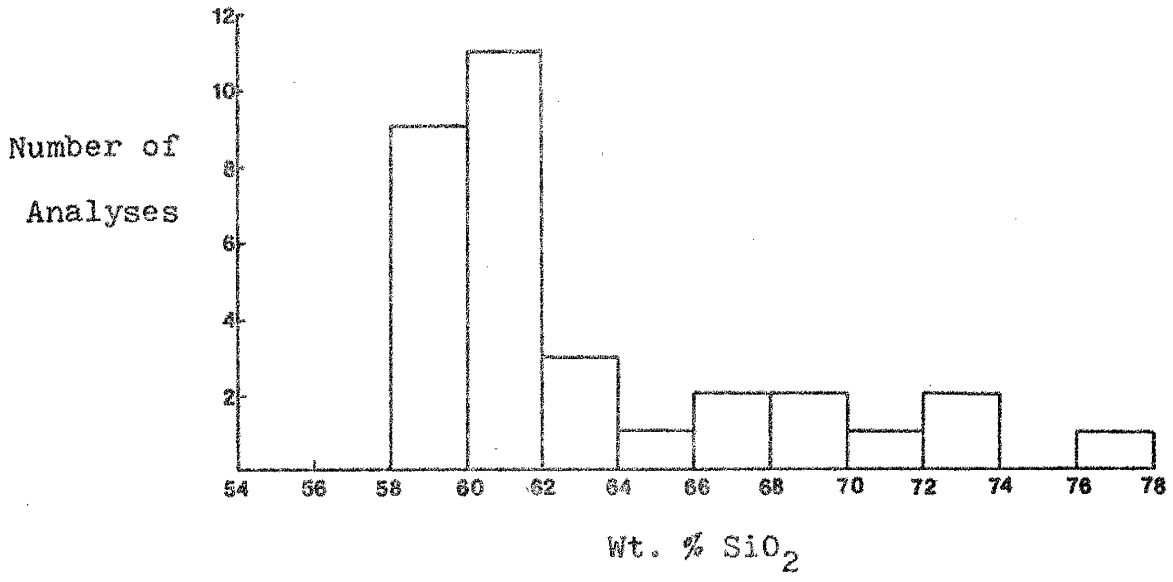

B. North Phipps section

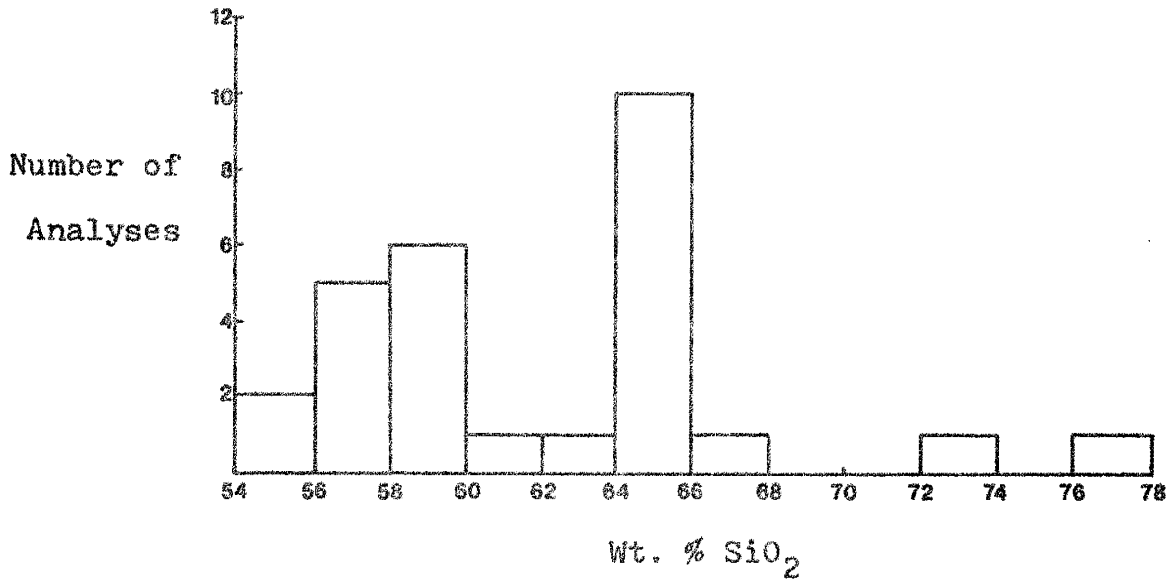

Figure 14. Frequency histograms of Wt. % SiO_2 verses Number of Analyses.

obtained. However, Hay (1966) has compiled a ternary diagram indicating compositional relationships among albite, potassium feldspar, and the dominantly alkalic zeolites which most commonly occur in sedimentary rocks. This diagram can be used to plot zeolites based on whole rock chemical analyses.

Figure 15A and 15B contain the zeolite plots prepared for the Wason and North Phipps measured sections. All points on the diagram are obtained by the method of Jensen (1976) which calculates equal volumes of oxide percentages based on one cation per oxide. Detailed use of the Jensen cation plot, a sample calculation, and tabulation of cation percentages in the plots are found in Appendix V.

The dominant zeolite present in these rocks is a zeolite which closely resembles both heulandite and clinoptilolite. Hay's diagram does not contain a heulandite field but does contain a clinoptilolite field. However, this is not a problem because heulandite group zeolites form a solid solution series between the Ca-rich end member, heulandite, and the alkali-rich end member, clinoptilolite (Boles, 1972). Therefore, most of the samples which plot in the clinoptilolite field are probably more like a combination of clinoptilolite and heulandite. This conclusion is supported by previously discussed X-ray diffraction studies and thermal stability tests which distinguish pure heulandite from pure clinoptilolite.

Symbols for Zeolites

ch=chabazite
cl=clinoptilolite
er=erionite
ph=phillipsite

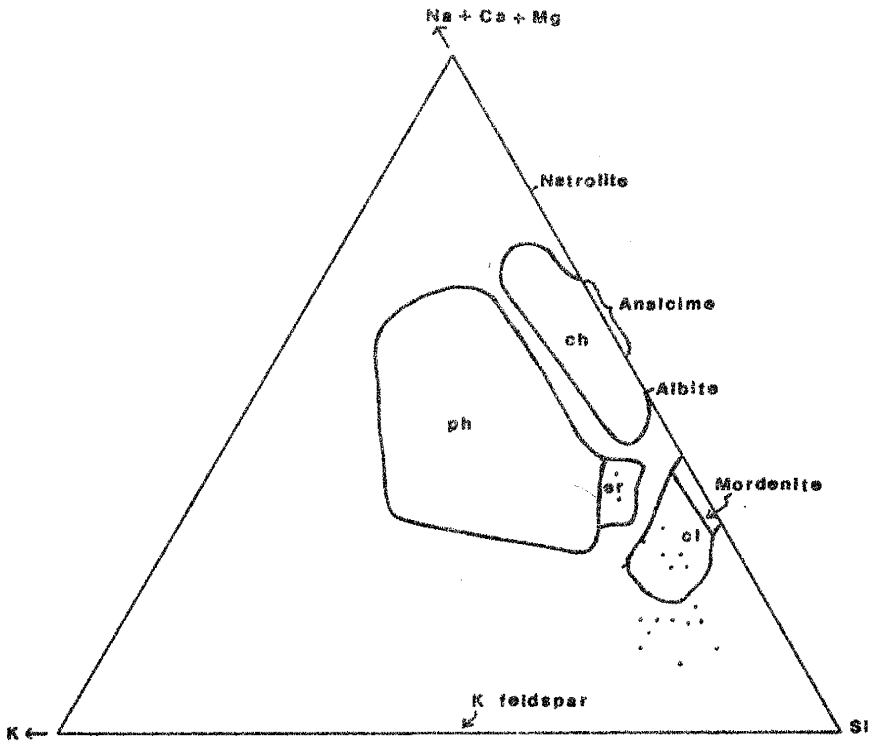

Figure 15A. Wason section cation plot.

Compositional relations of albite, potassium feldspar, and the dominantly alkalic zeolites which occur most commonly in sedimentary rocks. This diagram is the silica-rich part of a ternary diagram having as its end members the atomic proportions of Si, K, and Na+Ca+Mg. Modified from Hay (1966a). Atomic proportions calculated according to the method of Jensen (1976).

Symbols for Zeolites

ch=chabazite
cl=clinoptilolite
er=erionite
ph=phillipsite

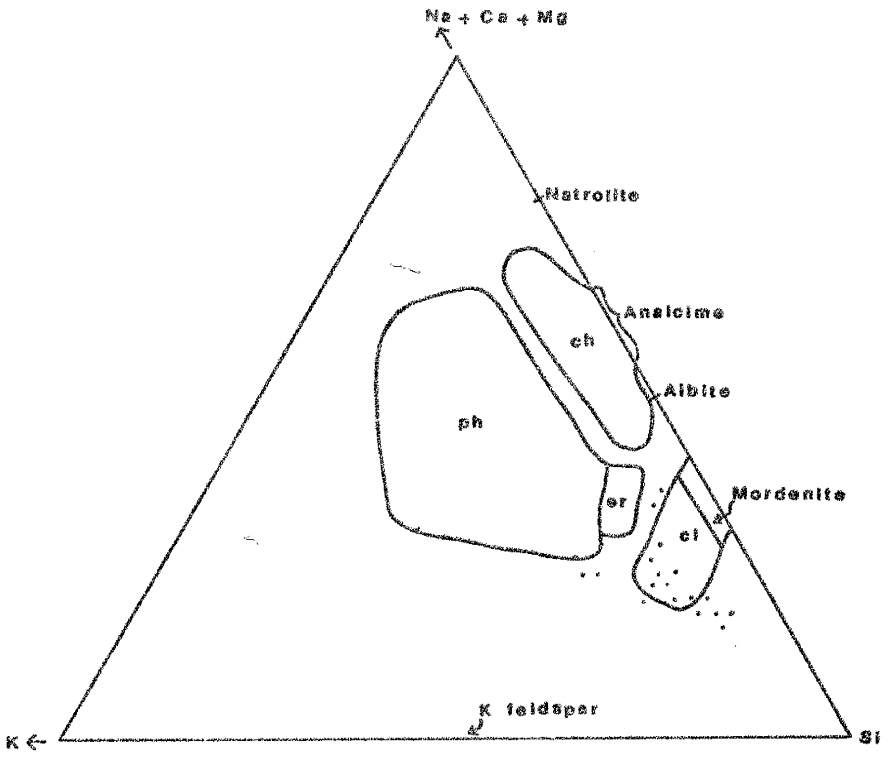

Figure 15B. North Phipps section cation plot.

Compositional relations of albite, potassium feldspar, and the dominantly alkalic zeolites which occur most commonly in sedimentary rocks. This diagram is the silica-rich part of a ternary diagram having as its end members the atomic proportions of Si, K, and Na+Ca+Mg. Modified from Hay (1966a). Atomic proportions calculated according to the method of Jensen (1976).

There is one problem with applying Hay's diagram to the zeolites found in these rocks. The diagram does not account for any unaltered glass which may still be present in these samples. Therefore, at best, Figure 15A & B can only be a qualitative representation of the zeolites present in the study area. In general, it appears that all points on the diagrams are probably shifted a small amount towards the Si-rich and potassium feldspar areas of the diagrams.

MECHANISM OF ALTERATION

CHEMICAL REACTIONS CONTROLLING THE ALTERATION PROCESS

Formation of the authigenic silicate minerals which occur in the Creede Formation, particularly the zeolites, require special geochemical and hydrologic conditions. In order for these minerals to form, the primary condition to be met is an abundance of appropriate starting materials. Volcanic glass is the most common starting material observed among zeolites formed in sedimentary rocks. Although, thick accumulations of biogenic silica, poorly crystalline clay minerals, and feldspars can also produce large quantities of zeolites (Hay, 1978).

In the Creede Formation this condition was easily met. Close proximity to vents in Fisher Mountain on the south side of the Creede caldera deposited abundant glass-rich material in the form of air-fall tuffs. In addition, the numerous surrounding ash-flow tuff sheets contributed a great deal of glass-rich volcanic detritus. In the Wason and North Phipps sections petrographic study has documented that most of the rocks once contained between 30 and 60% glass in the original matrix.

Due to the extreme reactivity of glass (Kerr, 1966) and its well known susceptability to chemical weathering (Gooding and Keil, 1978), leaching of volcanic glass can

easily occur in subsurface waters that originate as meteoric waters (Miola, 1970). Initial hydration and solution of only a small amount of glass is enough to set the authigenic mineral reaction sequence in motion. This immediately causes the alkalinity and salinity of the surrounding fluids to begin to increase, and the chemical parameters of the pore fluids become favorable for the formation of a clay mineral which is most often montmorillonite (Tank, 1969). In the Creede sediments, like so many other examples, montmorillonite and probably also celadonite were the first minerals to crystallize as the glass dissolved.

The early formation of both montmorillonite and celadonite is fovored by a low (K + Na)/H ion activity ratio and a pH between 7.0 and 8.0 (Hay, 1963, 1966; Surdam and Parker, 1972; Surdam and Sheppard, 1978). According to Hay (1963), the activities of ferrous and ferric iron determine whether montmorillonite or celadonite will form first. Montmorillonite contains dominantly ferric iron; thus, a lower ferrous activity (lower Eh) favors precipitation of montmorillonite over celadonite, which contains mainly ferrous iron (Barrows, 1980). From petrographic and scanning electron microscopic studies it is not possible to determine the relative ages of crystallization of these two minerals. However, fluids present at this point in the reaction sequence are only mildly alkaline and mildly saline. Compositionally, they still resemble typical ground

water which is characterized by slightly reducing conditions (Eh between -0.1 and -0.3), and a neutral to slightly alkaline pH between 7.0 and 8.0 (Garrels and Christ, 1965). Therefore, in this early stage of diagenesis, it seems likely that montmorillonite rather than celadonite formed first.

As glass continues to dissolve, the rate of dissolution eventually becomes greater than the rate at which montmorillonite and celadonite can consume cations being released into the pore fluids. Now the chemistry of the aqueous phase is favorable for the crystallization of zeolites rather than additional clay (Sheppard and Gude, 1969).

The formation of zeolites is favored by an increasing (K+Na)/H ratio, an increasing Si/Al ratio, and a decreasing activity of water (Hay, 1963, 1966; Sheppard and Gude, 1968, 1969; Surdam and Sheppard, 1978). Changes in these parameters also cause the pH to steadily rise (Surdam and Parker, 1972). Although zeolite crystallization is not directly related to the pH of the pore fluids, zeolitization does not begin until a pH of approximately 8.0 is reached. (Surdam and Sheppard, 1978).

Which zeolite crystallizes first depends on several factors: depth of burial of the sediments; temperature of any fluids present; and the chemistry of the pore fluids. In the Creede Formation chemistry of the pore fluids,

either passing through or trapped within the sediments, seems to have been the most important compositional parameter determining zeolite speciation. Ultimately, the amount and types of dissolved solids contained within the pore fluids are determined by the original composition of the dissolving glass.

In the Wason and North Phipps sections heulandite, clinoptilolite, and mordenite are the zeolites which have formed. From paragenetic relationships observed under the scanning electron microscope, it can only be concluded that heulandite and clinoptilolite crystallized simultaneously. In all samples where their distinctive wafer thin, coffin shaped structures are found, the two minerals cannot be identified separately. In addition, no relationships can be observed to suggest that some coffins grew before or after others. However, according to Hay (1978), clinoptilolite is considered an early forming zeolite and a precursor to other zeolites, specifically heulandite, analcime, and laumontite.

Based on Hay's examples, it is possible that the same sequence occurred in these sediments. Therefore, it is suggested that a small amount of pure clinoptilolite precipitated first from the glassy solution. This was soon followed by the crystallization of a heulandite-like zeolite or a pure heulandite which became the bulk of the zeolitic material to crystallize. Since X-ray diffraction patterns of heulandite and clinoptilolite are virtually identical,

whether this zeolite was pure heulandite or a heulandite-like zeolite cannot be determined at the present time. It also cannot be ascertained whether heulandite actually formed from a clinoptilolite precusor or whether each mineral precipitated separately from the glassy solution.

After crystallization of clinoptilolite and heulandite, the next zeolite to form in the Wason and North Phipps sections was mordenite. This event is well documented by scanning electron micrographs. All the mordenite crystals which could be observed were found lying on top heulandite group zeolite laths. According to Hawkins and others (1978), mordenite is very similar to clinoptilolite, compositionally and structurally, and can form over the same ranges of compositional parameters. These investigators contend that because clinoptilolite and heulandite are more hydrous minerals than mordenite, they should preferentially form at higher water activities and lower salinities. Clinoptilolite and heulandite contain 24 water molecules per unit cell while mordenite contains only seven. Thus, the observed paragenetic relationships are in agreement with the chemistry of mordenite crystallization.

Although decomposition of volcanic glass to montmorillonite and zeolites consumes a great deal of silica, this element is still in excess, and silica minerals are the next to crystallize after the zeolites (Iijima,

1961). In the Wason and North Phipps sections, it appears that chalcedony is the dominant authigenic silica mineral. This is well documented by radiating chalcedony crystals which are often final materials to fill in void spaces.

According to Hay (1966), Mariner and Surdam (1970), and Steven and Van Loenen (1971) deposition of opal also occurs at this point in the reaction sequence. Although opal is amorphous, it can be observed on X-ray diffraction patterns as a low bulge in the diffractogram extending between 20 and 30 degrees 2θ. On patterns obtained from size fractionation studies slight bulges were observed. Therefore, X-ray diffraction data on these samples suggest that minor amounts of opal formed.

The next authigenic mineral in this reaction sequence which usually forms is analcime. Analcime, a sodium-rich zeolite, is a very common constituent of saline alkaline lake deposits which form in closed hydrographic basins (Hay, 1966; Sheppard and Gude, 1969, 1973; Hay, 1970; Surdam and Parker, 1972; Surdam and Eugster, 1976). Analcime also commonly occurs in zeolite deposits which form by freely percolating ground waters in open hydrographic systems (Robinson, 1966; Hoover, 1968; Miola, 1970; Walton, 1975). Unlike clinoptilolite, evidence is quite convincing that analcime does not form directly from solution of volcanic glass, but always forms from a zeolite precusor (Hay, 1966; Sheppard and Gude, 1969, 1973; Surdam and Eugster, 1976).

The presence of analcime indicates that fluids in the pore spaces have reached moderate to high salinities (activity of water approximately 0.7), and a pH ranging between 9.0 and 10.0 (Surdam and Sheppard, 1978).

The formation of analcime from alkalic zeolites, particularly clinoptilolite, releases abundant potassium ion into solution (Tank, 1969). Thus, the reaction of montmorillonite to illite can easily occur due to increased potassium ion activity (Surdam and Parker, 1972). Formation of illite is controlled by a very high (Na + K)/H ion ratio, moderate salinity, moderate to high alkalinity, and low water activity (Tank, 1969). These conditions are usually attained in saline alkaline lakes or in ground waters which have been progressively enriched in dissolved solids through hydration and solution of volcanic glass. Consequently, illite, along with montmorillonite is the most common authigenic clay mineral associated with zeolitized pyroclastic deposits (Tank, 1969).

In the fluvial and breccia facies sediments analyzed from the Wason and North Phipps sections, abundant authigenic illite is present but no analcime has been found. However, significant quantities of analcime were found in lacustrine facies sediments located in the western portion of the Creede caldera (personal commun., Battory, 1982).

The final authigenic silicate mineral which can form through diagenesis of pryoclastic material is potassium

feldspar. According to most investigators, crystallization of this mineral represents pore fluids which have attained a pH greater than 9.5, and may contain a concentration of total dissolved solids in excess of 200,000 ppm (Jones, 1965; Eugster, 1970; Surdam and Sheppard, 1978). Authigenic potassium feldspar also forms from a zeolite precursor and has been observed replacing phillipsite, clinoptilolite, and analcime (Iijima and Hay, 1968; Sheppard and Gude, 1968, 1969, 1973; Surdam and Parker, 1972).

Authigenic potassium feldspar has been recognized in samples collected in the Wason and North Phipps sections. It has been identified on X-ray diffraction patterns form the 5 through 13 micron size fractions and has been observed with the scanning electron mocroscope. According to Surdam and Sheppard (1978), authigenic potassium feldspar is commonly associated with bedded saline minerals. However, in these two sections of the Creede Formation no saline minerals have been found.

AUTHIGENIC MINERAL PARAGENESIS

Based on the well documented chemical reaction sequence just discussed, a tentative statement of the authigenic mineral paragenesis can be summarized.

1. Hydration and solution of potassium-rich volcanic glass.

2. Precipitation of montmorillonite followed by celadonite from the glassy solution.

3. Continued hydration and solution of volcanic glass.

4. Precipitation of a silicic alkalic zeolite from the glassy solution, most commonly clinoptilolite.

5. Precipitation of heulandite from the glassy solution, or formation of heulandite by replacement of clinoptilolite precursors, or both.

6. Precipitation of mordenite from the glassy solution.

7. Precipitation of chalcedony and opal from the glassy solution.

8. Replacement of silicic alkalic zeolite precursor (clinoptilolite or heulandite) by the Na-rich zeolite, analcime. (Note: this event was not observed in samples from the Wason and North Phipps sections, but has been reported in other areas of the Creede Formation).

9. Replacement of montmorillonite by illite.

10. Replacement of silicic alkalic zeolite precursor (clinoptilolite or heulandite) by potassium feldspar.

In some cases the paragenetic sequence can be supported by grain relationships observed with the petrographic microscope or under the scanning electron microscope. In particular, steps 2, 4, 6, and 7 have been documented by research done for this thesis.

GEOLOGIC AND HYDROLOGIC ENVIRONMENT OF ALTERATION

Authigenic minerals formed by alteration of pyroclastic material can occur in numerous types of geologic and hydrologic environments. Hay (1966, 1978) reviews six such environments. However, only three of these environments are applicable to the alteration processes which have occurred in the Creede Formation. The three possible environments in which tuffaceous sediments at Creede could have been altered are: (1) alteration by ascending hydrothermal fluids; (2) alteration in a saline alkaline lake environment; and (3) alteration by relatively fresh meteoric ground waters.

Occurrences of hydrothermal zeolites are widespread. Some well known examples are found in Yellowstone Park, U.S.A. (Honda and Muffler, 1970); Wairakie, New Zealand (Steiner, 1953, 1955; c.f. Hay, 1978); and Onikoki, Japan (Seki et al., 1969; c.f. Hay, 1978). Hydrothermal deposits show a distinctly vertical mineral zonation (Hay, 1978). According to Hay (1978), the shallowest and coolest zones are characterized by the presence of clinoptilolite and mordenite, and progressively deeper zones commonly contain analcime, heulandite, laumontite, or wairakite. The presence of laumontite and wairakite in deposits of saline alkaline lakes or those formed by meteoric ground waters is unusual. Thus, their occurrence can be particularly diagnostic of alteration by hydrothermal fluids. Analcime

and heulandite, however, can form diagenetically or by hydrothermal fluids, and therefore are not so diagnostic. Associated authigenic minerals which often occur with hydrothermal zeolites are montmorillonite, celadonite, kaolinite, chlorite, fluorite, alunite, albite, or pyrite (Deffeyes, 1959; Robinson, 1966; Honda and Muffler, 1970; Hay, 1978)

Zeolites formed by diagenesis in saline alkaline lakes are the most common way in which zeolites form in sedimentary rocks. In the past 20 years numerous deposits formed in this manner have been documented around the world. Among the most classic examples described in the literature are the Eocene age Green River Formation of Wyoming (Hay, 1966; Surdam and Parker, 1972), and Pleistocene Lake Tecopa, Inyo County, California (Sheppard and Gude, 1968). Sheppard (1973) and Surdam and Sheppard (1978), have shown that these lakes are the result of fluids trapped in a closed hydrographic basin located where an arid to semi-arid climate once persisted or presently exists. Such regions are characterized by an evaporation rate which exceeds the amount of precipitation. With minimal influx of fresh water and no outlet for stagnent water, concentration of lake fluids by evaporation eventually produces a moderate to highly saline alkaline brine. The most common types of zeolites which occur in this environment are erionite, phillipsite, clinoptilolite, mordenite, chabazite, and

analcime (Surdam and Sheppard, 1978).

Many saline alkaline deposits show a distinctly lateral mineralogic zonation (Hay, 1978; Surdam and Sheppard, 1978). Where well developed, the succession of mineral zones forms roughly concentric to the basin perimeter. Hay (1966), Sheppard and Gude (1968, 1969, 1973), and Surdam and Parker (1972), have defined four basic zones: (1) an outer fresh water zone where volcanic glass (or other appropriate starting material) is either unaltered or partially replaced by clay minerals; (2) a moderately alkaline, moderately saline zone of alteration to silicic alkalic zeolites; (3) a more alkaline and saline zone characterized by analcime; and (4) a highly alkaline and saline zone where alteration is primarily to potassium feldspar.

Zeolites which form in a hydrographic setting characterized by ground waters that freely move in and out of a depositional basin are referred to as the 'open system type of zeolites (Hay, 1963, 1978; Walton, 1975; Mumpton, 1978). These deposits show a more or less vertical zonation due to ground water movement generally being in a downward direction (Hay, 1963; Walton, 1975). Diagenetic reactions proceed in much the same way as in saline alkaline lake deposits. Percolating ground waters react with unstable glassy material and become progressively enriched in dissolved solids. The major difference is that solutions in the open system model have a point of discharge from the

system. Concentration of these fluids occurs due to contact with more and more volcanic sediments undergoing solution and hydration.

Hay (1963) and Walton (1975) have described three mineralogic zones which characterize the open system zeolite deposits: (1) an upper zone between 200 and 500 meters thick in which fresh glass, montmorillonite, or possibly some opal are present; (2) a middle zone which can be 500 meters or more in thickness and is characterized primarily by clinoptilolite. Beds in this zone may contain greater than 90% zeolitic material; and (3) a basal zone characterized by analcime with or without potassium feldspar. The John Day Formation of Oregon (Hay, 1963), and The Vieja Group (Oligocene) of Texas (Walton, 1975) are excellent examples of this type.

The possibility that hydrothermal fluids were responsible for alteration of the Creede Formation deserves consideration. In the northern portion of the moat just north and west of the town of Creede, north trending fractures of the Creede vein system cut into the Creede Formation. Mineralization of the Creede system was caused by a convecting cell of hydrothermal-meteoric fluids (Steven and Eaton, 1975; Barton and Others, 1977). In both investigations referenced, schematic hydrologic models for ore deposition show a portion of this convecting cell moving through the Creede Formation. Therefore, hydrothermal

fluids probably did move through a restricted portion of the Creede sediments. However, that area was not studied in detail and it does not seem likely that fluids associated with the Creede vein system moved very far through the Creede Formation. Furthermore, the Creede vein system is approximately 1.8 m.y. younger than the Creede Formation (Steven and Others, 1967; Bethke and Others, 1976). It has been well documented that once hydration of volcanic glass begins, reactions which form zeolites can go rapidly to completion in approximately 1,000 years (Hay, 1964, 1966). Thus, it is probable that alteration of the Creede Formation had occurred well before the Creede vein system was mineralized.

Another possible mechanism exists which could cause zeolitization by hydrothermal alteration. During deposition of the Creede Formation, approximately 26.4 m.y. ago, this area was still a considerably active volcanic region. Thus, the geothermal gradient in the 1 km thick pile of sediments accumulating in the caldera moat was probably higher than normal. In addition, concurrent with sedimentation possibly hundreds of travertine bodies were being deposited by mineral springs. At the present time temperatures at which these springs were depositing travertine is unknown. Though it is still certainly possible that Creede Formation sediments may have been heated after deposition. Furthermore, several zeolites which characterize the

vertical zonation pattern found in hydrothermal zeolite deposits are also found in the Creede Formation. Unfortunately, the truely diagnostic ones have not yet been recognized at Creede, and the vertical section exposed today is not extensive enough to identify those zones.

However, evidence is also convincing that hydrothermal alteration was not responsible for the bulk of authigenic mineral formation which occurs in the Creede Formation. In the Creede Formation alteration, although variable in degree from bed to bed, is continuous both vertically and laterally. X-ray diffraction data indicate that zeolites are present throughout the entire vertical thickness. In addition, zeolitization can be observed to follow bedding planes over relatively long lateral distances. This widespread distribution of diagenetic mineral assemblages is cited as evidence against hydrothermal alteration (Hay, 1963; Hoover, 1968; Miola, 1970; Robinson, 1966;).

In Plate F note the white colored beds which stand out clearly against the buff colored sediments. These white beds correspond to samples that are considered highly zeolitized containing approximately 40% zeolitic material. The white zeolitized beds near the middle of the photograph can be traced laterally for 1.6 km. The zeolitized bed near the top right side of the photograph is approximately 200 meters long.

Finally, the mineral assemblages found in the Creede

Plate F. Creede Formation beds observed at a distance show extensively zeolitized white beds occur over long lateral distances.

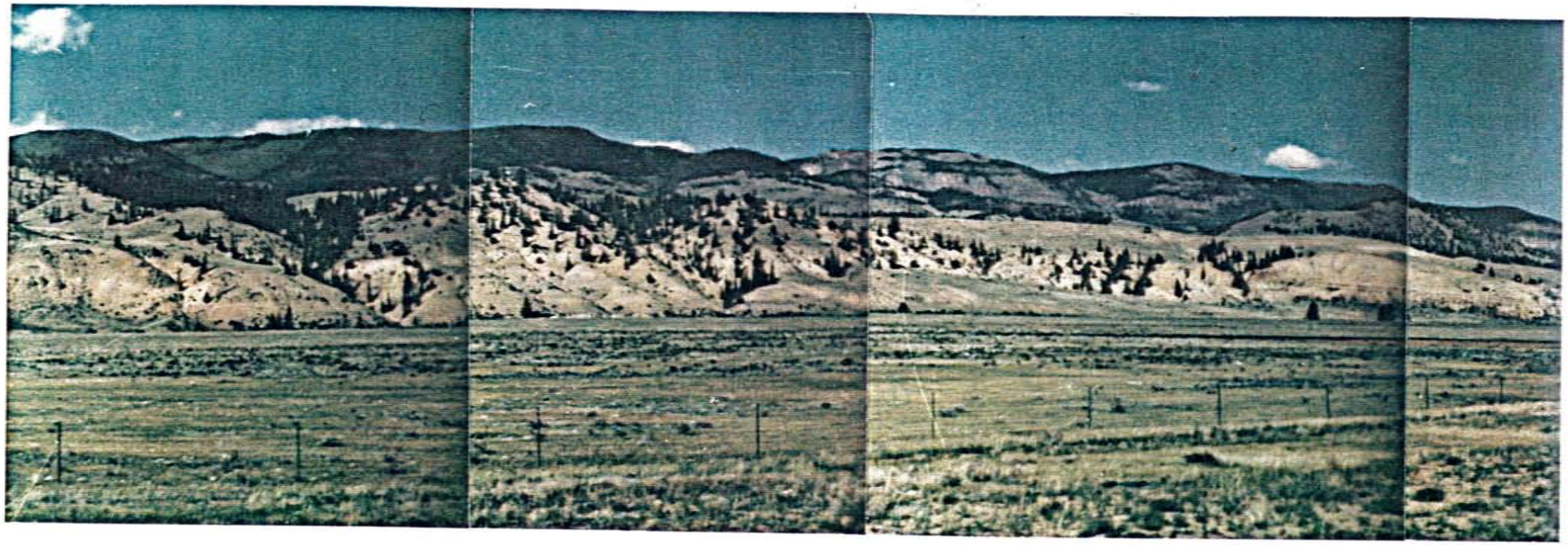

formation do not unequivocally support a hydrothermal origin. Laumontite and/or wairakite have not yet been identified. The rest of the authigenic silicates which do occur can form in both hydrothermal and low temperature diagenetic environments. A survey of the literature for this project has made it apparent that clinoptilolite, heulandite, mordenite, analcime, montmorillonite, and celadonite are more common in diagenetically formed deposits. At the present time not enough data has been collected to ascertain the role of hydrothermal alteration on diagenesis of the Creede Formation.

The possibility that diagenesis of a large portion of the Creede Formation occurred in a saline alkaline lake environment is a viable hypothesis. According to E. B. Leopold (written commun., 1973; c.f. Steven and Eaton, 1975) fossil flora collected in the Creede Formation suggests a montane environment with a cool temperate climate; higher slopes received moderate seasonal rainfall while lower areas like the Creede Formation were exposed to a warmer drier climate. This is very similar to the climate which exists today. The Creede area is part of semi-arid region which covers most of the Rocky Mountain geologic province and receives between 25 and 50 cm of average annual pecipitation (Batton, 1974, p. 104; Bloom, 1978, p. 312). Thus, it can be concluded that late Oligocene climate was also semi-arid, a prerequisite for formation of a saline alkaline lake.

There is also good evidence that small playa lakes developed in the central portions of the moat. At several localities along the Rio Grande River cliffs have formed up to 60 m high and sometimes extending for approximately 0.5 km along the river. The cliffs are dominantly composed of very finely bedded tuffaceous siltstones deposited in a lacustrine environment. In particular, abundant mudcracks and saline crystal casts now filled with calcite were observed at sections studied on the Broad Acres and Freemon Ranches (personal commun., Battory, 1982). Other characteristics such as ripple marks, absence of fossil fauna, and small scale disrupted bedding features support the presence of small playa lakes. Diagenetic alteration of the volcaniclastic sediments to the analcime facies in some areas further confirms the presence of such lakes.

However, in the Wason and North Phipps sections the possibility that authigenic silicates formed in saline alkaline lakes, does not appear so conclusive. Only the lower third of the Wason section contains beds from the lacustrine facies, and no beds in the North Phipps section have been deposited in a lacustrine environment. Where lacustrine beds do occur in the Wason section, finely bedded tuffaceous siltstones do not form considerable thicknesses of cliff forming sections like lacustrine facies in other localities. In addition, lacustrine sediments in the Wason section are frequently interupted by fluvial sandstones and

conglomerates. Therefore, lacustrine facies in this section are possibly more marginal lake facies than true lacustrine facies.

Furthermore, in these sections, even lacustrine facies of the Wason section , no supporting evidence for playa lakes has been observed. Mudcracks, ripple marks, and saline minerals or their casts are absent. Gypsum is present on some joint surfaces in the cliff-forming segment of the lacustrine facies. Though, by nature of its occurrence, deposition of gypsum appears to have been a later secondary event not related to zeolitic diagenesis. Finally, according to Mariner and Surdam (1970), the clinoptilolite and mordenite assemblage, which does occur in these sections, is more characteristic of fresher water deposits, whereas less siliceous zeolites like analcime are more indicative of the saline alkaline lake deposits.

The final possibility that diagenesis of the Creede Formation occurred in an open system must also be considered. Diagenesis of sediments deposited near the caldera rim, along the caldera sides, and possiblly as deltas near playa lake margins, may have occurred by the open system mechanism. The absence of lacustrine facies near the caldera sides, along with the dominance of fluvial and breccia facies in these sections, suggests that formation of playa lakes and concentration of lake fluids into saline alkaline brines did not occur everywhere in the

Creede Formation. Meteoric waters moving from the caldera rim towards centrally located playa lakes were in constant contact with highly reactive, glass-rich sediments. Thus, it is probable that pore fluids in the sediments became sufficiently enriched in dissolved solids to allow the formation of clay minerals, zeolites, silica minerals, and potassium feldspar, without calling on the saline alkaline lake mechanism.

During late Oligocene times, Steven and Ratte (1965), estimated a minimum possible thickness of the Creede Formation to be 620 meters. In most places sediments accumulated to 1 km or more in thickness. Even if the caldera rim was only 300 meters higher than playa lakes developing in the center of the moat, meteoric waters still had sufficient vertical thickness in which to percolate through for concentration of dissolved solids and for diagenetic reactions to occur.

For fluvial and breccia facies in the Wason and North Phipps sections, there is no evidence to indicate that fluids flowing through them were particularly saline. Relatively minor amounts of Na-montmorillonite formed, no analcime formed (the sodium-rich zeolite), and no saline minerals or casts were found. In order to have formed clinoptilolite, heulandite, and mordenite the pH must have been between 8.0 and 9.0 (Surdam and Sheppard, 1978), which is moderately alkaline. Thus, it is suggested that mildly

saline and moderately alkaline solutions characterized the fluids traveling through sediment pore spaces in this area of the Creede Formation.

The presence of authigenic feldspar is somewhat more problematic. Throughout the literature on zeolitization of pyroclastic material, formation of authigenic potassium feldspar is evidence that the pH of a given system has reached very high alkalinities (pH > 9.5), high concentrations of dissolved silica, and a high K/H ion ratio. It is suggested that in the Wason and North Phipps sections, alkalinities as high as 9.5 were probably not attained.

Based on stability relations which exist in the system K_2O-MgO-FeO-Al_2O_3-SiO_2-H_2O at 25 C and 1 atm. (Garrels and Christ, 1965, p.364), and those which exist in the system K_2O-Al_2O_3-SiO_2-H_2O at 25 C and 1 atm. (Stumm and Morgen, 1970, p. 404), authigenic potassium feldspar can form at lower pH's than 9.5. It is evident from these diagrams that the stability field of potassium feldspar is certainly larger at higher pH's. However, potassium feldspar can form at pH's as low as 4.0 provided that other conditions are optimum. Since primary crystals of orthoclase and sanidine are abundant in thin sections, it does not seem unreasonable that those materials ejected in a glassy state were also rich in potassium. Therefore, hydration and solution of potassium-rich volcanic glass allowed pore fluids in the

sediments to become sufficiently enriched in potassium and dissolved silica. Formation of potassium feldspar was then possible before extremely high alklinities and salinities were reached.

In summary, it is suggested that a combination of two hydrologic models were responsible for the bulk of zeolitic alteration which occurs in the Creede Formation. In the lower lying, more centrally located portions of the moat, a saline alkaline lake environment is the mechanism by which diagenesis occurred. Along the caldera sides and possibly near playa lake margins, an open system mechanism is the model which best explains how diagenesis occurred. However, many more sections need to be studied throughout the Creede Formation before these conclusions can be confirmed.

The most conclusive statement which can be made can only pertain to the sections on which this study was focused, the Wason and North Phipps sections. It is suggested that in these sections diagenesis occurred dominantly in a small scale open system environment. The lower 25 to 35 meters of section on the Wason Ranch may have been deposited as marginal lake facies. Relatively low salinities, moderate alkalines, and an abundant supply of a potassium-rich starting material, can adequately explain the authigenic silicate minerals present. Finally, conditions under which the bulk of these sediments were deposited support the open system model.

SUGGESTIONS FOR FUTURE STUDY

Certain aspects of this study warrant furthur investigation. The amount and types of authigenic minerals present in the Creede Formation need to be more quantitatively defined. In particular, determining the exact nature of which heulandite group zeolite species is present, is the foremost problem revealed by this study. A solution to this problem requires research into two additional procedures: (1) development of techniques for separating zeolites from other minerals, particularly those in the auhtigenic size range; and (2) development of techniques for separating one zeolite from another.

In this study heavy liquid density separations using a bromoform and acetone mixture were attempted. However, due to extremely small grain sizes of many minerals present, this procedure was unsuccessful. Among minerals a few microns in diameter, there is a large amount of surface area. Thus, surface tension forces are greater than that of the heavy liquid.

Today, quantitative electron microprobe analysis is being used by many researchers to resolve the kind of problems encountered in this study. With the microprobe exact chemical and structural parameters can be determined for a single zeolite crystal or other authigenic mineral. Thus, in order to complete the mineralogical and geochemical

description of the Creede Formation, research through quantitative electron microprobe analysis is strongly recommended.

Finally, extensive coring in a variety of locations around the moat to depths at which the Creede Formation is in contact with underlying volcanics, would be very useful. Determining the type and extent of authigenic mineral formation present in the cores and throughout the beds exposed today may help to more precisely define any vertical or lateral alteration zoning present.

REFERENCES CITED

Aletti, A., 1972, Polymorphism and crystal-chemistry of heulandites and clinoptilolites: Amer. Mineral., v. 57, p. 1448-1461.

Barrows, K. J., 1980, Zeolitization of Miocene volcaniclasti rocks, southern Desatoya Mountains, Nevada: Geol. Soc. America Bull. part I, v. 91, #4, p. 199-210.

Barton, P. B., Jr., Bethke, P. M., and Roedder, E., 1977, Environment of ore deposition in the Creede mining district, San Juan Mountains, Colorado: Part III. Progress towards interpretation of the chemistry of the ore-forming fluid for the OH vein: Econ. Geol., v. 72, p. 1-24.

Batton, L. J., 1974, Weather. Englewood Cliffs, New Jersey, Prentice-Hall Inc., 136p.

Bethke, P. M., Barton, P. B. Jr., Lanphere, M. A., and Steven, T. A., 1976, Environment of ore deposition in the Creede mining district, San Juan Mountains, Colorado: Part II. Age of mineralization: Econ. Geol., v. 71, p. 1006-1011.

Bloom, A. L., 1978, Geomorphology: A systematic analysis of late Cenozoic landforms. Englewood Cliffs, New Jersey, Prentice-Hall Inc., 510p.

Boles, J. R., 1972, Composition, optical properties, cell dimensions, and thermal stability of some heulandite group zeolites: Amer. Mineral., v. 57, p. 1463-1493.

Deffeyes, K. S., 1959, Zeolites in sedimentary rocks: Jour. Sediment. Petrol., v. 29, p. 602-609.

Emmons, W. H., and Larsen, E. S., 1923, Geology and ore deposit of the Creede district, Colorado: U. S. Geol. Survey Bull. 718, 198p.

Eugster, H. P., 1970, Chemistry and origin of the brines of Lake Magadi, Kenya: Mineral. Soc. Amer. Spec. Paper 3, p. 215-235.

Fisher, R. V., 1961, Proposed classification of volcaniclastic sediments and rocks: Geol. Soc. America Bull., v. 72, p. 1409-1414.

Garrels, R. M., and Christ, C. L., 1965, Solutions, minerals, and equlibria. San Francisco, Freeman, Cooper and Company, 450p.

_____and MacKenzie, F. T., 1971, The evolution of sedimentary rocks. New York, W. W. Norton and Company Inc., 397p.

Gooding, J. L., and Keil, K., 1978, Alteration of volcanic glass as a possible source of clay minerals on Mars: Geophys. Research Letters, Amer. Geophys. Union, Wash. D. C., v. 5, p. 727-730.

Hawkins, D. B., Sheppard, R. A., and Gude, A. J., 1978, Hydrothermal synthesis of clinoptilolite and comments on the assemblage phillipsite-clinoptilolite-mordenite, in L. B. Sand and F. A. Mumpton, eds., Natural Zeolites: Occurrence, Properties, Uses. Oxford, Pergamon Press, p. 337-343.

Hay, R. L., 1963, Stratigraphy and zeolitic diagenesis of the John Day Formation of Oregon: Univ. Calif. pub. in Geol. Sci., v. 42, p. 199-262.
_____1966, Zeolites and zeolitic recations in sedimentary rocks: Geol. Soc. Amer. Spec. Paper 85, 130p.
_____1970, Silicate reactions in three lithofacies of a semi-arid basin, Olduvai Gorge, Tanzania: Mineral. Soc. Amer. Spec. Paper, v. 3, p. 237-255.
_____1978, Geologic occurrence of zeolites, in L. B. Sand and F. A. Mumpton, eds., Natural zeolites: Occurrence, Properties, Uses. Oxford, Pergamon Press, p. 135-143.

Honda, S., and Muffler, L. P. J., 1970, Hydrothermal alteration in core from research drill hole Y-1, Upper Geyser Basin, Yellowstone Park, Wyoming: Amer. Mineral., v. 55, p. 1714-1737.

Hoover,D. L., 1968, Genesis of zeolites, Nevada Test Site, in Eckel, E. B., ed., Nevada Test Site: Geol. Soc. America Memoir 110, p. 275-284.

Iijima, A., 1961, Diagenetic alteration of some acidic tuffs in the Kushiro coal basin: Japanese Jour. Geol. and Geog. v. 32, p. 507-522.
_____and Hay, R. L., 1968, Analcime composition in tuffs of the Green River Formation of Wyoming: Amer. Mineral., v. 53, p. 184-200.

Jensen, R. L., 1976, A new cation plot for classifying subalkalic volcanic rocks: Ontario Division of Mines, Misc. Paper 66, 30p.

Jones, B. F., 1965, The hydrology and mineralogy of Deep Springs Lake, Inyo County, California: U. S. Geol. Survey Prof. Paper 502-A, 56p.

Keller, W. D., 1976, Scanning electron micrographs of kaolins collected from diverse environments of origin-I: Clay and Clay Minerals, v. 24, p. 107-113.

Kerr, G. T., 1966, Chemistry of crystalline aluminosilicates. I. Factors affecting the formation of zeolite A: Jour. of Phys. Chem., v. 70, p. 1047-1050.

Kerr, P. F., 1977, Optical mineralogy. New York, McGraw-Hill Company, 492p.

Krauskopf, K. B., 1967, Introduction to Geochemistry. New York, McGraw-Hill Company, 721p.

Larsen, E. S. Jr., and Cross, W., 1956, Geology and petrology of the San Juan region, Colorado; Cenozoic rocks, Creede Formation: U. S. Geol. Survey Prof. Paper 258, p. 167-172.

Lipman, P. W., and Mehnert, H. H., 1975, Late Cenozoic basaltic volcanism and development of the Rio Grande depression in the southern Rocky Mountains: Geol. Soc. Amer. Memoir 144, p. 119-154.

_____Doe, B. R., Hedge, C. E., and Steven, T. A., 1978, Petrologic evolution of the San Juan volcanic field, southwestern Colorado: Pb and Sr isotope evidence. Geol. Soc. Amer. Bull., v. 89, p. 59-82.

_____Steven, T. A., and Mehnert, H. H., 1970, Volcanic history of the San Juans as indicated by K-Ar dating: Geol. Soc. Amer. Bull. v. 81, no. 8, p. 2329-2352.

Mariner, R. H., and Surdam, R. C., 1970, Alkalinity and formation of zeolites in saline alkaline lakes: Sci., v. 170, p. 977-980.

Mehnert, H. H., Lipman, P. W., and Steven, T. A., 1973, Age of mineralization at Summitville, Colorado, as indicated by K-Ar dating of alunite: Econ. Geology, v. 68, p. 399-401.

Merkle, A. B., and Slaughter, M., 1968, Determination and refinement of the structure of heulandite: Amer. Mineral. v. 53, p. 1120-1138.

Moiola, R. J., 1970, Authigenic zeolites and K-feldspar in the Esmeralda Formation, Nevada: Amer. Mineral., v. 55, p.1681-1691.

Mumpton, F. A., 1960, Clinoptilolite redefined: Amer. Mineral., v. 45, p. 351-369.

_____1978, Natural zeolites: a new industrial commodity, in

L. B. Sand and F. A. Mumpton, eds., Natural Zeolites: Occurrences, Properties, Uses. Oxford, Pergamon Press, p. 3-27.

_____ and Ormsby, W. C., 1978, Morphology of zeolites in sedimentary rocks by scanning electron microscopy, in L. B. Sand and F. A. Mumpton, eds., Natural Zeolites: Occurrence, Properties, Uses. Oxford, Pergamon Press, p. 113-132.

Ratte, J. C., and Steven, T. A., 1967, Ash flows and related volcanic rocks associated with the Creede caldera, San Juan Mountains, Colorado: U. S. Geol. Survey Prof. Paper 524-H, 58p.

Robinson, P. T., 1966, Zeolitic diagenesis of Mio-Pliocene rocks of the Silver Peak Range, Esmeralda County, Nevada: Jour. Sed. Petrology, v. 36, p. 1007-1015.

Schmid, R., 1981, Descriptive nomenclature and classifcation of pyroroclastic deposits and fragments: Recommendations of the I.U.G.S. subcommission on the systematics of igneous rocks: Geology, v. 9, p. 41-43.

Scholle, P. A., 1979, A color illustrated guide to constituents, textures, cements, and porosities of sandstones and associated rocks. Amer. Assoc. Petroleum Geologists, Memoir 28, 201p.

Sheppard, R. A., 1973, Zeolites in sedimentary rocks: U. S. Geol. Survey Prof. Paper 820, p. 689-695.

_____ and Gude, A. J., 1968, Distribution and genesis of authigenic silicate minerals in tuffs of Pleistocene Lake Tecopa, Inyo County, California: U. S. Geol. Survey Prof. Paper 597, 38p.

_____ and Gude, A. J., 1969, Diagenesis of tuffs in the Barstow Formation, Mud Hills, San Bernadino County, California: U. S. Geol. Survey Prof.

_____ and Gude, A. J., 1973, Zeolites and associated silicate minerals in tuffaceous rocks of the Big Sandy Formation, Mohave County, Arizona: U. S. Geol. Survey Prof. Paper 830, 36p.

Smith, R. L., and Bailey, R. A., 1968, Resurgent calderas, in R. R. Coats, R. L. Hay, and C. H. Anderson, eds., Studies in volcanology: Geol. Soc. America Memoir 116, p. 613-662.

Steven, T. A., 1968, A critical review of the San Juan peneplain, southwestern Colorado: U. S. Geol. Survey Prof. Paper 524-I, 19p.

_____ 1972, Geologic environment of ore deposition in the Creede district, San Juan Mountains, Colorado [abs.]:

Econ. Geol., v. 66, no. 8, p. 1270.
_____ 1975, Middle Tertiary volcanic field in the southern Rocky Mountains, in B. F. Curtis, ed., Cenozoic history of the southern Rocky Mountains: Geol. Soc. America, Memoia 144.
_____ and Eaton, G. P., 1975, Environment of ore deposition in the Creede mining district, San Juan Mountains, Colorado: I. Geologic, hydrologic, and geophysical setting: Econ. Geol., v. 70, p. 1023-1037.
_____ and Epis, R. C., 1968, Oligocene volcanism in south-central Colorado, in R. C. Epis, ed., Cenozoic volcanism in the southern Rocky Mountains: Colorado School of Mines Quart., v. 63, no. 3, p. 241-258.
_____ and Friedman, I., 1968, The source of travertine in the Creede Formation, San Juan Mountains, Colorado: U. S. Geol. Survey Prof. Paper 600-B, p. B29-B36.
_____ and Lipman, P. W., 1976, Calderas of the San Juan volcani field, southwestern Colorado: U. S. Geol. Survey Prof. Paper 958, 35p.
_____ and Ratte, J. C., 1960, Relation of mineralization to caldera subsidence in the Creede district, San Juan Mountains, Colorado: Art. 8 in U. S. Geol. Survey Prof. Paper 400-B, p. B14-B17.
_____ and Ratte, J. C., 1964, Revised Tertiary volcanic sequence in the central San Juan Mountains, Colorado: U. S. Geol. Prof. Paper 475D, p. D62-D63.
_____ and Ratte, J. C., 1965, Geology and structural control of ore deposition in the Creede district, San Juan Mountains, Colorado: U. S. Geol. Survey Prof. Paper 487, 90p.
_____ and Ratte, J. C., 1973, Geologic map of the Creede quadrangle, Mineral and Saguach Counties, Colorado: U. S. Geol. Survey Geol. Quad. Map QQ-1053.
_____ and Van Loenen, R. E., 1971, Clinoptilolite-bearing tuff beds in the Creede Formation, San Juan Mountains, Colorado: U. S. Geol. Survey Prof. Paper 750-C, p. C98-C103.
_____ Mehnert, H. H., and Obradovich, J. D., 1967, Age of volcanic activity in the San Juan Mountains, Colorado: U. S. Geol. Survey Prof. Paper 575-D, p. D47-D55.

Stumm, W., and Morgam, J. J., 1970, Aquatic Chemistry. New York, John Wiley and Sons Inc., 583p.

Surdam, R. C., and Parker, R. D., 1972, Authigenic aluminosilicate minerals in the tuffaceous rocks of the Green River Formation, Wyoming: Geol. Soc. America Bull., v. 83, p. 689-700.
_____ and Eugster, H. P., 1976, Mineral reactions in the sedimentary deposits of the Lake Magadi region, Kenya: Geol. Soc. Amer. Bull., v. 87, p. 1739-1752.
_____ and Sheppard, R. A., 1978, Zeolites in saline,

alkaline-lake deposits, in L. B. Sand and F. A. Mumpton, eds., Natural Zeolites: Occurrence, Properties, Uses. Oxford, Pergamon Press, p. 145-174.

Tank, R., 1969, Clay mineral composition of the Tipton Shale Member of the Green River Formation (Eocene) of Wyoming: Jour. Sed. Petrology, v. 39, p. 1593-1594.

Walton, A. W., 1975, Zeolitic diagenesis in Oligocene volcanic sediments, Trans-Pecos Texas: Geol. Soc. America Bull., v. 86, p. 615-624.

LIST OF APPENDICES

Tables

APPENDIX I

Table I-1. Calibration Curve Statistics

ELEMENT	REGRESSION EQUATION	INFLUENCING ELEMENTS	CORRELATION COEFFICIENT	% REL. RMS ERROR
Si	multiple	Mg, Al, Ca, K	.99	0.54%
Al	multiple	Si, Mg	.99	0.0%
Fe	linear		.99	4.58%
Mg	multiple	Si, Al	.99	0.61%
Ca	multiple	Si	.99	1.20%
Na	linear		.99	9.15%
K	linear		.99	5.75%
Ti	linear		.99	6.73%

Table I-2. Variable instrumental conditions

ELEMENT	ABSORBER	TIME	CRYSTAL	COLLIMATOR	COUNTER
Si	20%	1 sec	RX4	fine	FPC
Al	50%	1 sec	TAD	fine	FPC
Fe	100%	2 sec	LiF200	coarse	SCN
Mg	100%	10 sec	TAD	coarse	FPC
Ca	100%	4 sec	LiF200	fine	FPC
Na	100%	10 sec	TAD	coarse	FPC
K	100%	4 sec	LiF200	fine	FPC
Ti	100%	20 sec	LiF200	coarse	SCN

(Note: FPC=Flow Proportional Counter; SCN=Scintillation Counter

APPENDIX II

Classification of Pyroclastic Deposits and Fragments

In order to understand the classification system and properly use Table II-3 (located on the next page), the following definitions must be given. These are taken directly from the IUGS publication (Schmid, 1981).

1. PYROCLASTIC: Consolidated and unconsolidated assemblages of individual crystals, crystal fragments, glass fragments, and rock fragments generated by disruption as a direct result of volcanic action. These must contain more than 75% pyroclasts by volume.

2. EPICLASTIC (volcanic and/or nonvolcanic): consolidated and unconsolidated aggregates of crystals, crystal fragments, glass fragments, and rock fragments that have been liberated from any type of pre-existing rock (volcanic or nonvolcanic) by weathering or erosion and transported from their place of origin by gravity, air, water, or ice.

3. TUFFITES (mixed pyroclastic-epiclastic rocks): rocks consisting of mixtures of pyroclasts and epiclasts. These must contain between 75% and 25% pyroclasts, and conversely between 25% and 75% epiclasts by volume.

APPENDIX II

Table II-3. Terms for Pyroclastic Rocks and Fragments

PYROCLASTIC	TUFFITES (mixed pyroclastic-epiclastic)	EPICLASTIC (volcanic and/or nonvolcanic)	AVG CLAST SIZE (MM)
Agglomerate, agglutinate, pyroclastic breccia	Tuffaceous conglomerate, tuffaceous breccia	conglomerate, breccia	64
Lapilli tuff			2
course	Tuffaceous sandstone	Sandstone	
(Ash) tuff			1/16
fine	Tuffaceous siltstone	Siltstone	
			1/256
	Tuffaceous mudstone, shale	Mudstone, shale	
100% pyroclastic	75% <----------	25%	0% by volume
	---------->	volcanic + nonvolcanic (+ minor amounts of biogenic, chemical sedimentary, and authigenic constituents)	

From the IUGS Subcommission on the Systematics of Igneous Rocks (Schmid, 1981).

APPENDIX III

Thin Section Photographic Plates

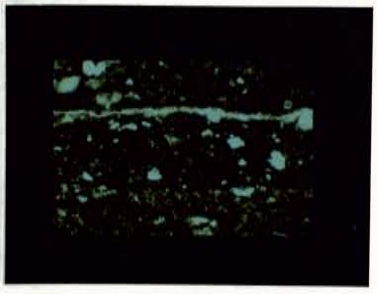

Plate 1. Tuffaceous siltstone.

3 mm

Sample 13-9; Magnified 100X; Plane light.

Plate 2. Pumice fragments in a tuffaceous siltstone.

5 mm

Sample 13-17A; Magnified 40X; Plane light.

Plate 3. Pumice fragments replaced by carbonate.

5 mm

Sample 13-17A; Magnified 40X; Crossed polars.

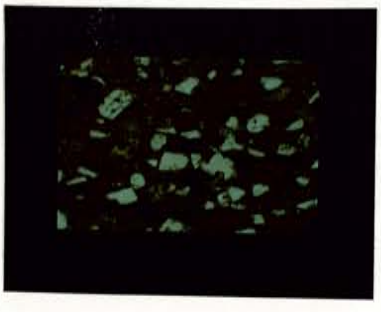

Plate 4. Tuffaceous sandstone.

5 mm

Sample 13-30; Magnified 40X; Plane light.

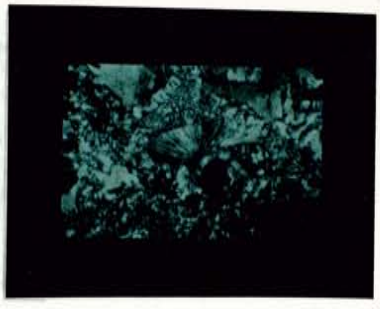

Plate 5. Radiating cluster of chalcedony crystals.

5 mm

Sample 30-12; Magnified 40X; Crossed polars.

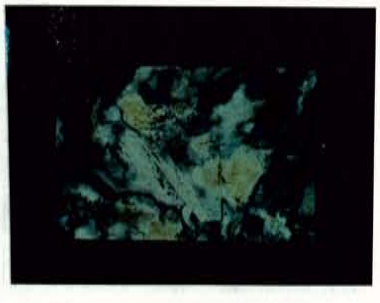

Plate 6. Wedge shaped tridymite twins.

3 mm

Sample 30-8; Magnified 100X; Crossed polars.

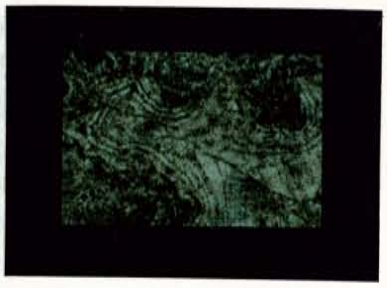

Plate 7. Coliform opal lining a cavity.

5 mm

Sample 30-17; Magnified 40X; Crossed polars.

Plate 8. Dipyramidal termination on detrital quartz.

5 mm

Sample 30-1; Magnified 40X; Crossed polars.

Plate 9. Euhedral sanidine in a glass-rich matrix.

5 mm

Sample 30-3; Magnified 40X; Crossed polars.

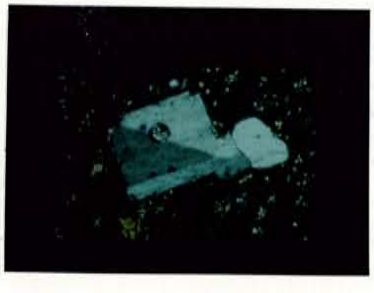

Plate 10. Fresh, euhedral plagioclase grain.

5 mm

Sample 30-3; Magnified 40X; Crossed polars.

Plate 11. Ash-flow lithic fragment.

5 mm Sample 30-16; Magnified 40X; Plane light.

Plate 12. Heulandite group zeolite crystals.

1 mm Sample 30-2; Magnified 320X; Plane light.

Plate 13. Glass shard replaced by gray zeolitic mat
and surrounded by clay minerals.
Sample 13-30; Magnified 320X; Plane light.

1 mm

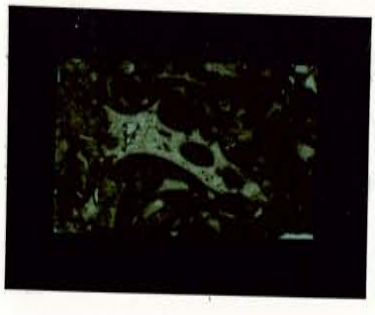

Plate 14. Well preserved vitroclast.

5 mm

Sample 30-1; Magnified 40X; Plane light.

Plate 15. Bent and broken biotite.

5 mm

Sample 30-10G; Magnified 40X; Crossed polars.

Plate 16. Hydromica, a variety of illite containing intergrowths of montmorillonite.

5 mm

Sample 30-2; Magnified 40X; Plane light.

Plate 17. Clay corona around a plagioclase lath.

5 mm

Sample 30-6; Magnified 40X; Plane light.

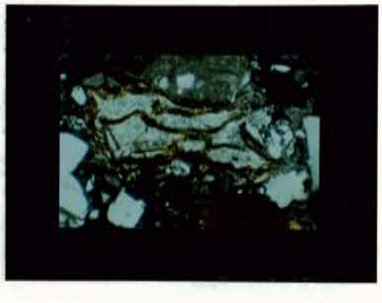

Plate 18. Fractured pyroxene filled with clay.

5 mm

Sample 30-7; Magnified 40X; Plane light.

Plate 19. Clay coronas surrounding glass shards.

3 mm

Sample 30-3; Magnified 100X; Plane light.

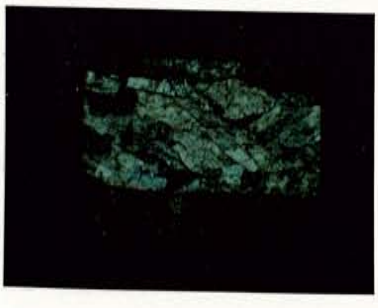

Plate 20. Plagioclase replaced by carbonate.

5 mm

Sample 13-7; Magnified 40X; Crossed polars.

APPENDIX IV

Scanning Electron Microscope

Photographic Plates

Plate 21. Authigenic illite showing micaceo habit.
10 μm
Sample 30-9; Magnified 1000X

Plate 22. Authigenic illite forming on edg a corroded feldspar grain.
13.25 μm
Sample 30-6; Magnified 350X.

Plate 23. Crenulated montmorillonite covering glass shards.
10 μm Sample 13-1; Magnified 1000X.

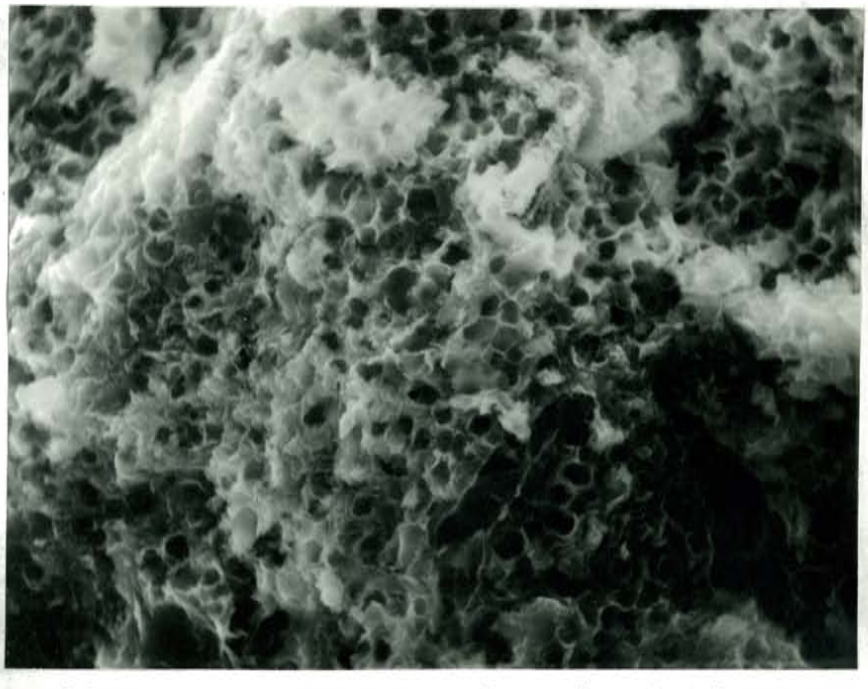

Plate 24. Honeycomb montmorillonite habit.
7.5 μm Sample 13-9; Magnified 1500X.

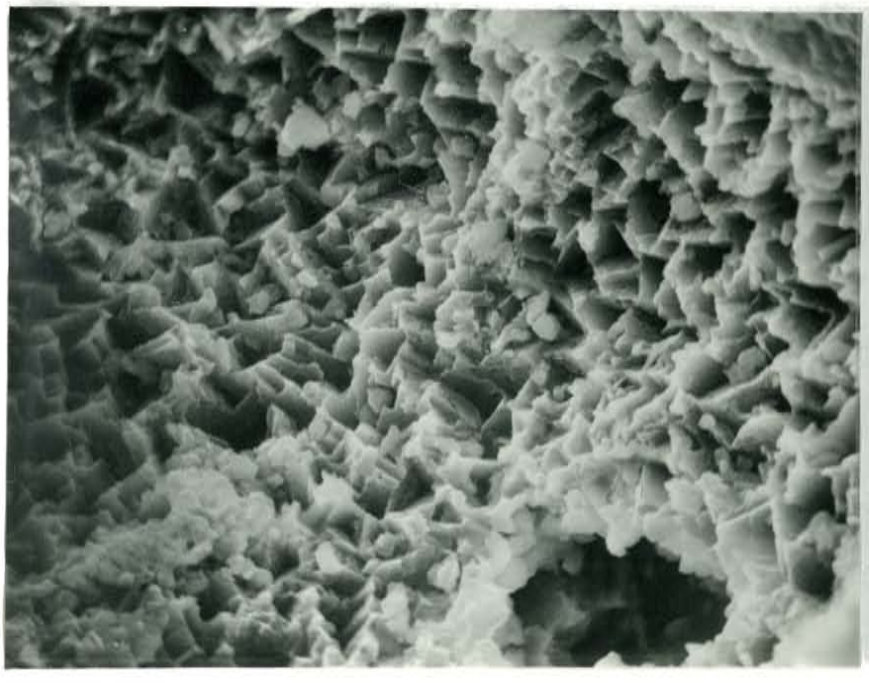

Plate 25. Interlocking montmorillonite crystals pervasively cover glassy surfaces. Sample 30-18; Magnified 1200X.

9.0μm

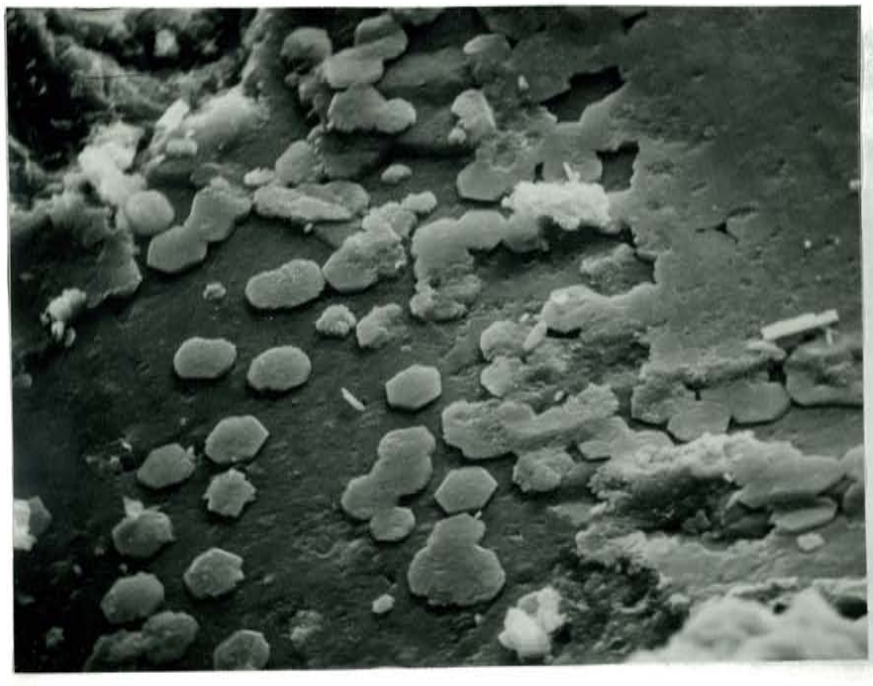

Plate 26. Pseudohexagonal basal kaolinite plates. Sample 13-1; Magnified 1300X.

8.5μm

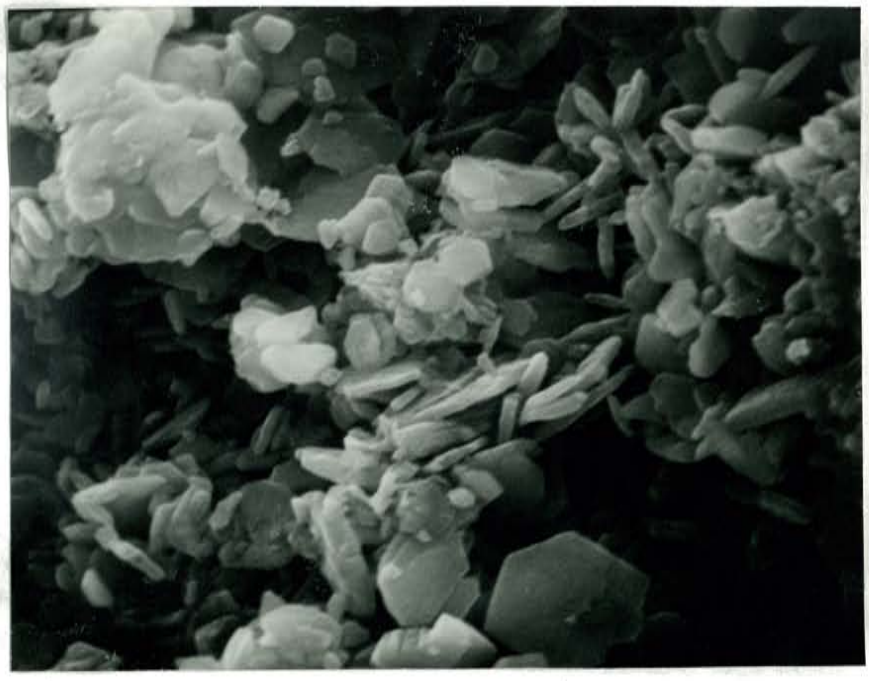

Plate 27. Kaolinite pseudohexagons.

8.0 µm Sample 13-14; Magnified 1400X.

Plate 28. Chlorite rosettes.

7.5 µm Sample 13-1; Magnified 1500X.

Plate 29. Wafer-thin, coffin-shaped, heulandite group zeolite laths.
10 µm
Sample 30-20; Magnified 1000X.

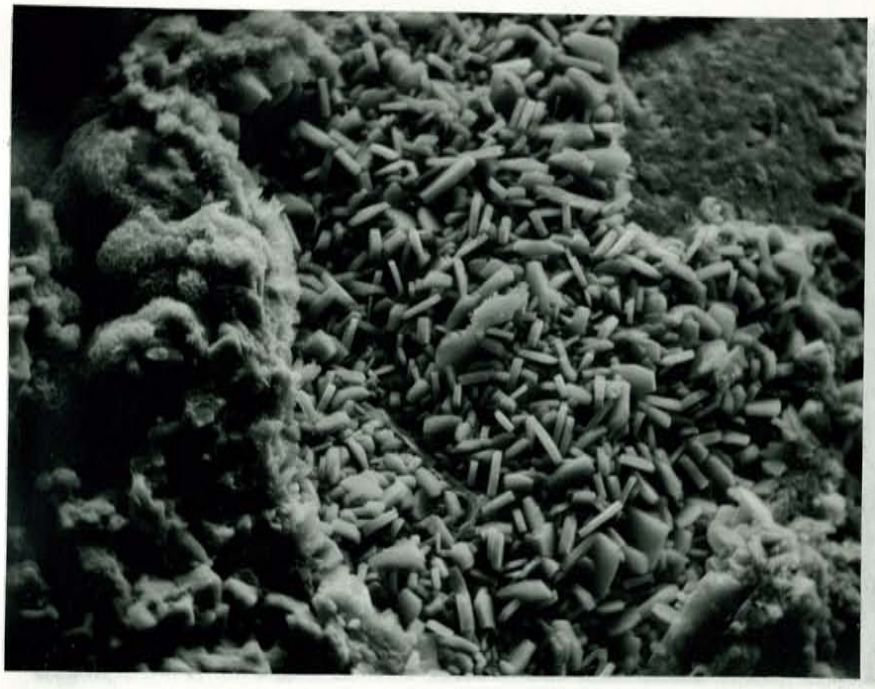

Plate 30. Heulandite group zeolite laths in center; clay mineral growth on left.
12.5 µm
Sample 30-22; Magnified 500X.

Plate 31. "Rats nest" mordenite crystal habit

7.5μm Sample 30-2; Magnified 1500X

Plate 32. Fibrous mordenite tuft containing hundreds of individual crystals.

10μm Sample 30-15A; Magnified 1000X.

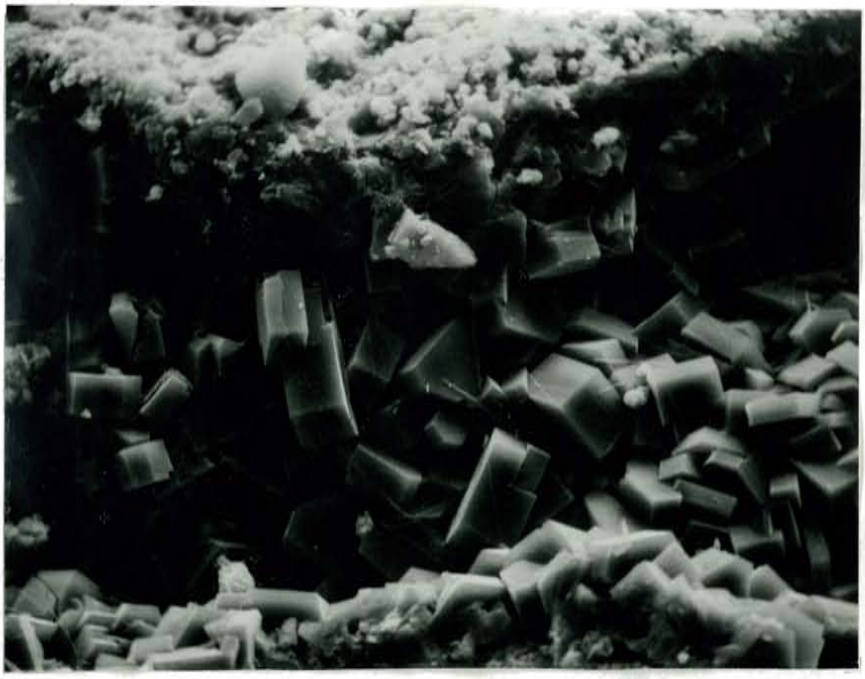

Plate 33. Potassium feldspar prisms growing in a pore space. (K-fsp = K-feldspar). Sample 30-15A; Magnified 1000X.

10 µm

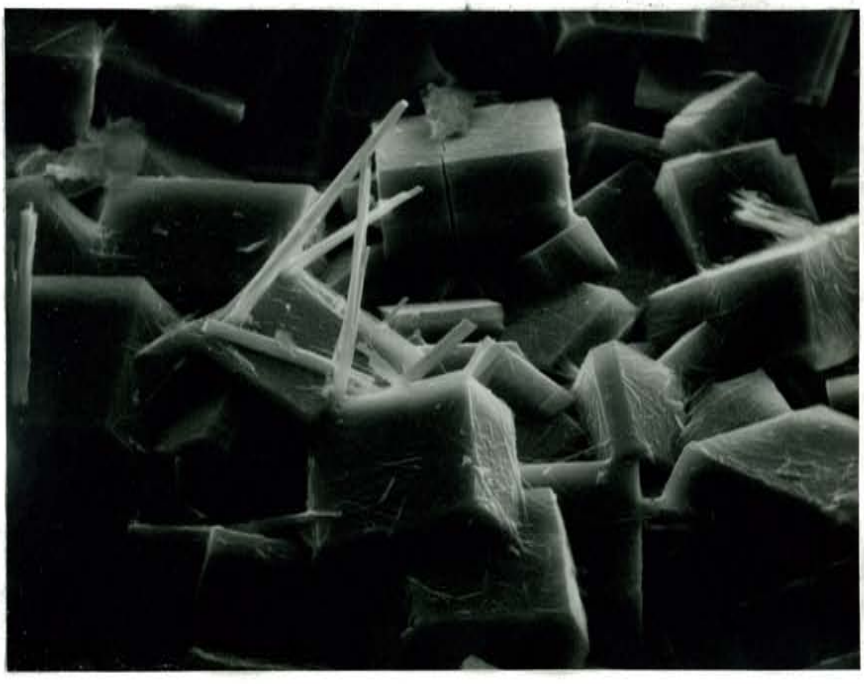

Plate 34. Acicular mordenite lying on top of stubby potassium feldspar prisms. Sample 30-3; Magnified 1000X.

10 µm

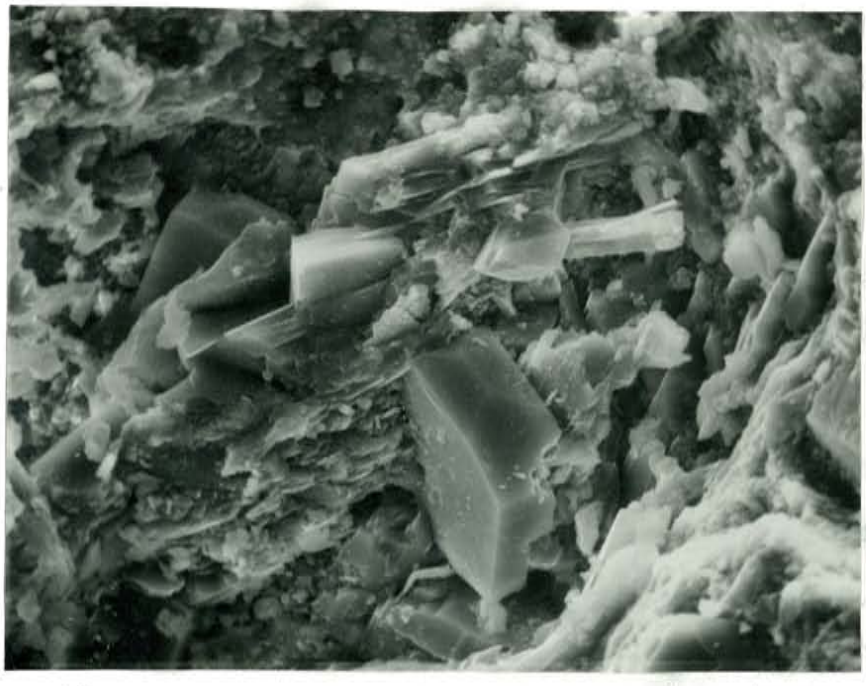

Plate 35. Well developed crystal terminations on authigenic potassium feldspar prisms. Sample 13-19; Magnified 900X.

10.5 µm

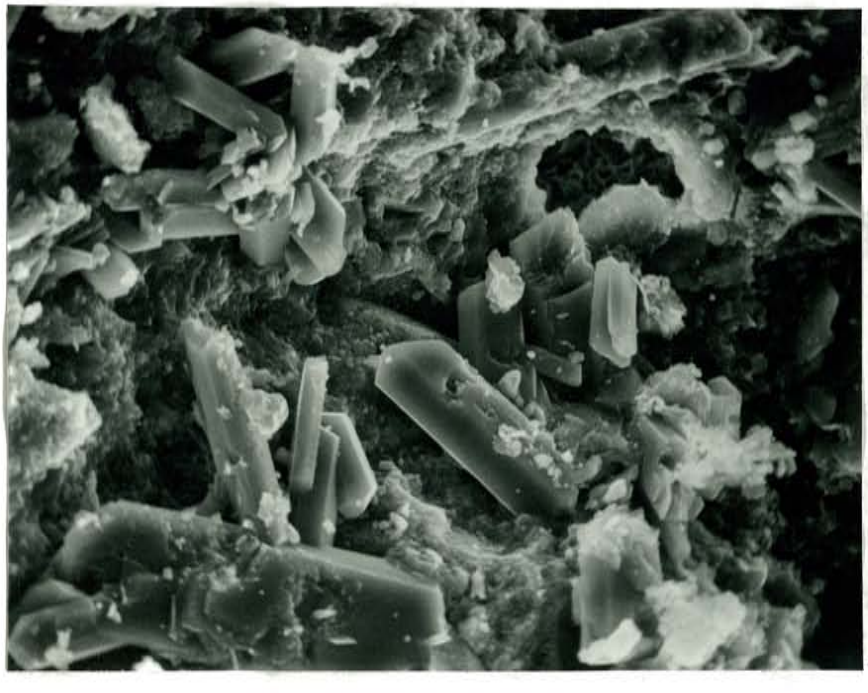

Plate 36. Secondary gypsum crystals lying on clay covered surface. Sample 13-3; Magnified 1000X.

10 µm

APPENDIX V

Detailed Use of the Jensen Cation Plot

The following exerpt is taken directly from L. S. Jensen's 1976 publication on Cation Plots for Classifying Subalkalic Volcanic Rocks.

The Jensen Cation Plot is a simple ternary plot of the volume of major element oxides found in a given rock. The argument for using volumes rather than weights is, it is much more accurate to compare equal volumes of rock than equal weights of rock. Weight percentages cannot show the quantitative relations which petrologists want to see (Barth, 1948; 1952; 1954; Eskola, 1954). This can be done by calculating the equivalent molecular proportions of the constituent oxides from their weight percentages (Table V-4). From the molecular proportions one can calculate atomic or cation percentages.

Oxygen (anions) form 90 to 95% of the volume of a rock. Atoms (cations) of Si, Al, Fe, etc. form less than 6% of the total volume of a rock; hence one molecule of MgO has essentially the same volume as one molecule of FeO. However, one molecule of FeO has nearly double weight of one molecule of MgO. In other words, in a rock where FeO and MgO form equal percentages by weight, MgO has nearly twice the volume of FeO in the rock.

Since one wants to retain a volumetric value rather than a weight measure, there is no advantage to breaking the molecules (oxides) into cations and anions (oxygens). It is simpler to calculate the percentage of each cation with its associated anion(s) (oxygen(s)) and retain the volumetric measure caused by the oxygen anion as explained above.

The cation (cation-oxide) percentages are proportional to the equivalent molecular proportions based on units containing one cation. Thus the proportion of Al_2O_3 is doubled, corresponding to $AlO_{1.5}$ as a unit; likewise $FeO_{1.5}$ instead of Fe_2O_3; $NaO_{1/2}$ instead of Na_2O; and $KO_{1/2}$ instead of K_2O.

Table V-4. Sample calculation of zeolite cation plot percentages: 13-1

	WEIGHT % RECALC. TO 100%	EQUIV. MOLEC. WEIGHT	CATION PROPOR. X 1000	% OF CATION	ZEOLITE CATION PLOT	
SiO_2	68.66	60	1144	64.74	64.74	82.54
$AlO_{1.5}$	16.65	51	326	18.45		
$FeO_{1.5}$	3.66	80	46	2.6		
MgO	1.43	40	36	2.04	2.04	
CaO	2.89	56	52	2.94	2.94	11.97
$Na_{0.5}$	2.40	31	78	4.41	4.41	
$K_{0.5}$	3.57	47	76	4.3	4.30	5.48
TiO_2	0.74	80	9	0.51		
	100.00		1767	99.99	78.43	99.99

Cation percentages are based on each oxide having one cation; therefore, for Al_2O_3, Na_2O, and K_2O, one half of the molecular weight is used.[2] To calculate the cation percentages, the original analysis is brought to a new total of 100%. It is then divided by the corresponding equivalent molecular weight and multiplied by 1000. These figures are added up and percentages of each cation can be calculated. For the zeolite plots SiO_2, MgO, CaO, $NaO_{1/2}$, and $KO_{1/2}$ are added up and brought to a total of 100.[2] The values for MgO, CaO, and $NaO_{1/2}$ are added to form the value for one apix, the SiO_2 value forms another apix, and $KO_{1/2}$ forms the value for the third apix.

Table V-5. WASON SECTION; Data on Zeolite Cation Plots

SAMPLE	CATION PLOT %'S			FIELD
	% SiO_2	% MgO + CaO + $NaO_{1/2}$	% $KO_{1/2}$	
1	83	12	5	cl
2	85	10	5	cl
3	85	8	7	
4	87	5	8	
5	85	8	7	
6A	84	7	9	
6B	80	12	8	cl
10A	86	8	6	
11	89	6	5	
12	76	19	5	er
13B	84	10	6	
14	84	8	8	
15	83	9	8	
16B	77	18	5	er
17A	80	14	6	cl
17B	86	9	5	near cl
18	81	15	4	cl
19	87	8	5	
20A	83	12	5	cl
20B	83	12	5	cl
22	84	12	4	cl
24	83	13	4	cl
27	85	10	5	cl
29	85	8	7	
30	84	10	6	
31	82	13	5	

Note: er=erionite field
cl=clinoptilolite

Table V-6. NORTH PHIPPS SECTION; Data on Zeolite Cation Plots

SAMPLE	CATION PLOT %'S			FIELD
	% SiO_2	% MgO + CaO + $NaO_{1/2}$	% $KO_{1/2}$	
1	85	10	5	cl
2	83	11	6	cl
3	82	10	8	near cl
4	86	10	4	near cl
7	84	10	6	cl
8	76	13	11	cl
9	83	11	6	cl
10A	82	12	6	cl
10B	88	9	3	
10C	86	9	5	near cl
10D	86	10	4	near cl
10E	81	13	6	cl
10F	87	9	4	
10G	81	14	5	cl
11	79	17	4	near cl
12	77	12	11	near ph
13	82	11	7	cl
14	78	12	10	near ph
15A	83	12	5	cl
15B	88	8	4	
16	82	11	7	cl
18	81	13	6	cl
19	76	13	11	ph
20	79	18	3	near cl
21	79	17	4	near cl

Note: ph=phillipsite field
cl=clinoptilolite field

APPENDIX VI

Table VI-7. Whole Rock Chemistry of U.S.G.S. Zeolite Standards (wt. %)

	SiO_2	Al_2O_3	TOTAL FE AS Fe_2O_3	MgO	CaO	Na_2O	K_2O	TiO_2	TOTAL
TX-2	73.9	11.5	0.92	0.84	1.52	1.30	0.59	.22	90.79
TP-10	67.7	13.1	1.63	0.60	1.69	3.70	2.04	.26	90.82
AMN-1	66.5	11.1	0.76	0.40	0.93	3.00	4.34	.08	87.13
SW3-2	58.2	17.6	2.09	0.80	1.00	9.90	0.77	.10	90.48
DO54H	62.3	11.6	4.51	0.96	1.67	3.00	2.42	.16	86.62
27053	65.4	12.5	1.33	0.90	3.07	1.00	3.32	.11	87.63
27063	68.4	10.8	1.74	0.40	2.00	1.00	4.47	.19	89.00
27083	63.4	12.2	1.33	1.70	3.37	1.40	1.12	.13	84.65

(Note: Zeolite standard, 27083, was the standard chosen for the drift pellet in all X-ray fluorescence analyses).

APPENDIX VII

Abbreviated Sample Descriptions

13-1: Course grained tuffaceous sandstone.

Pale gray to green unit with 1-5 cm thick iron oxide and organic laminae. Feldspar phenocrysts 0.5 to 1.0 mm are broken and angular, but still fresh. Well preserved vitroclastic texture. Diverse lithic fragments. Abundant biotite flakes 0.5 mm long.

X-ray diffraction indicates:
abundant: quartz, feldspar, biotite
moderate: calcite, gypsum, montmorillonite, clinoptilolite, illite
minor: celadonite, mordenite
trace: tridymite, chlorite, kaolinite.

13-2: Medium grained tuffaceous sandstone.

Pale gray to green unit with abundant sulfur staining. Feldspar phenocrysts 0.5 mm long, are broken and angular, but still fresh. Well preserved vitroclastic texture and abundant pumice fragments ~1 mm long. Diverse lithic fragments.

X-ray diffraction indicates:
abundant: quartz, feldspar, biotite
moderate: calcite, gypsum, montmorillonite, clinoptilolite, illite;
minor: celadonite, mordenite.

13-3: Tuffaceous conglomerate.

Pale grayish purple to chalky white unit. Abundant, diverse lithic fragments 1-10 mm long in a siltsize ashy matrix. Several areas of patchy carbonate replacement.

X-ray diffraction indicates:
abundant: quartz, feldspar, biotite
moderate: calcite, gypsum, montmorillonite, heulandite, illite
minor: celadonite, mordenite
trace: tridymite.

13-4: Tuffaceous siltstone.

Very pale gray, thinly bedded unit with 1 cm thick layers. Carbonized plant imprints on shaley partings. Unbroken feldspar laths and biotite flakes 0.1-0.5 mm long.

X-ray diffraction indicates:
abundant: quartz
moderate: feldspar, biotite, calcite, montmorillonite, heulandite
minor: celadonite, mordenite, illite

13-5: Tuffaceouus conglomerate.

Pale yellow massive unit with occasional bands of white or sulfur yellow zones 2-3 cm thick. Abundant, diverse lithic fragments 1-10 mm wide in a siltsize ashy matrix.

X-ray diffraction indicates:
abundant: quartz, feldspar
moderate: calcite, gypsum, biotite, heulandite group zeolite
minor: montmorillonite, mordenite, illite
trace: celadonite

13-6: Tuffaceous siltstone.

Well bedded unit alternating between pale gray (13-6A) and mustard yellow (13-6B) layers 12-15 cm thick. 13-6A contains abundant laminations < 0.01 mm thick. Feldspar and biotite flakes 0.1-0.5 mm long. 13-6B contains abundant white pumice fragments 1-4mm long with tiny acicular crystals inside. Both siltstone varieties contain unbroken, fresh feldspar phenocrysts, and well preserved vitroclastic texture. Despite the color differences, both samples have the same mineralogy.

X-ray diffraction indicates:
abundant: quartz
moderate: feldspar, biotite, calcite, gypsum, montmorillonite, clinoptilolite
minor: celadonite, mordenite, illite

13-7: Carbonate-rich tuffaceous conglomerate

Pale yellow, pale gray, and off white unit with 10 cm wide vugs containing brown bladed calcite crystals. Abundant, diverse ash-flow and Creede Formation lithic fragments 1 mm to 3 cm long. Many pore spaces filled with radiating chalcedony crystals or patchy carbonate replacement material.

X-ray diffraction indicates:
abundant: calcite
moderate: quartz, feldspar, biotite, gypsum,

heulandite

13-9: Tuffaceous siltstone.

Pale brownish gray, paper thin bedded unit with profuse laminations < 0.01 mm thick. Carbonized plant imprints along shaley partings sometimes with sulfur staining. Feldspar laths and biotite flakes are euhedral, unbroken, fresh, and 0.1-0.5 mm long.

X-ray diffraction indicates:
abundant: quartz, montmorillonite
moderate: feldspar, calcite, heulandite group zeolite
minor: biotite, celadonite, mordenite

13-10: Carbonate-rich tuffaceous siltstone.

Thinly bedded unit alternating from an ashy, white, very poorly consolidated layer at base (13-10A) to a pale brownish gray layer at top (13-10B). Biotite flakes and feldspar laths are euhedral, unbroken, and 0.1 mm long. Well preserved vitroclastic texture in both varieties. 13-10A is dominantly siltsize but does contain some 3-5 cm long lithic fragments at base of unit and fines upward.

X-ray diffraction indicates:
13-10A-abundant: feldspar
moderate: quartz, gypsum, calcite, montmorillonite, heulandite
minor: celadonite, mordenite
13-10B-abundant: calcite
moderate: quartz, biotite, montmorillonite, heulandite
trace: celadonite

13-11: Tuffaceous siltstone.

Pale buff to pale gray, paper thin bedded unit with a few layers up to 1.5 cm thick. Forms blocky exposure. Carbonized wood imprint along shaley partings. Biotite flakes and feldspar laths are euhedral, unbroken, and 0.1-0.5 mm lomg.

X-ray diffraction indicates:
abundant: quartz
moderate: feldspar, biotite, gypsum, calcite, montmorillonite, heulandite
minor: celadonite, mordenite

trace: illite, clinoptilolite, kaolinite

13-12: Tuffaceous conglomerate.

Off white and buff unit, very poorly consolidated with little matrix material. Abundant and diverse ash-flow lithic fragments 1-5 cm long.

X-ray diffraction indicates:
abundant: feldspar, calcite
moderate: quartz, biotite, gypsum, heulandite, illite
minor: montmorillonite
trace: celadonite

13-13: Medium and coarse grained tuffaceous sandstone.

Well bedded, buff to pale gray unit alternating between medium grained (13-13A) and coarse grained (13-13B) layers. Both varieties contain biotite flakes 0.5-2.0 mm long and euhedral but broken up feldspar laths 0.1-2.0 mm long. Organic laminae < 0.01 mm thick.

X-ray diffraction indicates:
13-13A-abundant: feldspar
moderate: quartz, tridymite, biotite, calcite, gypsum, heulandite, illite
minor: mordenite
13-13B-abundant: quartz, biotite
moderate: feldspar, tridymite, calcite, gypsum, heulandite, illite
minor: mordenite

13-14: Tuffaceous siltstone.

Pale gray to white, paper thin bedded unit with some layers 5-10 mm thick. This unit contains lenses 5 cm long by 2.5 cm wide, filled with coarse grained, medium to dark gray, very poorly consolidated ashy material. Carbonized wood imprints on shaley partings. Euhedral, unbroken feldspar laths and biotite flakes 0.1-0.5 mm long. Organic laminae < 0.01 mm wide. Abundant glass shards present.

X-ray diffraction indicates:
abundant: quartz
moderate: feldspar, biotite, gypsum, montmorillonite, heulandite, illite
minor: celadonite, mordenite
trace: kaolinite

13-15: Carbonate-rich tuffaceous siltstone

Pale to white, paper thin bedded unit randomly interbedded with 0.1-0.5 mm thick medium gray layers and lenses of poorly consolidated ash. Abundant glass shards and pumice fragments. Euhedral, unbroken feldspar laths and biotite flakes 0.1 mm long. Much carbonate replacement.

X-ray diffraction indicates:
abundant: quartz, biotite
moderate: feldspar, calcite, gypsum, montmorillonite, heulandite, illite
minor: celadonite, mordenite

13-16: Tuffaceous siltstone and fine grained sandstone

Buff and pale gray, well bedded unit alternating between paper thin, carbonate-rich tuffaceous siltstone (13-16A), abd very fine grained, carbonate-rich, tuffaceous sandstone (13-16B). 13-16B forms beds several cm thick, contains abundant pumice fragments 2-4 mm long, and has well preserved vitroclastic texture.

X-ray diffraction indicates:
13-16A-abundant: quartz, calcite
moderate: biotite, heulandite
minor: feldspar
13-16B-abundant: calcite
moderate: tridymite, feldspar, biotite, heulandite
minor: montmorillonite,
trace: celadonite, clinoptilolite, kaolinite

13-17A: Tuffaceous siltstone.

Pale buff to white, paper thin bedded unit, with carbonized plant imprints along shaley partings. Clusters of silicate-rich and carbonate-rich replacement patches. Abundant organic laminae. Euhedral, unbroken feldspar laths and biotite flakes 0.1-0.5 mm long. Abundant pumice fragments, some stained with sulfur or iron oxide.

X-ray diffraction indicates:
abundant: calcite
moderate: quartz, tridymite, feldspar, biotite, gypsum, heulandite, illite
minor: montmorillonite, mordenite
trace: celadonite, clinoptilolite

13-17B: Medium grained tuffaceous sandstone.

Pale pinkish to buff, well bedded unit interbedded with 1-2 mm thick, pale to medium gray, siltsize ash layers. Organic laminae <0.05 mm wide. Fresh, euhedral, but broken feldspar laths and biotite flakes 0.5-1.0 mm long.

X-ray diffraction indicates:
abundant: quartz, feldspar, biotite
moderate: tridymite, calcite, heulandite, illite
minor: montmorillonite, mordenite, gypsum
trace: celadonite

13-18: Coarse grained tuffaceous sandstone.

Pale gray to white, very poorly consolidated, extremely porous and permeable unit. 1 cm thick bands of iron oxide alteration throughout the unit.

X-ray diffraction indicates:
abundant: feldspar, biotite, gypsum
moderate: quartz, tridymite, calcite, heulandite, illite
trace: clinoptilolite

13-19: Tuffaceous siltstone.

Dark brown, well bedded unit with 5 mm to 4 cm thick layers. Contains small white pumice fragments 1-3 mm wide, large pinkish gray pumice fragments up to 3 cm long, and medium gray lenses of siltsize ash up to 4 cm long. Abundant solution features and some ooids observed.

X-ray diffraction indicates:
abundant: quartz
moderate: tridymite, feldspar, biotite, calcite, gypsum, heulandite
minor: montmorillonite, illite
trace: celadonite, clinoptilolite

13-20: Coarse and fine grained tuffaceous sandstone.

Buff to white, well bedded unit alternating from coarse grained layers (13-20A) to fine grained layers (13-20B) which range from 1 mm to 2 cm thick. Coarse grained, cm thick beds more prevalent at base of unit. 13-20A contains abundant pumice fragments and well preserved vitroclastic

texture. 13-20B contains abundant organic laminae, and occasional interbedded pale gray, 1-2 mm thick, siltsize ashy layers.

X-ray diffraction indicates:
13-20A-abundant: feldspar
moderate: quartz, biotite, montmorillonite, heulandite, illite
minor: calcite
trace: tridymite, kaolinite
13-20B-abundant: feldspar, biotite
moderate: quartz, tridymite, calcite, montmorillonite, heulandite, illite

13-22: Coarse grained tuffaceous sandstone.

Pale gray to white, well bedded unit with 5-8 cm thick layers. Fresh, euhedral but broken up feldspar laths and biotite flakes 1-1.5 mm long.

X-ray diffraction indicates:
abundant: feldspar
moderate: quartz, tridymite, biotite, heulandite
minor: illite, calcite

13-24: Coarse grained tuffaceous sandstone.

Pale gray to off white, well bedded unit with beds ~ 8 cm thick. Fresh, euhedral, but broken up feldspar laths and biotite flakes 1-1.5 mm long. 1-2 cm layering evident within beds by alternating colors between pale gray and white.

X-ray diffraction indicates:
abundant: feldspar
moderate: quartz, biotite, heulandite, illite
trace: calcite, tridymite

13-25: Carbonate-rich tuffaceous siltstone.

Pale gray to white, paper thin bedded unit with 1-1.5 mm thick layers. Occasional creamy yellow layers. Sparse carbonized plant imprints. Well preserved vitroclastic texture.

X-ray diffraction indicates:
abundant: calcite
moderate: quartz

trace: feldspar, biotite, heulandite group zeolite, illite, kaolinite

13-26: Tuffaceous siltstone and bedded carbonate.

Paper thin bedded, pale gray to white, carbonate-rich tuffaceous siltstone (13-26A) with well preserved vitroclastic texture, separated in middle of unit by an ~ 20 cm thick, dark gray brown, autobrecciated limestone.

X-ray diffraction indicates:
abundant: calcite
moderate: quartz
trace: feldspar, biotite, heulandite group zeolite

13-27: Medium grained tuffaceous siltstone.

Nearly pure white, well bedded unit with 2-5 cm thick layers. Unusual iron oxide alteration spots, 1-2 mm in diameters throughout unit. Euhedral but broken up feldspar laths and biotite flakes 0.1-0.5 mm long.

X-ray diffraction indicates:
abundant: feldspar, biotite
moderate: quartz, tridymite, calcite, heulandite illite
minor: montmorillonite
trace: celadonite, mordenite

13-28: Carbonaceous coarse grained tuffaceous sandstone.

Dark to medium gray, well bedded unit with 5 mm to 3.5 cm thick layers. Occasional interbedded buff colored layers ~ 5 mm thick. Feldspar laths 1-2 mm long are unusually broken up, more rounded than usual, but still fresh in appearence. Abundant carbonate cement.

X-ray diffraction indicates:
abundant: calcite
moderate: quartz, feldspar, biotite
minor: illite
trace: heulandite group zeolite

13-29: Tuffaceous siltstone.

Very pale gray, paper thin bedded with some layers 5 mm wide. Sparse carbonized plant remains along shaley partings. Well preserved vitroclastic texture.

X-ray diffraction indicates:
abundant: quartz
moderate: tridymite, feldspar, biotite, calcite, heulandite, montmorillonite, illite
minor: celadonite

13-30: Medium grained tuffaceous sandstone.

Alternating layers of very pale gray ashy material with heavily iron oxide stained layers. White layers 2-3 mm thick, and are less permeable and porous than 5 mm thick iron stained layers. Euhedral, angular, fresh, somewhat broken up feldspar laths and biotite flakes ~ 0.5 mm long.

X-ray diffraction indicates:
abundant: feldspar, biotite
moderate: quartz, heulandite, illite
minor: montmorillonite
trace: tridymite, celadonite

13-31: Coarse grained tuffaceous sandstone.

Poorly consolidated, pale gray unit with profuse iron oxide staining throughout unit. Very porous and permeable. Feldspar and biotite laths average 1-2 mm long.

X-ray diffraction indicates:
abundant: feldspar, biotite
moderate: quartz, heulandite, illite
trace: tridymite

30-1: Tuffaceous conglomerate.

Light buff to off white unit with 30-60 cm thick beds. Diverse ash-flow lithic fragments 1-5 mm long comprising 15-20% of the unit in a very fine, ash size, glass rich matrix. Feldspar laths and biotite flakes 0.5-1.0 mm long, fresh, euhedral but broken up, and mostly contained in ash-flow fragments. Well preserved vitroclastic texture. Feldspar-tridymite spherulites in matrix.

X-ray diffraction indicates:
abundant: quartz
moderate: tridymite, feldspar, biotite, calcite, montmorillonite, heulandite,
minor: celadonite, mordenite, illite

30-2: Tuffaceous conglomerate.

Light buff to off white unit with 10-20 cm thick beds. Diverse ash-flow lithic fragments 1-7 mm long comprising 30-35% of the unit in a medium ash size, glass rich matrix. Feldspar laths and biotite flakes 0.5-1.0 mm long, are fresh, angular, broken, and mostly found in ash-flow fragments. Feldspar-tridymite spherulites in matrix. Well preserved vitroclastic texture with some acicular crystals observable inside glass shards.

X-ray diffraction indicates:
abundant: quartz, feldspar
moderate: tridymite, biotite, calcite, heulandite, montmorillonite
trace: celadonite, mordenite, illite

30-3: Tuffaceous conglomerate.

Light buff to off white unit with 10-20 cm thick beds. Diverse ash-flow lithic fragments 5-15 mm long comprising 15-20% of the unit in a very fine ash size, glass rich matrix. Feldspar laths and biotite flakes 0.5-1.0 mm long and mostly found in lithic fragments. Glassy matrix full of feldspar microlites and broken glass shards.

X-ray diffraction indicates:
abundant: quartz, feldspar
moderate: biotite, calcite, montmorillonite heulandite
minor: celadonite, mordenite, illite
trace: tridymite, kaolinite

30-4: Fine grained tuffaceous sandstone.

Off white to slight pale green unit with beds 3-7 mm thick. Occasional pale green siltsize laminations 1-3 mm thick which contain elongated pumice fragments 1-2 mm long. Euhedral, unbroken feldspar laths and biotite flakes < 0.1 mm long. Layering defined by oriented microlites and glass shards.

X-ray diffraction indicates:
abundant: quartz, feldspar
moderate: biotite, calcite, montmorillonite, heulandite
minor: illite
trace: celadonite, mordenite

30-5: Bedded carbonate.

Pale gray unit with beds 2-4 mm thick. Appears to have once been a tuffaceous siltstone and is now nearly all recrystallized to calcite due to direct association with a travertine spring. Outcrop seen in Photographic Plate C.

X-ray diffraction indicates:
abundant: calcite
moderate: quartz, feldspar

30-6: Coarse grained tuffaceous siltstone.

Medium to pale gray unit with beds 10-25 cm thick. Fresh, angular, and broken feldspar laths and biotite flakes 1-2 mm long. A few ash-flow lithic fragments and numerous travertine chips 2-3 mm long. Glass rich matrix with abundant carbonate cement.

X-ray diffraction indicates:
abundant: calcite
moderate: quartz, feldspar, biotite
montmorillonite
minor: heulandite
trace: illite

30-7: Tuffaceous conglomerate.

Light buff to off white unit with beds 15-25 cm thick. Diverse ash-flow lithic fragments 1-4 mm long. Very fine, ash size, glass rich matrix. Well preserved vitroclastic texture.

X-ray diffraction indicates:
abundant: quartz, feldspar
moderate: heulandite
minor: biotite, gypsum
trace: calcite, celadonite, mordenite, illite, chlorite

30-8: Tuffaceous mudflow.

Off white, massive, moderately consolidated, chaotic unit with beds up to 1 m thick. Fine to medium ash size, crystal rich matrix containing large, angular ash flow lithic fragments 7-15cm in diameter. Clasts very randomly oriented and floating in the matrix.

X-ray diffraction indicates:
abundant: feldspar
moderate: quartz, biotite

minor: illite
trace: calcite, tridymite, celadonite

30-9: Coarse grained tuffaceous sandstone.

Buff colored unit with 10-25 cm thick beds. Fresh, euhedral, but broken feldspar laths 0.5-3.0 mm long. Crude layering defined by very coarse and medium to coarse grained layers. Very coarse layers have pumice fragments 1-3 mm long and occasional ash-flow fragments up to 5 mm long. Medium to coarse layers have better preserved vitroclastic texture.

X-ray diffraction indicates:
abundant: quartz, feldspar, biotite
moderate: montmorillonite, heulandite, illite
minor: celadonite, mordenite
trace: kaolinite

30-10: Coarse and fine grained tuffaceous sandstone

Buff colored unit with 10-25 cm thick beds alternating regularly from coarse to fine grained layers. Pumice fragments 1-3 mm long, biotites 0.5-1.0 mm long, glass rich matrices, and occasional feldspar-tridymite spherulites in matrix occur throughout unit and are not restricted to fine or coarse beds. Euhedral feldspars 0.1-0.5 mm long in fine grained layers. More broken up, 1-2 mm long feldspars in coarse grained layers.

X-ray diffraction indicates:
abundant: quartz, feldspar, biotite
moderate: montmorillonite, heulandite
minor: tridymite, calcite, celadonite, mordenite, illite

30-11: Coarse grained tuffaceous sandstone.

Medium to light buff colored unit with 10-25 cm thick beds. Strongly zoned, very broken feldspar laths 0.5-3.0 mm long. Occasional lenses of tuffaceous siltstone 5-9 cm long lying parallel to bedding. 10-15% pumice fragments 2-4 mm long, some rounded, some stretched. Medium, ash size, glass rich matrix with feldspar microlites and minor amounts of tridymite.

X-ray diffraction indicates:
abundant: quartz, feldspar, biotite, calcite
moderate: montmorillonite, heulandite, illite

trace: tridymite

30-12: Tuffaceous mudflow.

Medium buff colored, massive but poorly consolidated, chaotic unit with beds 30-50 cm thick beds. Many rounded clasts 2-10 cm in diameter in matrix and in much larger clasts and boulders up to 50 cm wide. Clasts very randomly oriented and float in matrix. Many clasts are bleached white. Abundant feldspar-tridymite spherulites in matrix. Outcrop seen in Photographic Plate D.

X-ray diffraction indicates:
abundant: feldspar
moderate: quartz, biotite, tridymite
trace: illite

30-13: Coarse grained tuffaceous sandstone.

Medium buff colored unit with beds 10-20 cm thick. Euhedral but broken feldspar laths 1-2 mm long. A few lithic fragments ranging from 3-10 mm.

X-ray diffraction indicates:
abundant: quartz, feldspar, biotite
moderate: tridymite, calcite, montmorillonite, heulandite, illite
trace: celadonite, mordenite

30-14: Tuffaceous mudflow.

Medium buff colored, massive, well consolidated, chaotic unit with no individual beds discernable. Clasts more angular than other mudflow units and range from 1-9 cm in diameter. Clasts float in a fine to coarse, glass rich, ash size matrix. Some feldspar-tridymite spherulites.

X-ray diffraction indicates:
abundant: feldspar
moderate: quartz, biotite
trace; tridymite, illite

30-15A: Coarse grained tuffaceous sandstone.

Off white to very pale green unit with 5 cm thick beds. Euhedral but broken feldspar laths and biotite flakes 0.5-1.0 mm long. Medium ash size, glass rich matrix with some tridymite twins and abundant feldspar microlites.

X-ray diffraction indicates:
abundant: feldspar
moderate: quartz, biotite
minor: heulandite
trace: calcite, illite

30-15B: Tuffaceous conglomerate.

Off white to very pale green massive bed about 1 m thick. Diverse ash-flow lithic fragments 3-7 mm in diameter, some elongated. Feldspar laths are euhedral, not very broken, and 0.1-0.5 mm long. Fine ash size, glass rich matrix.

X-ray diffraction indicates:
abundant: quartz
moderate: feldspar, biotite, calcite, heulandite
minor: montmorillonite, illite
trace: celadonite, mordenite

30-16: Tuffaceous conglomerate.

Off white, massive, poorly consolidated bed about 1 m thick. May be same unit as 30-15B but too much undifferentiated Creede Formation in between to be certain. Feldspar laths are 1-1.5 mm long. Diverse ash-flow lithic fragments 3-7 mm with occasional clasts up to 12 mm long. Fine to medium ash size, glass rich matrix.

X-ray diffraction indicates:
abundant: feldspar
moderate: quartz, biotite, heulandite
minor: montmorillonite
trace: celadonite, mordenite, illite

30-17: Bedded carbonate:

Gray to brown bed about 40 cm thick. Looks like a conglomerate composed of rounded pieces of travertine that are concentrically banded. Pore spaces filled with carbonate cement and very fine grained feldspar laths probably < 0.05 mm long.

X-ray diffraction indicates:
abundant: calcite
minor: quartz, feldspar, biotite, heulandite

30-18: Coarse and fine grained tuffaceous sandstone.

Light buff unit with 10-20 cm thick beds alternating between fine and coarse grained layers. Coarse layers have abundant pumice fragments 2-5 mm long and a few as large as 7 mm. Euhedral, broken feldspars in coarse layer 1-1.5 mm long. Less broken feldspar 0.5 mm in fine grained layer.

X-ray diffraction indicates:
abundant: feldspar
moderate: quartz, biotite, calcite
minor: montmorillonite, heulandite, illite

30-19: Carbonaceous coarse grained tuffaceous sandstone.

Dark to pinkish gray, 15 cm thick bed separating the fine and coarse sandstone unit below and an entirely coarse grained unit above. Feldspars 1-2 mm long, euhedral, and fresher than 30-18 but still broken. Pore spaces filled with carbonate cement.

X-ray diffraction indicates:
abundant: feldspar
moderate: quartz, biotite
trace: tridymite, illite

30-20: Coarse grained tuffaceous sandstone.

Light buff to off white unit with beds 5-10 cm thick. Carbonate patches throughout matrix 1-2 mm wide that may have once been pumice fragments. Rest of matrix glass rich, and full of shards and vessicles.

X-ray diffraction indicates:
abundant: feldspar
moderate: quartz, biotite, calcite,
montmorillonite, heulandite
minor: illite
trace: mordenite

30-21: Coarse grained tuffaceous sandstone.

Unit may be same as 30-20 except for being a darker buff color, slightly coarser grained, more biotite rich, and more poorly consolidated.

X-ray diffraction indicates:
abundant: quartz, feldspar, biotite
moderate: calcite, montmorillonite, heulandite,

illite
trace: celadonite, mordenite

30-22: Fine and coarse grained tuffaceous sandstone.

Pale gray to white unit, well bedded, and alternating between fine and coarse grained layers. Fine grained layers contain 25-30% pumice fragments 1-2 mm long. Coarse grained layers contain 30-35% pumice fragments 5-10 mm long with excellent relict compacted glass texture. Well preserved vitroclastic texture throughout the unit.

X-ray diffraction indicates:
abundant: calcite
moderate: quartz, feldspar, biotite
montmorillonite, heulandite
minor: illite
trace: mordenite

30-23: Tuffaceous siltstone.

Carbonate-rich bed with layers 2-4 mm wide. Glass rich matrix with abundant feldspar microlites. Well defined layering throughout unit.

X-ray diffraction indicates:
abundant: calcite
moderate: quartz
minor: feldspar, biotite, heulandite

This thesis is accepted on behalf of the faculty of the Institute by the following committee:

Adviser

January 22, 1982
Date